Alma Mater Studiorum – Università di Bologna

DOTTORATO DI RICERCA IN
SCIENZE CHIMICHE
Ciclo XXVI
Settore Concorsuale di Afferenza: 03/A1
Settore Scientifico Disciplinare: CHIM/01

FLOW FIELD–FLOW FRACTIONATION FOR SIZE ANALYSIS AND CHARACTERIZATION OF NANOPARTICLES FOR APPLICATION IN LIFE SCIENCES

Presentata da: **Francesco Borghi**

Coordinatore dottorato:
Prof. Aldo Roda

Relatore:
Prof. Pierluigi Reschiglian

Esame finale anno 2014

TABLE OF CONTENTS

Abstract

Nanotechnologies are rapidly expanding because of the opportunities that the new materials offer in many areas such as the manufacturing industry, food production, processing and preservation, and in the pharmaceutical and cosmetic industry [1-3]. Size distribution of the nanoparticles determines their properties and is a fundamental parameter that needs to be monitored starting from the small scale synthesis up to the bulk production and in the quality control of nanotech products on the market. This concept holds true especially because on particle size and particle size distribution (PSD) depend some important characteristics of nanoparticles such as stability, toxicity and functioning (just to name a few). An example is the distribution of nanoparticles in different biological compartments with the result that the same chemical species can be toxic or not according to its size, while in the context of drug delivery and cosmetic industry [4], specific targets require well-defined size distributions (in anticancer therapy, nano particles between 70 and 200 nm are used drug vector while micro particles can act as cell- like tumor vaccines).

As a consequence of the increasing number of application the EU regulatory authorities is implementing the EU's groundbreaking chemicals legislation of nanomaterials. Aims are the *benefit of human health and the environment as well as the innovation and competitiveness of chemical industry*. Companies have to comply with the legislation, advance the safe use of chemicals, provide information on chemicals and address chemicals of concern. This introduces the obligation for companies that make use of nanomaterials both to compliance with such regulations and to acquire and use analytical platforms that allow the assessment of the size parameters of the nanomaterials they use. This duty is considered to be of capital importance, so that the problem of the

characterization of nanosized materials has recently been summarized in the slogan *'no data, no market'*.

Size exclusion chromatography (SEC) is nowadays the golden standard for size separation of dispersed samples, because of its simplicity of use, relative low number of parameters to be kept under control for the experiments, ease method set up, and most of all because its hyphenation with UV-Vis, Refractive index or fluorescence detection makes it possible to have an analytical platform with the appealing feature of easy and rapid method development and relatively easy method validation. Such features have been historically enough for chemical laboratories, especially in the industry, to choose SEC as standard technique, especially when reproducibility of analysis is of capital importance because the research is carried on on the cooperation of different laboratories. However SEC separation have some drawbacks, that become very important for niche application, when it might fail for two main reasons: (1) it covers a low Mw range of separation and (2) analysis conditions are rigid and separation method is very sensitive to parameters such as pH, ionic strength and type of anion and cation of the carrier solution.

It is a matter of fact that Asymmetric Flow Field-Flow Fractionation (AF4) and Hollow Fiber Flow Field-Flow Fractionation (HF5) have both separation range far away broader than SEC and analysis conditions are much more flexible. For this reasons the scientific community is starting to propose AF4 and HF5, if not the promised next golden standard, at least a valuable and effective complementary technique to SEC. However, it is necessary to distinguish between the flexibility and wide applicability of FFF, from the costs related to this flexibility. As an example it is true that almost every carrier solution can be used as mobile phase since the FFF channel is simply empty and separation relies on physical principles rather than on chemical interactions. But on the other hand, like it happens in SEC, sometime there are only few buffers, pH or ionic strengths that allow for a proper separation. Therefore the FFF flexibility in daily use is sometime lower than a

theoretical speculation would suggest. However, for niche applications it is still true that FFF offers interesting features, which can be used to investigate complex issues.

In my thesis, I propose Asymmetrical Flow Field-Flow Fractionation iphenated with Multiangle light Scattering (MALS), Differential Refractive Index (DRI) and UV-Vis detection as analytical platform to determine particle size distribution and gain a deep characterization of nanoparticles in dispersion. AF4 is a separation technique consisting in the size separation according to the hydrodynamic radius of the analytes, while MALS coupled with DRI and/or UV-Vis detection allow for the independent determination of the radius of gyration or root means square radius (r_g or RMS) and molecular mass (M_w) of the analytes.

Its uses are applied to different samples with the purpose to address some specific issues. In particular Section 2 is focused on the field of liposomal technologies: it aims to discuss in depth that several technique are today used for the size and morphological characterization of lipidic vesicles (Chapter 3), but despite liposomal technologies were introduced decades ago, still today the analytical challenges they put on the table suffer the lack of a size based separation and characterization technique, applicable in a wide series of dispersing medium, and able to provide deep insight both on morphological or structural aspects and into functional aspect of liposomes. Chapter 4 is devoted to the investigation of the particle size distribution and aggregates formation of liposomes dispersed in different medium, while in Chapter 5 the functional features of a liposomal drug vector in terms of its biological and physical interaction with blood serum components is put into the spotlight. A deep and comprehensive approach to understand the behavior of lipid vesicles in terms of drug release and fusion/interaction with other biological affine species is described, together with weaknesses and strength of the developed method.

Section 3 contains two chapters both devoted to the rapid screening and fast dimensional characterization of functional nanoparticles. Chapter 6 is focused in particular on the size

characterization and size stability of a new generation of metastable drug vectors: the Metal Organic Frameworks. The conjugation of the vector with various azidothymidine analogues in evaluated, together with size and size stability of particles. Chapter 7 shows that it is possible to successfully use HF5-ICP-MS for the rapid screening of the presence of nanoparticles in samples of tattoo inks. This chapter, rather than describe a deep and comprehensive characterization, aims to show that with few steps it is possible to gain qualitative information on the content of metallic particulate in the sample.

Section 1: The Flow Field-Flow Fractionation Technique

Chapter 1 – Field-Flow Fractionation

1.1 – Introduction on FFF: nature, mechanism and operational modes

Field-flow fractionation (FFF) is a family of flexible elution techniques capable of simultaneous separation and measurement. Its sample domain extends across a broad macromolecular-colloidal-particulate continuum from about 1 nanometer to more than 100 micrometers [5].

These techniques are based on the action of two fields: separation is achieved through a laminar flow of mobile phase and a perpendicular force-field, as illustrate in Figure 1.

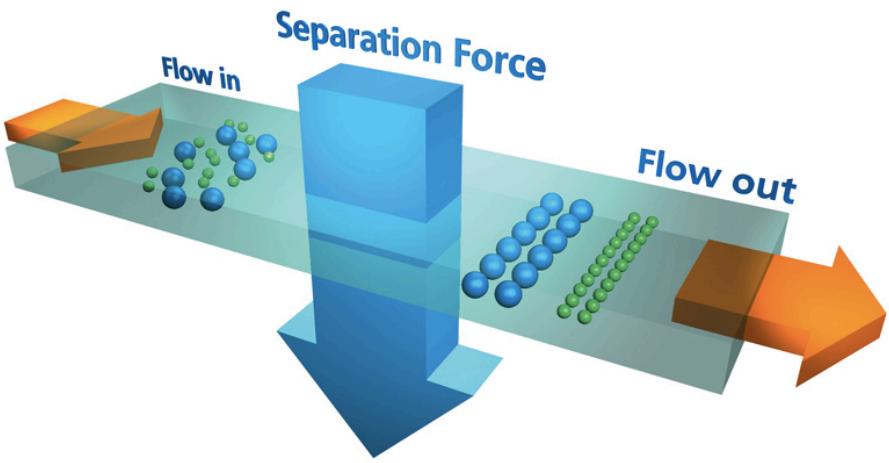

Figure 1: FFF works in the basis of the action of two perpendicular fileds.

FFF sub-techniques are distinguished and classified according to the great number and type of applicable force-field: FFF is therefore extraordinarily versatile.

The most common sub-techniques and the corresponding force-field are listed in Table 1.

Field type	Technique
Cross-flow (Fl)	Flow FFF (FlFFF)
	Hollow – fiber (FlFFF)
Sedimentation (Sd)	Sedimentation FFF (SdFFF)
	Centrifugal (SdFFF)
	Gravitational FFF (GrFFF)
Thermal (Th)	Thermal FFF (ThFFF)
Electrical (El)	Electrical FFF (ElFFF)
Magnetic (Mg)	Magnetic FFF (MgFFF)
Dielectric (Dl)	Dielectric FFF (DlFFF)

Table 1: applicable Force-field and corresponding FFF techniques.

An FFF system is composed by an empty channel with at least one capillary dimesion: this makes FFF a soft fractionation technique, highly biocompatible and suitable for samples of biological interest [6, 7].

Once injected in the separation channel, analytes take position across a laminar flow, whose profile is parabolic, with maximum velocity in the channel center and minimum close to channel wall. This position determines many important parameters, such as selectivity, efficiency and others. Most of all the elution order and the two possible operational mode in FFF, namely normal mode and Steric-Hyperlayer, are determined:

(1) Normal mode: analytes are pushed by the field toward the lower potential wall, the accumulation wall, and their local concentration increases with decreasing distance from the wall itself. A concentration gradient is then created, and it promotes a diffusive transport which opposes the transport generated by the external force-field. When both are

balanced, the sample reaches a position of dynamic equilibrium with a determined distance from the accumulation wall. According to this distance analytes penetrates the parabolic flow profile and exerience different flow velocity and separation occurs.

(2) Steric-Hyperlayer mode: for micrometric particles, the diffusive transport opposing the force-filed is negligible. Therefore particles originate a layer whose tickness depends on the size of the particles themselves. Larger particles forme thicker layers and penetrates into regions of the parabolic flow profile of higher speeds, and are eluted faster. During elution, the movement of particles towards the accumulation wall is balanced by the so-called lift-forces, which are induced by the mobile phase flow. Therefore the larger the particles the earlier they elute.

1.2 – Flow Field-Flow Fractionation

Flow Field-Flow fractionation (FlFFF) is in absolute the most diffuse and versatile FFF technique. The separation is obtained as a combination of a parabolic flow and perpendicular flow (cross-flow) of carrier solution, the latter constitutes the external force-field. Asymmetric Flow Field-Flow Fractionation (AF4) and Hollow Fiber Flow Field-Flow Fractionation are the FlFFF technique who experienced the main success and development, they are in fact the widest used among commercially available FFF techniques.

Separation results from the application of a flow stream of carrier within a capillary channel together with a perpendicular, hydrodynamic flow. Since the separations depends only upon the carrier flows applied, because of the lack of a packed stationary phase and since no chemical interactions or shear stress/degradation mechanism are involved, AF4 has a unique gentle separation mechanism: issues like shear forces or particle alteration are

therefore avoided. Furthermore analyses are feasible in a wide series of dispersing medium.

The separation device is a flat channel with a trapezoidal shape and capillary height, as shown in Figure 2.

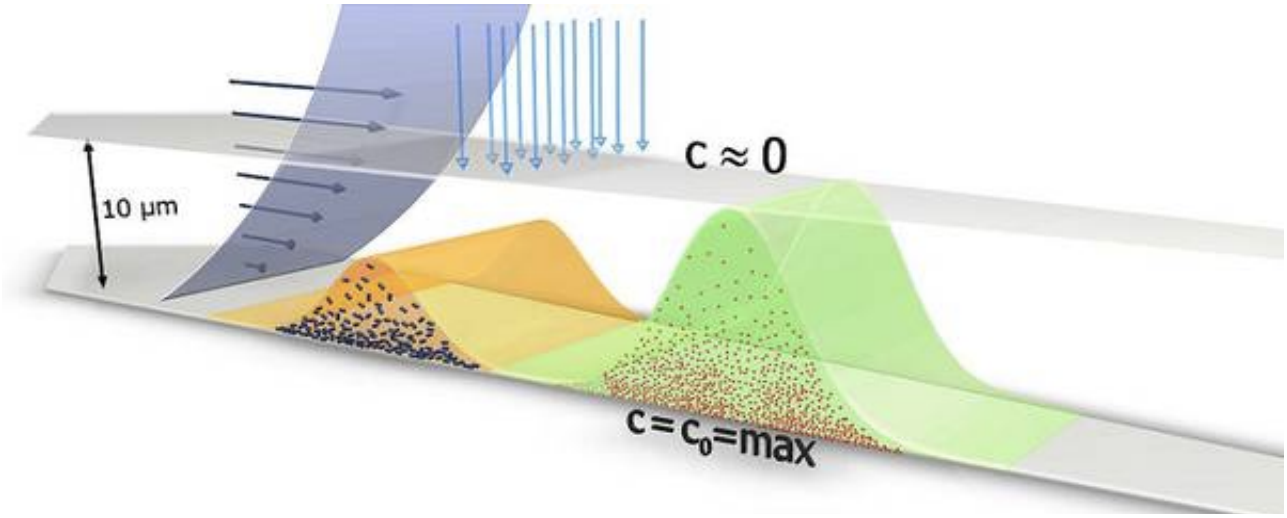

Figure 2: AF4 channel

For the sample analysis, particles are at first introduced in the channel and a focussing step takes place by applying two opposing streams of carrier, allowing the sample to concentrate on a narrow band. When the elution starts, a stream of carrier drives particles toward the channel, while the perpendicular hydrodynamic field is applied, as indicated by dark blue arrows and light blue arrows in Figure 2. This causes the particles to be driven toward the accumulation wall (the inferior surface of the channel), and their concentration to builds up against the wall. A concentration gradient is therefore created, and causes the particles to diffuse away from the wall because of an opposing, diffusive flux. Different particles form layers of different thicknesses, and the greater the thickness the higher the elevation at which the cloud of particle travel along the channel because and penetrates into a faster streamline of the parabolic flow profile. Therefore, in AF4 retention times of particles are inversely proportional to their diffusion coefficient (D), and directly proportional to the hydrodynamic diameter [8]. A pump generates the two perpendicular

flows by splitting the longitudinal flow, into a second one (the cross-flow) across the accumulation wall (the only permeable wall of the channel).

1.3 – Asymmetric Flow Field-Flow Fractionation (AF4)

In normal mode AF4, analytes concentration as a function of the distance from the accumulation wall, *c(x),* depends upon the forces generated by the cross-flow stream (first term of equation 1) and the opposite, duffusive flux (second term of equation 1):

$$J_x = u(x)c(x) - D\frac{dc(x)}{dx} = 0 \qquad (1)$$

From equation 1 the expression for *c(x)* can be obtained:

$$c = c_0 \exp\left[\frac{-|u(x)|}{D}\left(1 - \frac{x^2}{w^2} + \frac{x^3}{2w^3}\right)\right] \qquad (2)$$

Where c_o is the analyte concentration at *x*=0, that is close o the accumulation wall, as indicated in Figure 2.

The ratio $D/u(x)$ is expressed as l, it represents the mean distance from the accumulation wall and. The retention parameter λ depends upon l:

$$\lambda = \frac{l}{w} = \frac{D}{|u(0)|w} \qquad (3)$$

In FFF theory there is an equation relating λ *and R*, the approximated form is:

$$R \cong 6\lambda \tag{4}$$

The retention parameter can be obtained from experimentally, it is in fact the ratio between t_0 (void time) and t_r (retention time):

$$R = \frac{t_0}{t_r} \tag{5}$$

Both t_0 and t_r can readly be calculated, according to the following two equations:

$$t_0 = \frac{V^0}{V_C} \ln\left\{1 + \frac{V_C}{V_{out}}\left[1 - \frac{w}{V^0}\left(b_0 z' - \frac{b_0 - b_L}{2L} z'^2 - y\right)\right]\right\} \tag{6}$$

$$t_r = \frac{V^0}{V_C} \frac{|u_0| w}{6D} \ln\left\{1 + \frac{V_C}{V_{out}}\left[1 - \frac{w}{V^0}\left(b_0 z' - \frac{b_0 - b_L}{2L} z'^2 - y\right)\right]\right\} \tag{7}$$

where V_0 is the void volume, V_c and V_{out} are the velocities of longitudinal and cross-flow, respectively. Equation 7 is of capital importance since it highlights the proportionality between retention time and diffusivity of particles, since both t_r and D appear. On the other hand, the Stokes-Einstein equation relates the diffusion coefficient D to the hydrodynamic diameter *d* of particles:

$$D = \frac{KT}{3\pi\eta d} \tag{8}$$

For this reason in AF4 it is usually reported that the retention time is inversely proportional to the diffusion coefficient and proportional to the hydrodynamic radius of particles:

$$t_r \propto \frac{1}{D} \qquad\qquad t_r \propto d_h$$

The following equation explicits the raltionship between t_r and the hydrodynamic diameter of the eluted species, that can be directly calculated from the experimental retention time value:

$$r_h = \frac{2kTV_0}{\pi\eta V_c w^2 t_0} t_r \qquad (9)$$

1.4 – Hollow Fiber Flow Field-Flow Fractionation

Historically AF4 has been the first FIFFF technique commercially available. However in the recent years another technique has gained increasing interest: the Hollow Fiber Flow-Field Flow Fractionation (HF5).

HF5 is based on the same principles of AF4 for the size-based separation of colloids so that the same sequence steps is shared in both techniques: sample injection, sample focusing and relaxation, sample elution with an external field generated by a stream of carrier solution. Also sample separation modes are the same and governed from the same principles: diffusive flux in normal mode, and steric volume of particles together with lift forces in steric hyperlayer mode. The main difference is due to the geometry of the separation device: in HF5 it is a cylindrical, empty channel, rather than a trapezoidal , flat one.

The retention ratio is expressed according to the following equation:

$$R = \frac{t_0}{t_r} \cong \frac{4D}{Ur_f} \qquad (10)$$

Because channel volume in HF5 is tens of time lower compared to that of AF4, it allows for channel miniaturization. This is a key feature because some key advantages were achieved with HF5: lower sample dilution that leads to lower detection limit and higher sensitivities, lower mobile phase consumption. Also detector flow is lower, a feature which makes HF5 the elective FlFFF technique for the on-line coupling with MS. Furthermore channels are more easy to handle and disposable: for application in biochemistry problems like run to run carry over and sterility are with HF5 fixed.

Chapter 2 – Detection in FFF

2.1 - Introduction

Once analytes are separated a detector is required to determine when the sample is eluted. Detection in FFF can be performed both off-line and on-line. In the first case the eluate is collected for subsequent analyses. When performed on-line, one or multiple detectors are placed after the separation system, virtually with no limitation on the number. The most common detectors are UV-Vis, Refractive Index (RI), fluorescence (FL) and Multi Angle Light Scattering (MALS) detectors; furthermore, increasing application of FFF on-line coupled with MS, especially ICP-MS are now available on the literature. Some limitations are still to be overcome for the coupling with other ionization source; up to now the main problems are (1) the high salt concentration required for separation which suppress ionization; and (2) the high detector flow that introduces technical issue to be fixed for the correct working of the FFF-MS systems.

2.2 - UV/Vis Spectrophotometry

UV-Vis detection is widely used for the characterization of colloids. It is relatively cheap, quite easy to handle and the on-line coupling with FFF apparatus easy. It allows for the characterization of the spectroscopic features of samples, and this is very interesting because often colloids have size dependent properties, that can be investigated.

The major drawback of UV-Vis detection is that it is a concentration detector, and for an optimal use signal should be proportional only to the concentration of analytes. However, when the sample is a colloid, the bigger the particles the more signal is generated because of scattering of photons rather than to absorption. As a consequence, sample quantification is not straightforward because the UV signal is actually a turbidimetric measure. The sensitivity varies according to particles size, with consequent underestimation of the population of bigger particles. The more particle size approaches detection wavelength the more this phenomenon affects the measurement.

2.3 – Differential Refractive index (DRI) detection

DRI detectors experienced a great success in colloid characterization because they are the best choice for dissolved polymers, especially when separated with SEC columns. When analysing narrowly dispersed samples, DRI signal can be converted directly to a concentration profile, but with increasing sample polidispersity this holds not always true: signal response is proportional not only to particle concentration but also to particle size. For these reasons RI detection experiences the same limitation of UV-Vis detection. Furthermore DRI detectors require the pressure of the separation system quite stable. It is the case of SEC whose methods are nothing more than a single step of isocratic flow and isocratic mobile fase. On the contrary, AF4 methods often require flow gradients to separate particles in a reasonable time, causing pressure drifts or progressive pressure drops in the DRI cell, making this detection technique hardly applicable.

2.4 – Light Scattering

Light scattering (LS) methods are broadly used for the size analysis of colloids. LS is a non-destructive technique, it is widely used both in batch mode and on-line coupled with separation techniques, such as SEC and FFF. This configuration allows at first to size separate particles and then to analyse a series of ideally mono-dispersed slices of sample, so that the information content is higher than in the case of a batch mode analysis whose result in terms of particle size would be just a mean.

Dynamic light scattering (DLS) is often coupled with FFF, it measures the diffusivity of samples by processing the interference profile decays generated by particles in brownian motion. Diffusivity is then turned into the hydrodynamic radius of particles through the Stokes-Einstein equation. DLS is easy to couple with FFF systems, however its use is sometime limited. It is a matter of fact that for a good DLS experiment, measurement time should be at least some tens the time that interference profiles takes to completely decay.

As a consequence detector flow in FFF has to be tuned according to the DLS need to detect particle for a sufficient time, which is a severe complication during FFF method development and experiments. Bigger particles take more time to decay, so that for example it is easy to correctly characterize few nanometres proteins, but hard to characterize tens or hundreds nanometres radius nanoparticles. Such a procedure is particularly time consuming when nothing but decrease elution flow can be done.

Multiangle light scattering was first coupled with FFF during the 90s [9]. The theory on size and mass calculation based on static light scattering has been extensively explained. Briefly, when refractive index increment (dn/dc) and sample concentration are known, MALS can provide Mw while, independently from concentration or other sample specification and without assumption on particle conformation or shape, it provides the root mean square (RMS) radius, which represents the mass-averaged distance of each mass element of the NP from its centre of gravity.

MALS detection does not require any calibration step, in this sense it is an absolute method: particle size and Mw are computed by using the physical phenomenon of scattering that occurs when a colloidal sample is illuminated by photons. A MALS detector has multiple diodes arranged around the sample cell so that the angular intensity of scattered light is measured as a function of angle. The Zimm formalism [10] relates these quantities trough the following equation:

$$\frac{K^{*}c}{R(\theta,c)} = \frac{1}{M_{w}P(\theta)} + 2A_{2}c \qquad (11)$$

where $R(\theta,c)$ is the excess Rayleigh ratio of the solution and depends from the scattering angle θ and concentration c; M_w is the weight-averaged solute molar mass; A_2 is the second virial coefficient in the virial expansion of the osmotic pressure, while K^* is a

constant. *P*(θ) describes the angular dependence of the scattered light, and is related to the rms radius. The expansion of *P*(θ) to first order gives:

$$P(\theta) \approx 1 - \frac{16\pi^2 n_0^2}{3\lambda_0^2}\left\langle r_g^2 \right\rangle \sin^2\frac{\theta}{2} \qquad (12)$$

where r_g is the RMS radius.

If a sample is very diluted and its concentration tends to zero ($c \rightarrow 0$), the second term of eq. 10 can be neglected, and the quantity directly measured from every diode in the MALS cell, *R(θ)* is directly proportional to M_w:

$$\frac{R(\theta,c)}{K^* c} = M_w P(\theta) \qquad (13)$$

Combination of eq. 12 with eq. 13 results in eq. 14, which shows that by plotting $\frac{R(\theta,c)}{k^* c}$ as a function of $sin^2(\theta/2)$, the result is a series of point that upon linear regression give a curve with slope equal to r_g and intercept equal to M_w:

$$\frac{R(\theta,c)}{K^* c} = M_w - \frac{16\pi^2 n_0^2}{3\lambda_0^2} M_w \left\langle r_g^2 \right\rangle \sin^2\frac{\theta}{2} \qquad (14)$$

If both Mw and RMS radius distributions are known, particle shape and density information are accessible (deriving from the Mw to RMS ratio). MALS detection is applicable in the range 10 nm – 1 μm, and since scattering intensity increases with particle size, the bigger the former the higher the sensitivity.

Section 2: FlFFF to address challenges in liposome technology

Chapter 3 – Liposome characterization

3.1 – Liposomes

Liposomes and phospholipid vesicles are composed of one or multiple double layers of lipids or phospholipods that surround an aqueous core [11]. They form spontaneously upon mechanical agitation of an aqueous solvent and lipids. The size of liposomes may vary from tens of nanometers to tens of micrometers, and they can be unilamellar or multilamellar according to the number of lipid bilayers. It is a common practice to classify liposomes as a function of these characteristics, the three main classes are:

- SUVs (Small Unilamellar Vesicles), for particle size smaller than 100 nm;
- LUV (Large Unilamellar Vesicles), for particle size in the range 100 - 800 nm,
- MLVs (Multilamellar Vesicles), for micrometer sized particles.

Several techniques are nowadays available for liposome synthesis. MLV dispersions can be obtained by rehydration of a lipid film, sonication of this dispersion leads to the formation of SUVs [12], which may also be obtained by extrusion through filters of suitable porosity [13, 14], or by high pressure homogenisation [15]. LUV can be prepared using techniques suche as detergent removal from a dispersion of micelles [16] or by reverse phase evaporation [17].

Liposomes are interesting for their ability to incorporate both hydrophilic compounds (in the aqueous core), as well as lipophilic or amphiphilic compounds (in the lipid membrane) [18]. As drug vector devices liposomes have high versatility, thanks to their structure, to their biocompatibility, to the wide choice of phospholipid compositions, and last but not least thanks to the use of additives such as cholesterol or species able to target their fate, like antibody or proteins [19, 20]. A number of liposomal formulations are undergoing clinical trials for FDA approval, or have already been approved (AmBisome ® - Amphothericin B; Doxil ® / Caelyx ® - doxorubicin; and DaunoXome ® - daunorubicin, to report some examples).

3.2 – Morphological and functional characterization of liposomes

Monitor the size and size distribution of liposomes is crucial because of several aspects. First of all, during manufacturing processes PSD provides important information on preparation techniques and for process optimization, from the small-scale synthesis to the industrial scale-up.

Furthermore, particle size affects physical stability of liposomes, since phenomenon like fusion of vesicles of small size or aggregation of MLVs are common.

Most of all, PSD is important on the context of the applications in medicine and drug delivery. Size and structure tune the ability to incorporate or encapsulate pharmaceutical compounds: while for lipophilic and amphiphilic compounds high ratios between membrane thickness and core volumes is required, the opposite is for hydrophilic drugs, as shown in Figure 3.

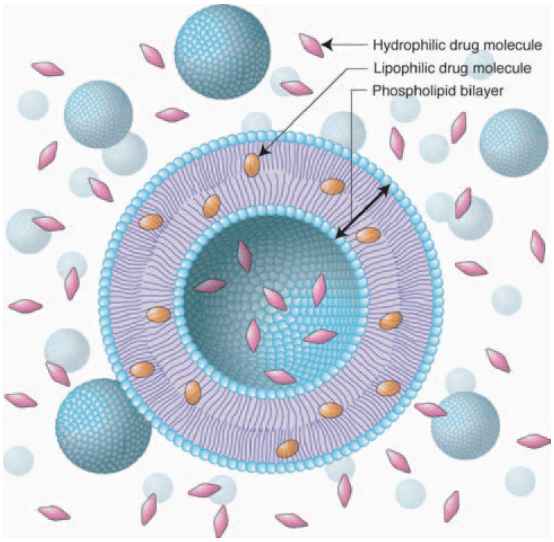

Figure 3: Liposome incorporating lipophilic drug in the lipid bilayer and hydrophilic drug in the aqueous core

Vectorization of chemotherapeutic agents is one of the main application of liposomes as drug carriers, because of the great number of advantages of this formulation:

(1) protection of chemotherapeutic agents from metabolism and degradation during circulation in the blood stream;

(2) administration of poorly soluble agents;

(3) administration of high doses limiting toxic effects;

(4) high local concentration of the drugs in the target site.

Both particle size and PSD determine the fate of liposomes: parenchymal cells of the liver absorb small size vesicles with radius up to 70 nm, while liposomes larger than 300 nm accumulate in the spleen. PSD affects bio-distribution [21], as an example cancerous tissues have a very high permeability according to particle size: a cut-off of 400 - 600 nm was determined for liposomes which penetrate through the tumour cells.

3.3 – Common techniques for liposome characterization

Despite a wide choice of techniques is available for liposome characterization, up to now no analytical techniques have been established for separation and particle size distribution analysis of liposomes, especially when the broad size range of liposomes has to be covered and characterization in the dispersing medium is required. These aspects are discussed in the next sections.

3.3.1 – Microscopy techniques

Scanning electron microscopy (SEM) and transmission electron microscopy (TEM) are often used, since they allow for a direct observation of vesicles. However, sample preparation is labour intensive, negative staining and high vacuum analysis conditions are required. Moreover, drying procedures may induce conformational changes of vesicles, thus limiting the applicability of these techniques to liposome observation in their native state [22]. Environmentally Scanning Electron Microscopy (ESEM), is also used because of the possibility to observe wet systems without conductive coating, but detailed information about surface and architecture of vesicles, observable with TEM or SEM, are lost [23]. Cryo-TEM allows for a direct observation of colloids in the vitrified frozen hydrate state, thus very close to the native state of samples. Information about size, shape, lamellarity, tridimensional structure of single lipid vesicles are accessible. Sample preparation is relatively fast compared to other microscopy techniques, however it is quite critical for fragile particles like liposomes, because of the possibility to generate and observe artefacts due to the freezing and drying processes that induce morphological changes or rearrangements of the particle structure. Cryo-TEM is therefore an useful tool to investigate specific structural aspects of particles [24] rather than PSD.

Altogether, this holds true for microscopy techniques (with the exception of ESEM): they are not able to analyse vesicles in the dispersing medium and do not provide PSD

measurements unless a relevant number of observation are performed to have statistical significant data.

3.3.2 – Atomic force microscopy

Atomic Force Microscopy (AFM) is one of a number of scanning probe microscopy techniques that image a sample surface with a sharp tip or probe. Several papers have been published on the characterization of liposomes and on the investigation of specific issues [25] [26]. For the analysis liposomes are immobilized onto a smooth surface and then scanned by the AFM tips. On a comprehensive study on the use of AFM for liposome characterization [25] it was demonstrated that this technique could be suitable for the analysis of liposome size, but some problems were highlighted. Analysis on dispersion is possible only immediately after sample deposition because medium evaporation cause vesicles rearrangements in less than 10 minutes, liposomes are not stable once deposited on the mica surface [23] and, finally, it has been suggested to obtain images in the so called non-contact mode, otherwise, with tapping or contact mode deformations of lipid layers occur. Nevertheless even with non-contact mode some vesicle deformation or rearrangements were observed.

3.3.3 – Light Scattering techniques

Dynamic Light Scattering (DLS) is a widespread and well-established technique for PSD measurements [27-30]. Sample manipulation is easy and analysis fast, but in batch mode a DLS experiments provides relatively low information. When sample has wide and/or multimodal size distribution, PSD evaluation is limited or biased, restricting the DLS-based analysis to non-complex samples with narrow distribution. One way to get through this problem is to study the angular dependence of scattered light [31]. Such a LS-based technique is Multi Angle Light Scattering (MALS). Together with DLS, MALS represents

one of the few absolute methods for particle sizing and molar masses determination and it is able to work over a wide range without the use of any standard [10].

3.3.4 – Size-separation techniques

As already discussed in chapter the optimal use of LS based detection rely on the on-line coupling with size-separation techniques. By coupling SEC or FFF to LS detection it is possible to reduce sample complexity and to study of a series of ideally monodispersed slices of sample [32]. Size exclusion chromatography (SEC) and HPSEC have been applied for lipid vesicles separation. They are based on the same principle, i.e. size-dependent permeation of solubilized molecules or dispersed molecular aggregates through the gel. Liposomes elution is mainly related to their size and shape, however a series of other variables influence retention behaviour and recovery [33], among which flexibility or rigidity of bilayers. Liposomes interactions with the gel matrix are often observed, they derive from the chemical nature of the gel, the lipid bilayer composition and the encapsulated material (if any). Column pre-saturation has often found to be necessary [34, 35] and mechanical interactions or shear forces are likely to induce vesicle degradation or severe alteration of the original PSD of samples.

AF4 is extensively used for liposome characterizaiton [35-41]. Interesting features are the lack of a packed stationary phase and absence of chemical interactions or shear stress/degradation mechanism are involved: particle alteration is therefore avoided. Furthermore and analysis are feasible in a wide series of dispersing medium. However, sample carry-over is a possible issue, and membrane pre-saturation is often necessary.

Chapter 4 – Characterization of a lipidic dispersion for ophthalmic use

4.1 – Introduction

Emulsions of nanosized, phospholipid vesicles have shown able to restore the microenvironment of damaged ocular surfaces [42]. This chapter is focused on several aspects of the size characterization of a lipidic vesicle dispersion for ophthalmic use. The vesicles are constituted of an aqueous and a lipid phase. Main components of the lipid phase are the physiological constituents of the lachrymal fluid (phospholipids and medium-chain triglycerides). The lipid components have shown able to protect the ocular surface by forming a thin hydrophobic barrier that is similar to the lipid layer of the lachrymal film. It was demonstrated that exposure of cells to phospholipid vesicles may also result in unidirectional movement of cell cholesterol to the vesicles [43].

Possible uptake of cholesterol on phospholipid vesicles is of therapeutic relevance since biochemical studies have focused that the excess of intracellular cholesterol may inhibit cell proliferation [44]. The actual uptake level depends on the interaction of the vesicle lipid components with cholesterol. The uptake process likely involves aggregation/re-assembly of the phospholipid bilayer, which should be evaluated using a non-destructive technique for biophysical analysis of self-assembling colloidal structures.

As already stated PSD is a key feature of liposomes, since it affects a number of properties including *stability*, *drug encapsulation* and *bio-distribution*, with influence on therapeutic effects when drug-loaded liposomes are used.

In this work we propose an hyphenation of AF4 and MALS as a mature, efficient, and time saving technique for liposomes characterization, and to show its performances for the (a) characterization of vesicles in different osmolarity conditions of the carrier liquid in order to investigate its effect on PSD, and detection of aggregates when they form even in very low amounts; (b) evaluation of cholesterol uptake capability in different carriers in order to establish the vesicles reactivity with respect to the osmolarity of the dispersing medium: for

this purpose experiments in both pathologic and physiologic osmolarity condition were performed; (c) evaluation of cholesterol uptake upon spiking of vesicles with increasing cholesterol uptake.

4.2 – Materials and Methods

4.2.1 – Samples

Lipimix emulsions (Tubilux Pharma, Pomezia, Italy) were available on the market as formulations for ophthalmic use. They are constituted of an aqueous phase, and of a lipidic phase which components are the physiological constituents of the lachrymal fluid. The main components are: phospholipids, medium chain triglycerides, soybean oil, glycerin, α-tocopherol, and distilled water. Samples were stored at 4°C in the dark, as the manufacturer suggests.

All the samples were diluted 1:20 in carrier solution. Injection volume was set to 10 µL.

Carrier solution was phosphate buffer (salt purchased from Sigma Aldrich) at pH = 7.4 and different osmolarities (9, 19, 38, 75, 150 and 300 mOsm/L). Cholesterol was purchased from Biolabo, (as part of a chod-pap test kit).

4.2.2 – Instrumental setup

AF4-MALS analysis was performed by using a 1100 Series HPLC system (Agilent Technologies, Palo Alto, CA), connected to a control module to control AF4 flow rates and operations (Eclipse 3, Wyatt Technology Europe, Dernbach, Germany). Detection was performed by a MALS DAWN HELEOS detector (Wyatt Technology Corporation, Santa Barbara, CA). Carrier solutions were degassed using an on-line vacuum degasser Agilent, 1100 series (Agilent Technologies).

The separation device was a 265 mm long channel (Wyatt Technology Europe), equipped with regenerated cellulose membrane (Nadir) with a molecular weight cut-off of 10 kDa. The channel spacer was 250 µm tick, with trapezoidal shape (upstream width b_0 = 16 mm; downstream width b_L = 4 mm).

Figure 4 reports the flow program used for vesicles fractionation.

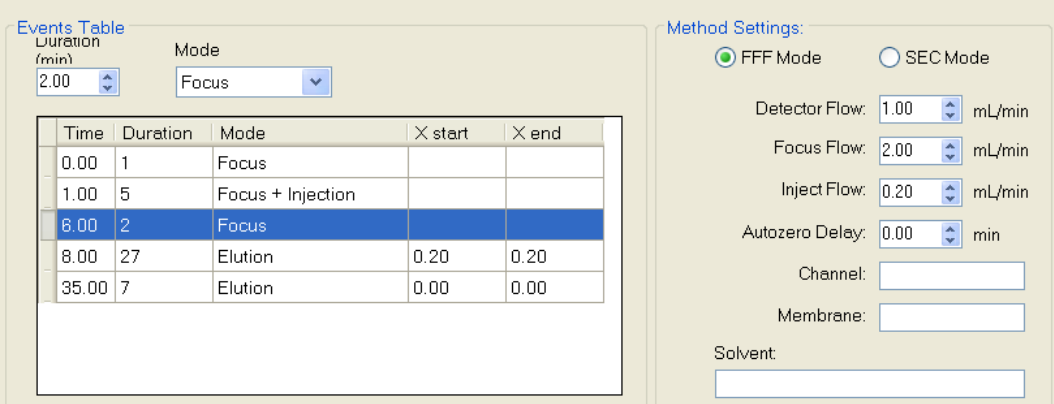

Figure 4: Flow program for the fractionation of liposomes

In details the following steps constitutes the flow program: 1 minute focus flow (2 mL/min) was applied to equilibrate the flows. Than 5 minutes injection (at a flow rate of 0.2 mL/min) in focus mode were applied in order to allow the sample to reach the channel, and two further minutes of focus were used to allow for a complete relaxation. After the focus step the elution starts. Detector flow had been set to 1 mL/min, while a constant perpendicular hydrodynamic field of 0.2 mL/min, namely the cross flow, was applied.

4.3 – Results & Discussion

4.3.1 – Lipimix in different carrier solutions

Figure 5 reports the LS fractograms of Lipimix. Samples were prepared by dilution of vesicles 1:20 in mediums of different osmolarity (respectively 9 mOsm/L; 19 mOsm/L; 38 mOsm/L; 75 mOsm/L; 150 mOsm/L; 300 mOsm/L), while fractograms were obtained by elution of each sample using as carrier the same medium in which vesicles were diluted. Salt composition was kept constant, while salt osmolarity varied. Laser Scattering signals were recorded at 18 different angles of the MALS detector, and relative scattering intensities at 90 degrees are reported.

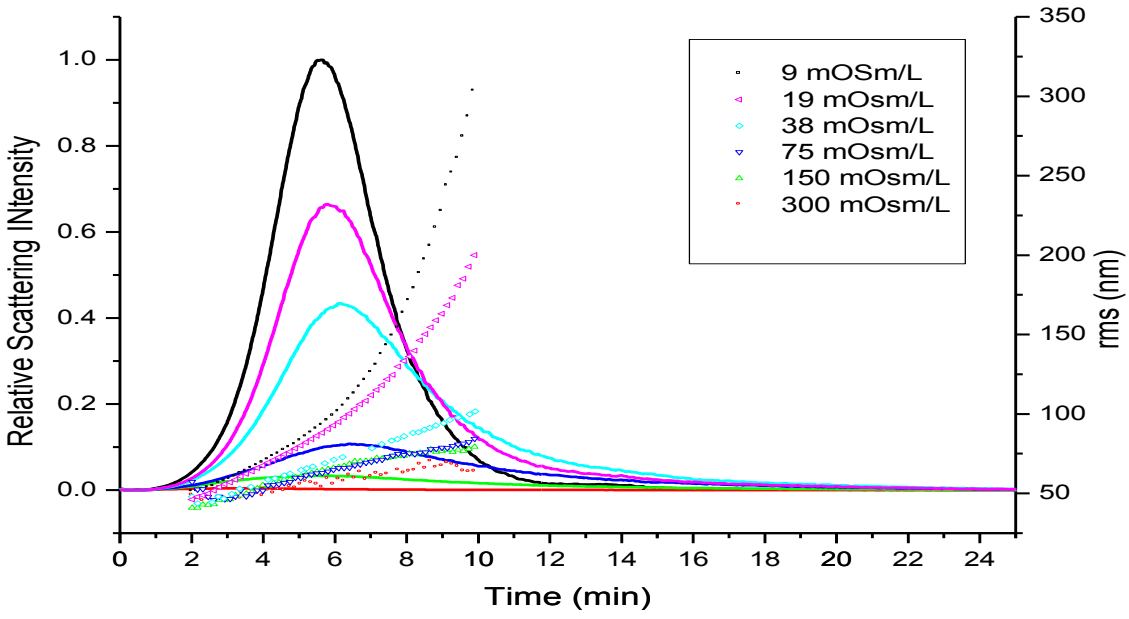

Figure 5: Full lines: LS traces @ 90° of Lipimixeluted in different osmolarity conditions (9, 19, 38, 75, 150, 300 mOsm/L); Empty squares: RMS radii (nm).

As already explained in chapter 2.4, it is possible to retrieve the RMS distribution in correspondence of the peaks directly from the profile of scattering intensity. RMS radii traces are represented as squares in Figure 5 and PSD are reported in Table 2.

Osm/L ($\cdot 10^{-3}$)	RMS (nm)	tr (min)
9	50 – 350	5.6
19	50 – 200	5.8
38	50 – 100	6.1
75	50 – 80	6.4
150	50 – 75	5.8
300	50 – 60	3.3

Table 2: RMS radius and retention times of Lipimix diluted and run in different carriers

As it can be seen, with decreasing osmolarity there is a change in particle size distribution: in 9 mOsm/L carrier the particle radius span from about 50 nm to 350 nm, the range becomes narrower with increasing osmolarity so that it is 50 nm to 75 nm for 300 mOsm/L carrier solution. It is clear that particle size of the vesicles is influenced from the carrier solution, and it increase with decreasing osmolarity. This can be due to potential aggregation/reassembling of particles.

It can be observed that there is a difference in retention time with decreasing nanoparticles RMS radius when the osmolarity of the carrier solution decreases from 75 mOsm/L to 9 mOsm/L. This is not consistent with retention theory since elution time is proportional to D^{-1} (the diffusion coefficient) and D is proportional to r^{-1} (with r hydrodynamic particle radius), that is, the smaller the hydrodynamic radius of the particle the earlier it elutes. By comparing the ionic strength of each eluted sample, it can be noticed that the higher the ionic strength the higher the retention time. It is known and fully accepted that ionic strength plays an important role in FFF, and it is of particular relevance when one consider the migration of charged particles (as phospholipid nanovesicles are) in proximity of the

accumulation wall. Particles at low ionic strength elutes relatively far away from the accumulation wall compared to those eluted on higher ionic strength. In the first case a decrease of the electric double layer is responsible for the particle to closer approach the accumulation wall, while at low ionic strength the opposite occur because of an increased electric double layer. For this reasons the velocity of migration is different because different is the interaction with the longitudinal, hydrodynamic field. However it is not clear why 150 mOsm/L and 300 mOsm/L did not join this trend.

4.3.2 – Lipimix in different carrier solutions

A qualitative but smart method for the detection of small quantities of aggregates is the observation of LS fractograms recorded at low angles. The MALS detector records the scattering intensities at 18 different angles with respect to the laser beam source. It is known that the scattering intensity at each angle of detection is proportional to the mass concentration of sample and to the RMS radius of the particles. The concentration of sample has the same contribution at every angle (there is not angular dependence of scattering intensity from concentration). But this holds not true for particle size when the scattering is not isotropic. In this case, the higher the RMS radius, the more the photons are scattered on the opposite side of the laser beam source, that means, according to the scattering theory reference axis, at small angles. As a consequence, observing the fractograms at lower and lower angles, the contribution of particle size to the intensity of LS signal gradually increases. For this reason it becomes easier to appreciate the presence of aggregated/reassembled particles, even when they are present in a very low amount.

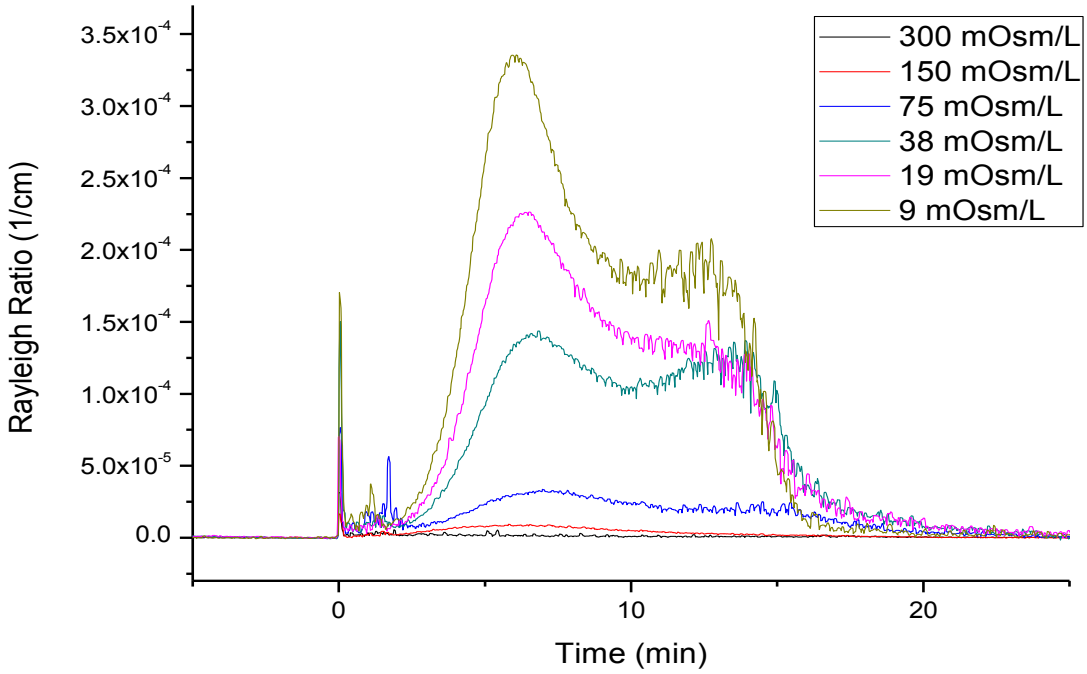

Figure 6: Rayleigh Ratio @ 14.45° for Lipimix in different carriers

In Figure 6 the scattering patterns of Lipimix at 14.45° in different osmolarity are reported: in 300 mOsm/L carrier there is a broad and noisy band, and it is even not possible to identify any peak, and the same is observed for 150 mOsm/L carrier. In 75 mOsm/L carrier the profile is different and constituted by a first band, followed by a second, less intense band, at higher retention time. In 19 mOsm/L and 9 mOsm/L carriers, patterns definitely show the presence of a second band.

This observation, together with the already discussed change in RMS radius distribution showed in Table 2, suggests a conformational change of vesicles that can be ascribed to the change in osmolarity of the mobile phase.

4.3.3 – Uptake of cholesterol in different osmolarity conditions

We also investigated the possibility of unidirectional movement of cholesterol from the dispersing medium to the lipid bilayer of the Lipimix nanovesicles. For this aim six samples were prepared: two vials of Lipimix diluted 1:20 in 2.7, 300, 316 mOsm/L carrier

solution. Injection volume was set to 10 µL. The choice of such carriers was done to investigate the uptake of cholesterol in different conditions: 316 mOsm/L is the osmolarity associated to the so called dry eye disease; 300 mOsm/L is the normal eye osmolarity, while there are not studies reporting hypo-osmolarity conditions of the human eye. To one of every couple of vials an aliquot of cholesterol was added, so that the injections corresponded to 10 µL of Lipimix 1:20 in carrier solution + 200 ng of cholesterol.

Three couples of fractograms are reported in Figure 7A, B and C, each one corresponding to the injection of Lipimix as it is and to Lipimix after the addition of cholesterol.

With 2.7 mOsm carrier solution there is clear change in particle size, with radii spanning from 56 nm to 314 nm before uptake and 108 nm to 300 nm after uptake. This suggests an actual cholesterol uptake. As for 300 mOsm/L carrier solution the dispersion span 45 nm to 60 nm before uptake and the particle size increase to 65 – 90 nm after uptake. Finally, looking at the 316 mOsm/L fractograms it can be noted that the RMS traces span the interval of 50 – 120 nm before uptake and 60 – 150 nm after uptake.

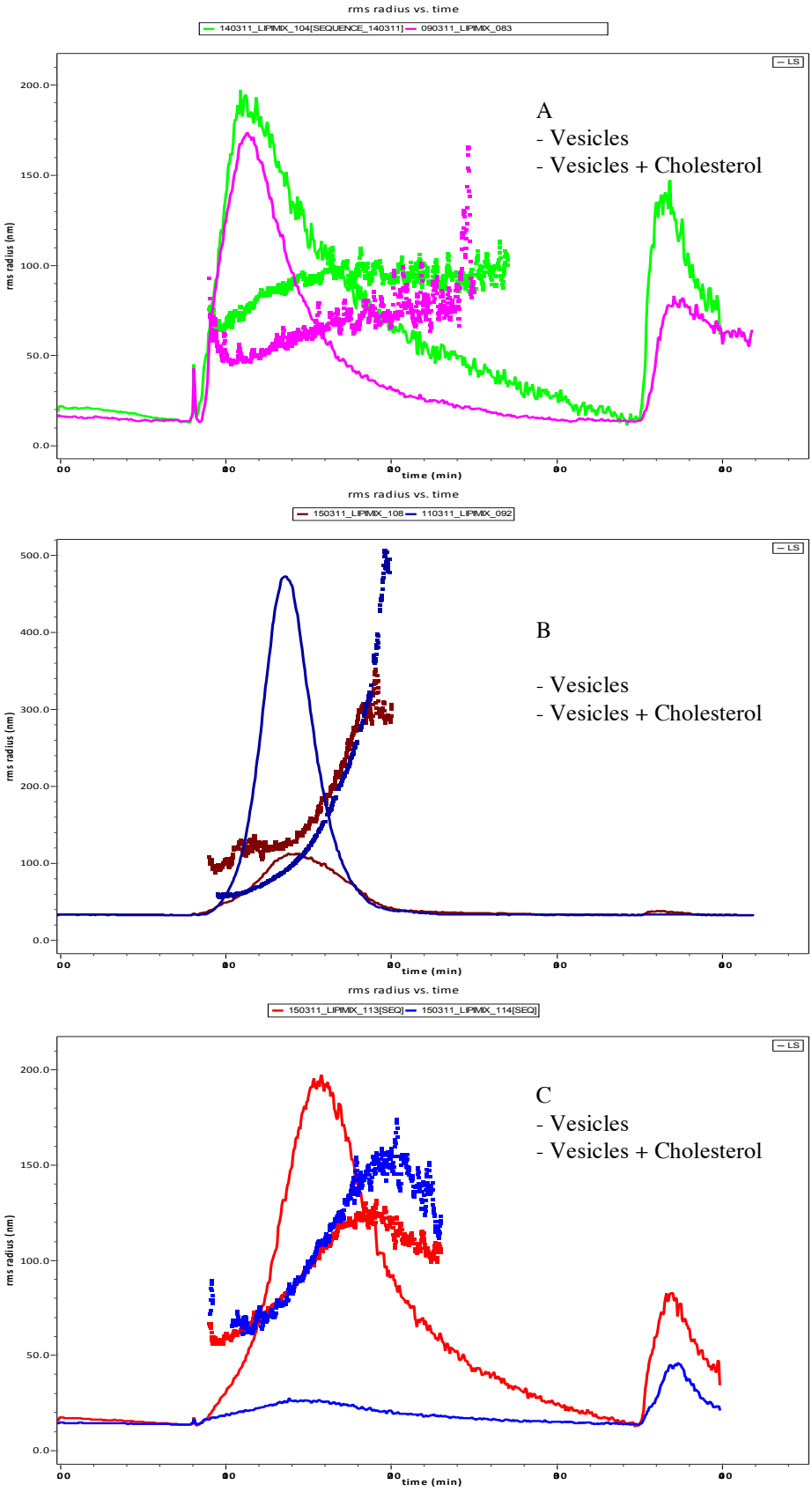

Figure 7: LS traces at 90° of lipimix vs lipimix + 200 ng cholesterol, in (A) 300 mOsm/L Carrier; (B) 2.7 mOsm/L carrier; and (C) 316 mOsm/L carrier

4.3.4 – Uptake of increasing amount of cholesterol 300 mOsm carrier

In the last part of this work we studied the ability of vesicles to interact with increasing amount of cholesterol, together with the ability of the technique to detect particle size changes even when the added cholesterol is low (compared to the 200 ng reported in the previous section). 300 mOsm/L carrier solution was chosen as it is the physiologic osmolarity on the ocular surface. Vesicles where diluted 1:20 in carrier and than an aliquot of cholesterol was added in the vial, so that for an injection volume of 10 µL the injected amount was 10 µL of limpimix 1:20 + 25 ng of cholesterol and 100 ng of cholesterol.

As it can be seen in Figure 8 with 25 ng of cholesterol particle size increase, the effect is more evident with 100 ng of cholesterol.

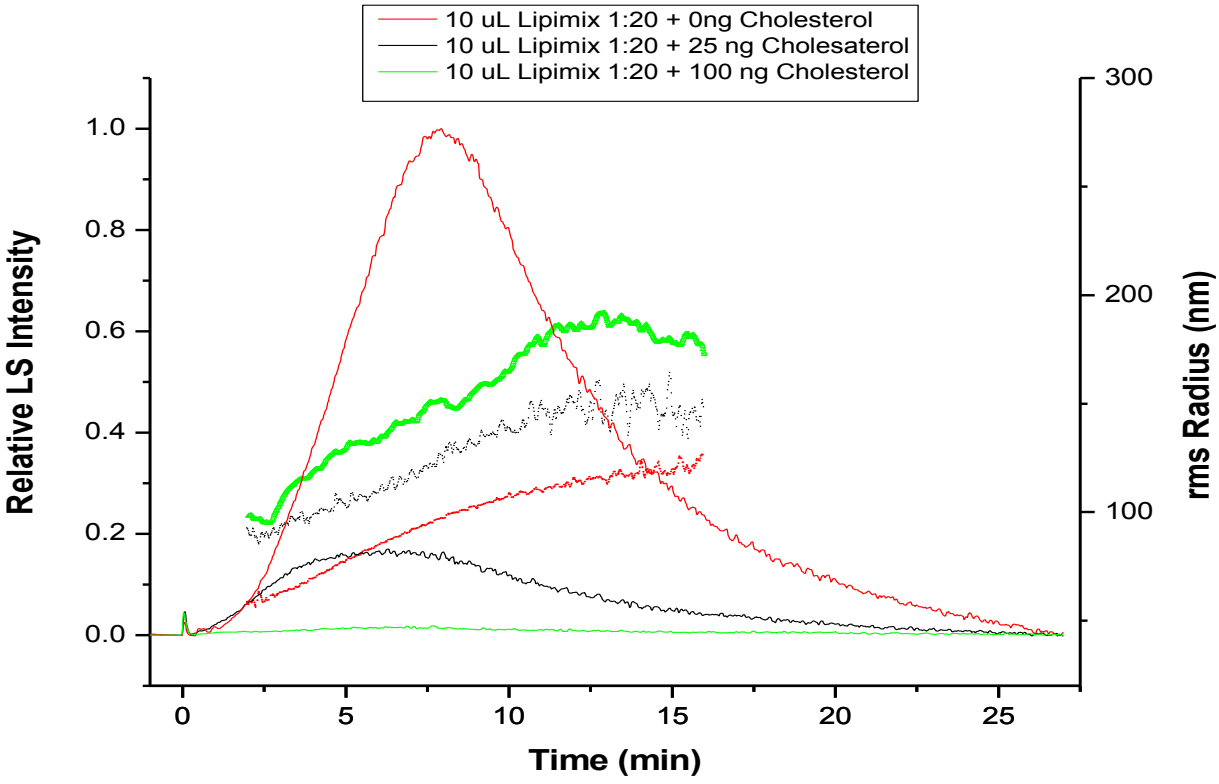

Figure 8: LS traces of Lipimix with increasing amount of added cholesterol Red: Lipimix + 0 ng of cholesterol; Black: Lipimix + 25 ng of cholesterol; Green: Lipimix + 100 ng of cholesterol.

4.4 – Conclusions

AF4-MALS has here shown to be a suitable tool for the rapid assessment of lipid vesicles dispersions. (a) AF4 allowed for a rapid size separation, while MALS detection showed to be able to detect small quantities of aggregates: by simply observe signals at low angles it was straightforward to detect small quantities of aggregates and relate their formation as a consequence of the osmolarity of the carrier; (b) it was possible to evaluate the vesicles uptake as a function of increasing amount of added cholesterol in physiological conditions (thus constant osmolarity of the carrier) and to evaluate the cholesterol uptake of vesicles as a function of the dispersing medium by varying its osmolarity.

Chapter 5 – Liposomes as Elacytarabine vector: an evaluation of the interactions with blood serum components

5.1 – Introduction

Acute myeloid leukemia (AML) is a genetically heterogeneous group of leukemia, which evolves in bone marrow failure, anemia, fatal infection, bleeding, and organ infiltration. The standard therapy against AML follows two main objectives: complete remission through an induction therapy followed by a post-remission (consolidation) therapy with the aim to stabilize the conditions gained during complete remission and prolong it. However the majority of patients relapse, giving rise to a more resistant leukemia, which up to now have no specifically approved therapy. [45].

Nowadays the most common approach is to administer cytarbine, but several mechanism of drug resistance inhibits its benefits [46-48]. A strategy to improve its therapeutic effect is the administration of elacytarabine[49] which is the fatty acid derivative (elaidic acid ester) of cytarbine (Figure 9), synthesized through an esterification reaction between elaidic acid(trans-9-octadenoic acid) and the deoxycytidine analogue cytarabine specifically designed to improve antileukemia activity [49].

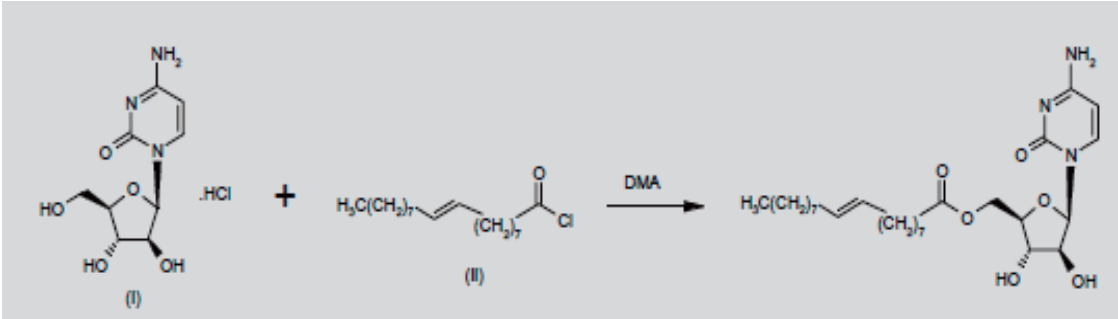

Figure 9: synthesis of elacytarabine: (I) Cytarabine, (II) elaidic acid ester

However elacytarabine is insoluble in water and for parenteral administration it is solubilized trough an egg phospholipid liposome formulation [50, 51] a form in which liposomes act as drug vector once injected in the blood stream. When lipidic particles are injected they come into contact with circulating lipoproteins and cell membranes and they have deleterious effects when infused in excess due to the perturbation of several

metabolic processes, like exchange and transfer of lipids and apolipoproteins, enzymatic hydrolysis of triacylglycerols and phospholipids, and internalization by different tissues. To limit as much as possible the metabolic perturbations due to the intravenous administration of exogenous phospholipids, the emulsion has to be infused at a low rate, and should contain the minimal amount of excess phospholipids [52].

Since liposomes is a rather old technology, discovered and first published in the sixties [11] several attempts to study their interactions with blood serum component have been done [53-55]. The first approach was to set-up simulated and simplified physiological conditions so that only the variables and parameters of interest were to be taken into account. From a practical point of view, this approach consists on the creation of purpose made samples, so that for example, Liu D. et al elucidated the interactions of liposome with serum proteins, through a series of experiments using standard or purified serum proteins and lipoproteins [56], and the same did Cwiklinska A. et al. [57]. Another approach is to administer liposomes to mices for a subsequent blood test, and analysis of pre-treated, purified blood samples with technique such as SDS-PAGE separation, western blot and ELISA assay [58]. Also nowadays, despite in literature hundreds of studies on this subject are reported, it seems that most of them are in-vitro studies consisting on the incubation of liposomes with serum component and subsequent analysis with various assay [59]. In this context, it is relevant to report that the interactions of liposomes with blood serum components is a problem that has not been faced through the use of size based separation technique like AF4.

Since it is of capital importance, this chapter is focused on the study of the fate of the elacytarabine drug molecules due to interactions of liposomes once exposed to the biological compound of the blood serum.

The ability of AF4 to size separate blood serum components such as HDL, LDL VLDL and chylomicrons has already been reported both for standard and purified samples [60]; the

technique has been shown to be effective also to fractionate untreated, whole blood serum [61].

In this study AF4-MALS is for the first time further developed to identify the blood serum species having interaction with the drug carrier, by means of size separation of liposome carrying elacytarabine from blood serum components and in particular lipoproteins.

A first method developed on analytical scale shows that the liposomes retention time band is partially overlapped to the serum lipoproteins peak and overloading problems still persist after different channel lengths and flow gradients were tested. Instead, a method developed on micro-preparative scale improved separation and avoided co-elution of liposome with serum lipoproteins, allowing (i) to study liposome / lipoproteins interactions (ii) a conformational analysis of liposome, serum lipoproteins, and liposome-lipoprotein complexes done by collecting fractions from the AF4-MALS system and analyzing them with QELS and (ii) to inject amount of sample high enough for collection for further HPLC analysis.

The study confirmed the presence of interactions between liposomes and lipoproteins depending on two main parameters: sample ratio and incubation time. Interactions are more evident with increasing time and with increasing liposome to serum ratio; we evaluate 1:100 as the lower limit for the detection of liposome in serum. For this ratio liposomes are still detectable in the fractogram. The conformational analysis showed a change in conformation due to sample interactions, which ends up in aggregation phenomena between liposomes and lipoproteins. HPLC–UV analysis revealed two serum species to be responsible for the higher drug uptake: IgG and HDL fraction, the former having probably high affinity for the apolar lipidic tag of elacytarabine molecules and for liposomes lipidic components. The elacytarabine was also found in lipoproteins fractions, with high amount.

5.2 – Samples and Methods

5.2.1 – Sample – Analytical scale characterization

In this work the following samples were used:

(1) a well-characterized serum sample;

(2) CP-4055 liposome formulation;

(3) CP-4055 liposome formulation plus the well-characterized serum sample in various ratios, as reported on every section of this paragraph;

(4) reference samples: Human Serum Albumin (HAS) and an immunoglobulin (IgG).

A healthy donor whose blood serum has been monitored (in terms of protein and lipidic content) for six month right before the starting date of this project provided the serum sample. The following parameters were considered relevant for this study: Albumin (69 kDa), 45 g/L and 21.8 mmHg and globulines (a_1, a_2, b, g) (140 kDa), 25 g/L. Also the lipidic composition in terms of total cholesterol (COLT = 208 mg/dL), triglycerides (TG = 67 mg/dL), and HDL cholesterol (HDL = 85 mg/d) was monitored. The following table reports the last blood analysis of the subject.

Proteine Plasmatiche	Componenti principali	Percentuale	Valore
Totali			6.4 -8.3 g/dL
rapporto albumina/globuline			1.13 - 1.94
albumina		53 - 66 %	3.5-5.0 g/dL
globuline alfa 1	α1-antitripsina, α1-glicoproteina acida, α1-lipoproteina,	1.9-4.5 %	0,14 - 0,33 g/dL
globuline alfa 2	α2-macroglobulina, aptoglobina, ceruloplasmina, α2-lipoproteina	6.5-13 %	0,48 - 0,96 g/dL
globuline beta 1	transferrina, β-lipoproteine	4 - 6 %	0,3 - 0,44 g/dL
globuline beta 2	Complemento C3	1 - 3 %	0,07 - 0, 22 g/dL
globuline gamma	IgA, IgD, IgE, IgG e IgM	10.5-21 %	0,77 - 1,54 g/dL

Table 3: Concentration of serum proteins of the donor

The liposomes were provided by Clavis-Pharma. The formulation is composed of vesicles which are mostly unilamellar, with a declared size distribution ranging from 10 nm up to 200 nm. The surface charge is negative because of the ionized phosphate groups of the phospholipids they are composed by. Liposomes were always filtered before use (both for injection and previous mixing with serum) using 1.2 µm regenerated cellulose (RC) or poly-ether sulfone (PES) filters to avoid possible aggregates of vesicles and prevent elacytarabine microcrystal to damage the fractionation system.

Samples containing both CP-4055 liposome formulation and serum sample were prepared and injected. From a general point of view, two ratios of elacytarabine mixed with serum sample were mostly used, namely 1:20 and 1:200 (liposome/serum, v/v) as they represent the typical situation of end and beginning of infusion to the patient, respectively. The formulation is in fact administered in the time frame of 24 hours, at the rate of 1,9 g/hour, with a consequent time dependent variation on the ratio of liposomes and serum in the blood stream.

The reference samples were albumin from human serum (HSA A3782 Sigma, Human Albumin, purity > 99%, free of fatty acids) and a commercial monoclonal antibody (IgG, Mw 150 kDa, from a pharmaceutical formulation).

The following tables summarize the samples used. As for CP-4055 liposomes + serum (1:200 - sample I) and CP-4055 liposomes + serum (1:20 - sample II) of table 2 the volumes are chosen so that the mass of liposomes is constant despite their ratio with serum varies.

Sample	Concentration	Injected volume	Injected amount
	mg/mL	µL	Mg
Serum	/	4 or 40	/

CP-4055 liposomes	10	2	20
CP-4055 liposomes + serum (1:200 - **sample I**)	0.5 + Serum*	40	20
CP-4055 liposomes + serum (1: 20 - **sample II**)	5 mg/mL + Serum**	4	20
HSA	10	18	180
IgG	40	2.5	100

Table 4: Sample I: Liposomes diluted 1:200 in blood serum (serum to liposome ratio to mimic the beginning of the infusion); Sample II: Liposomes diluted 1:20 in blood serum (serum to liposome ratio to mimic the end of the infusion)

5.2.2 – Sample – Overloading study

The purpose of this section was to ascertain if the fractograms were affected by overloading and aspecific or method dependent phenomenon, and to determine the maximum injectable amount of sample. Two series of injections using the AF4 method number 2 reported in Figure 11 were done. The first aimed to verify the overloading effect due to total load (Table 5) by injecting increasing amount of a sample with constant liposome to serum ratio (Sample I, ratio 1:20).

Sample	Concentration	Injected volume	Injected amount
CP-4055 liposomes + serum, 1:20	5 mg/mL+ Serum	4; 2; 0.5 μL	20; 10; 2.5 μg

Table 5: series of injection with the aim to verify the overloading effect due to total load. Three injection with different volumes of sample with the liposome to serum ratio of 1:20 (sample II) were done. Total injection amount in μg is also reported.

The second series consists on injections of samples with increasing liposome to serum ratio in order to increase the amount of injected liposomes. Three samples with liposome to serum ratios equal to 1:20, 1:10 and 1:5 were prepared. By increasing the ratio, the injected amount of liposome duplicates (20 μg, 40 μg and 80 μg, respectively) while the

corresponding injected mass of proteins decreases, so that the total amount does not vary significantly.

Sample	Injected volume (µL)	Liposomes mass (µg)	Serum protein mass (µg)	Total injected amount (µg)
CP-4055 liposomes + serum, 1:20	4	20	228	248
CP-4055 liposomes + serum, 1:10	4	40	216	258
CP-4055 liposomes + serum, 1:5	4	80	192	272
CP-4055 liposomes	2	20	/	/

Table 6: series of injection with the aim to increase the load of liposomes. Liposome to serum ratio are 1:20, 1:10 and 1:5. Liposome load duplicates, serum protein decreases, so that the variation of total injected amount is kept as low as possible.

5.2.3 – Sample – Micro-preparative scale characterization

Since the analytical scale characterization was affected by overloading issues, an AF4 method with channel with higher thickness (w= 490 μm) was tested in order to increase the injected amount. Samples are reported in Table 7.

Sample	Concentration	Injected volume	Injected amount
Serum		10 μL	
Serum		15 μL	
CP-4055 liposomes	10 mg/mL	10 μL	100 μg
CP-4055 liposomes + serum, 1:20	5 mg/mL+ Serum	4 μL	20 μg

CP-4055 liposomes + serum, 1:20	5 mg/mL+ Serum	10 μL	50 μg
CP-4055 liposomes + serum, 1:20	5 mg/mL+ Serum	15 μL	75 μg

Table 7: samples injected for the characterization of samples on the micro-preparative scale

5.2.4 – Sample - Liposome-lipoproteins interactions: incubation time and serum to liposome ratio

In order to study the liposome-lipoproteins interactions, the effect of the following parameters were studied:

(1) incubation times (measurement of liposome + serum blends at t=0, 12 and 24 hours at room temperature);

(2) serum to liposome ratios;

Samples are reported in Table 8.

Sample	Concentration	Injected volume (μL)	Injected amount (μg)
CP-4055 liposomes + serum, 1:20	5 mg/mL+ Serum	15	75
CP-4055 liposomes + serum, 1:50	2 mg/mL+ Serum	15	30
CP-4055 liposomes + serum, 1:100	1 mg/mL+ Serum	15	15

Table 8: for the micro-preparative characterization three ratios of liposome to serum samples were prepared: 1:20, 1:50 and 1:100.

5.2.5 – Conformational analysis

A conformational analysis was performed by evaluation of the RMS/rh ratio, using MALS detection for RMS radii and DLS analysis to determine hydrodynamic radii on the collected fractions.

Sample concentration and injected amount are summarized in Table 9.

Sample	Concentration	Injected volume	Injected amount
Serum		4 or 40 μL	
CP-4055 liposomes	10 mg/mL	2 μL	20 μg
CP-4055 liposomes + serum, 1:20	5 mg/mL+ Serum	15 μL	75 mg

Table 9: sample set of the conformational study

5.2.6 - HPLC-UV drug analysis of collected fractions

The micro-preparative AF4-MALS method was applied to two different liposomes + serum samples in order to collect fractions for the study of elacytarabine drug molecule distribution among the blood serum components.

Seven fractions were collected: HSA, IgG, LDL, lipoprotein band 1, lipoproteins band 2, chylomicrons, and field release. The HPLC-UV analysis was performed by means of a method optimized for elacytarabine quantification.

Sample concentration and injected amount are summarized in Table 10.

Sample	Concentration	Injected volume	Injected amount
CP-4055 liposomes + serum, 1:20	5 mg/mL+ Serum	15 μL	75 μg
CP-4055 liposomes + serum, 1:100	1 mg/mL+ Serum	15 μL	15 mg

Table 10: Samples injected for the fraction collection and drug quantification.

5.3 – Instrumental setup

The commercial AF4 system was the model Eclipse 3 (Wyatt Technology Europe, Dernbach, Germany). HPLC system was a 1100 Series HPLC system (Agilent Technologies, Palo Alto, CA).

Detection was performed by a DAWN HELEOS, MALS detector (Wyatt Technology Corporation, Santa Barbara, CA, USA). ASTRA software version 6 (Wyatt Technology Corporation) was used to handle signals from the detectors and to compute the RMS values.

The DLS instrument was a Dynapro Nanostar, all the measurements were done in batch mode in quartz cuvette, upon fractionation and fraction collection.

HPLC-UV for elacytarabine quantification was done at Clavis-Pharma, Oslo, Norway.

5.3.1 - AF4 methods: Analytical scale and micro-preparative scale characterization

A double approach is here presented for sample separation: at first two analytical scale method are proposed and strength and drawbacks are discussed, then a micro-preparative scale method is presented to overcome some issue related to the first. The differences between method depends mainly upon the channel volume: for the analytical scale method a 152 mm channel with a 250 μm thickness spacer and a 175 mm channel with a 350 μm thickness spacer were used, while for the micro-preparative scale method a significant increase on channel volume is obtained though the choice of a 175 mm channel whit a 490 μm spacer.

All the measurements were dome using 0.85 g/L sodium nitrate solution (10 mM ionic strength), to ensure a sufficient ionic strength generally required for liposome fractionation [37]. The carrier solution contains also 22 g/L of glycerol with the purpose to balance the osmotic pressure of the carrier with respect to that of liposome core, and prevent osmotic

stress of the liposomes [39] and 200 mg/L sodium azide to prevent bacterial growth without significantly alteration of the ionic strength.

Two methods were tested for the characterization of serum, liposomes and serum with liposomes. Flow conditions are reported in Figure 10 and Figure 11.

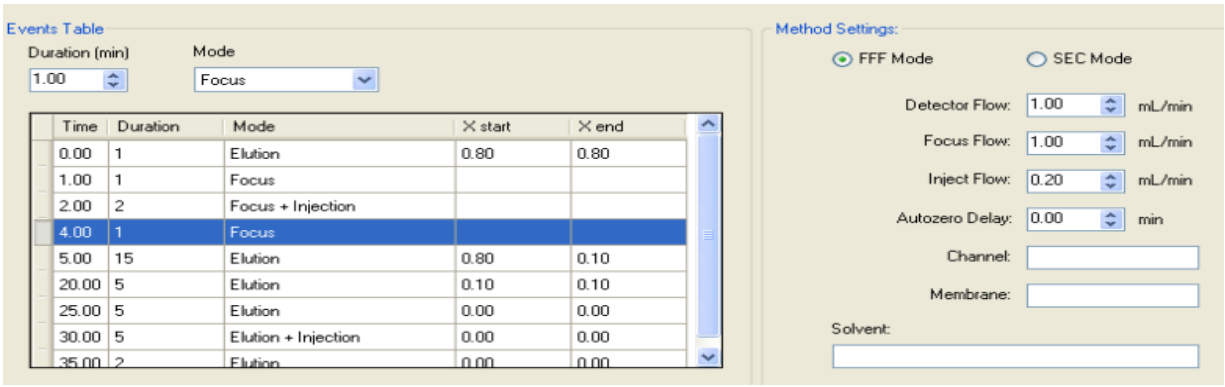

Figure 10: AF4 method 1, used for analytical scale characterization

In method 1 detector flow and focus flow are both 1 mL/min. An elution and a focus step of one minute each at the beginning of the method serve to equilibrate the flows inside the channel. Then samples is introduced into the channel with an injection flow of 0,2 mL/min and focused for 3 minutes. For the elution, an initial cross-flow rate of 0,8 mL/min was set, and then linearly decreased to 0.10 mL/min in 15 minutes. The crossflow rate was then kept constant for 5 min, and finally set to 0.0 mL/min for 5 min. The channel was 152 mm long, 16 mm wide, and 250 µm thick. Regenerated cellulose membranes with a 10 kDa cutoff were used.

In order to improve separation in the region between IgG and serum lipoproteins (where the peak maximum of liposomes lays) method 2 was set up (Figure 11).

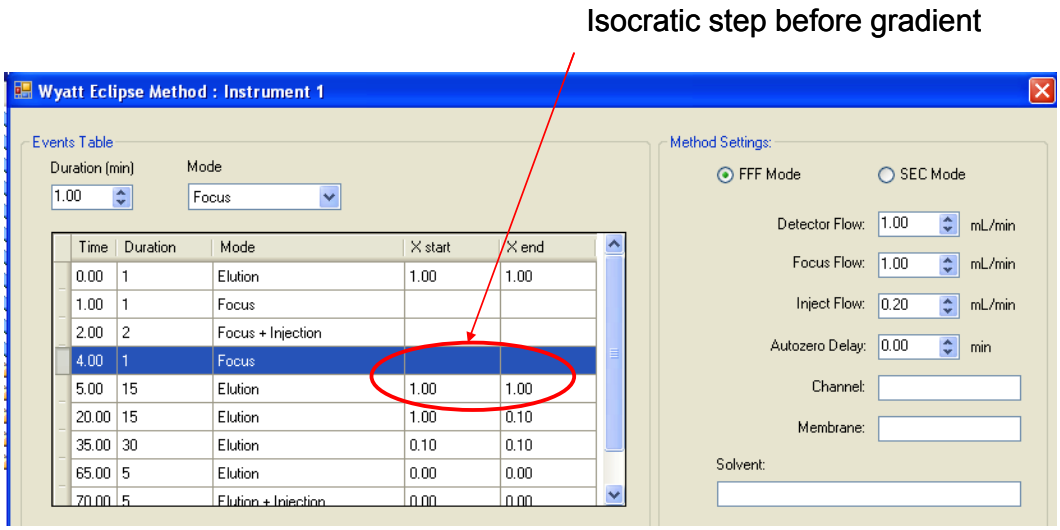

Figure 11: Method 2, used for analytical scale characterization (spacer thickness 350 µm) and for micropreparative scale characterization (spacer thickness 490 µm thickness).

The initial steps (until sample focusing) are the same of method 1. Focus flow and detector flow were again 1 mL/min while initial cross flow was set to 1 mL/min ant kept constant for 15 minutes. After the isocratic step the cross flow linearly decreases to 0,10 mL/min and then a second isocratic step of 0,10 mL/min crossflow lasts for 30 minutes for the complete elution of sample. 5 minutes of elution and 5 minutes of elution with an inject flow of 0,2 mL/min and no cross flow are introduced to wash channel and inject tubings. This flow program was used with a 350 µm thickness spacer for the analytical scale method, and with a 490 µm thickness spacer for the micro-preparative scale characterization and for sample collection for further analysis on DLS and HPLC-UV. The channel was 175 mm long, 16 mm wide, regenerated cellulose membranes with a 10 kDa cut-off were used.

5.4 – Results & Discussion

5.4.1 – Analytical scale characterization

The first purpose of this section is to characterize on an analytical scale a CP-4055 sample and a mixture of CP-4055 with serum (sample I and sample II, see sample section, Table 4). The aim is to identify the bands for liposomes and lipoprotein subpopulations in the fractograms and to evaluate the degree of separation between liposomes and lipoprotein subpopulations.

The laser scattering profiles of liposomes fractionated with the analytical scale method reported in are shown in Figure 12.

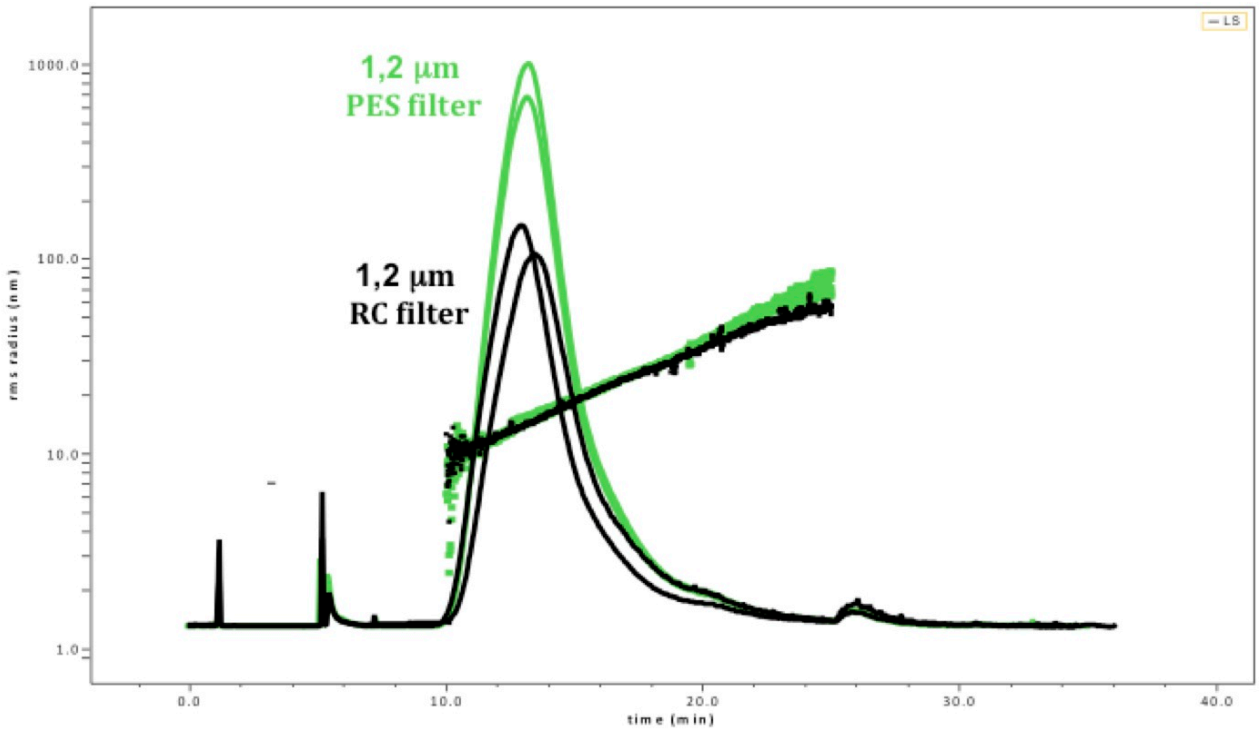

Figure 12: AF4-UV/Vis-MALS of CP-4055 liposome samples; two repeated runs with PES and RC filters used for sample preparation.

The fractogram is constituted by a quite symmetrical peak at circa 13 min, and a low signal due to the field release at 25 min. From the MALS detector the RMS radius distributions are calculated; particle size ranges from 10 nm up to 100 nm, with a monomodal

distribution, and no liposome aggregates are observed in correspondence of the tail of the peak (no particles with radius higher than 100 nm), or in correspondence of the field release at 25 minutes. The material of the filters (PES or RC) used for sample preparation does not seem to have a significant effect on sample size distribution. Since a slightly lower sample recovery is obtained using RC filters, all the results described in the next sections were obtained using PES filters.

In a first attempt to identify the elution bands of the protein subpopulations which constitute a serum samples, the method 1 used for liposomes was also applied for the fractionation of serum sample and for the reference samples (HAS and IgG); the laser scattering traces are reported in Figure 13 where blue, red and green lines are the results of serum, HAS and IgG fractionation, respectively.

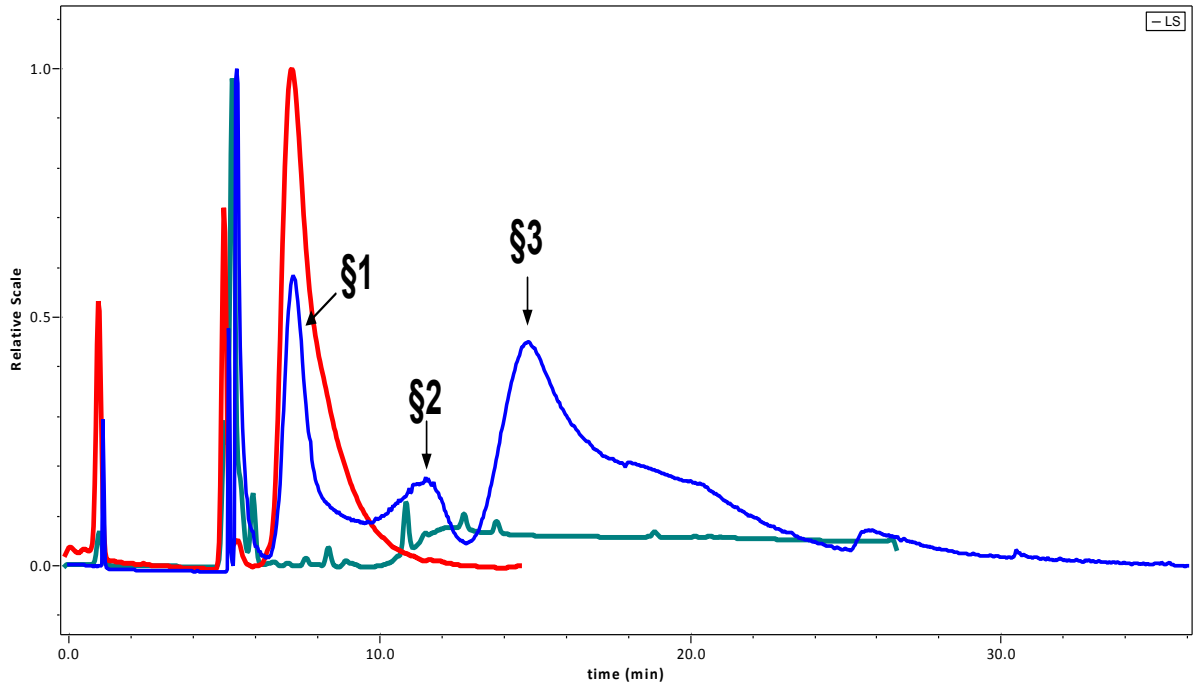

Figure 13: AF4-UV/Vis-MALS of serum, HSA and IgG.

Three main bands, §1 at 7 min, §2 at 11,5 min and §3 at 15 min respectively, characterize the serum sample fractogram (blue trace). They were identified from the comparison of the retention times of the reference samples, which were 7 min for HAS and 12 min for IgG.

Based on these results and on previous AF4 data of serum samples with different methods reported in literature [61], we could assign in the serum profile peak §1 to HAS and peak §2 to serum immunoglobulins. However a slight difference in retention time between human serum IgG (11 min) and reference IgG (12 min) is observed, with the latter eluting later: a reasonable explanation of this phenomenon may be due to the reference IgG which is a pharmaceutical immunoglobulin coming from a different species. At last, in serum fractogram the §3 band eluting in the time range 12-20 minutes may be generically assigned to the serum lipoproteins.

In order to investigate possible interactions of liposomes with blood serum lipoproteins during elacytarabine infusion time, sample I and II were injected and the fractograms compared to that of serum and liposomes alone.

Figure 14 shows the fractographic profile of the serum sample, CP-4055 liposome and serum sample added with CP-4055 liposome (Sample I, Table 4).

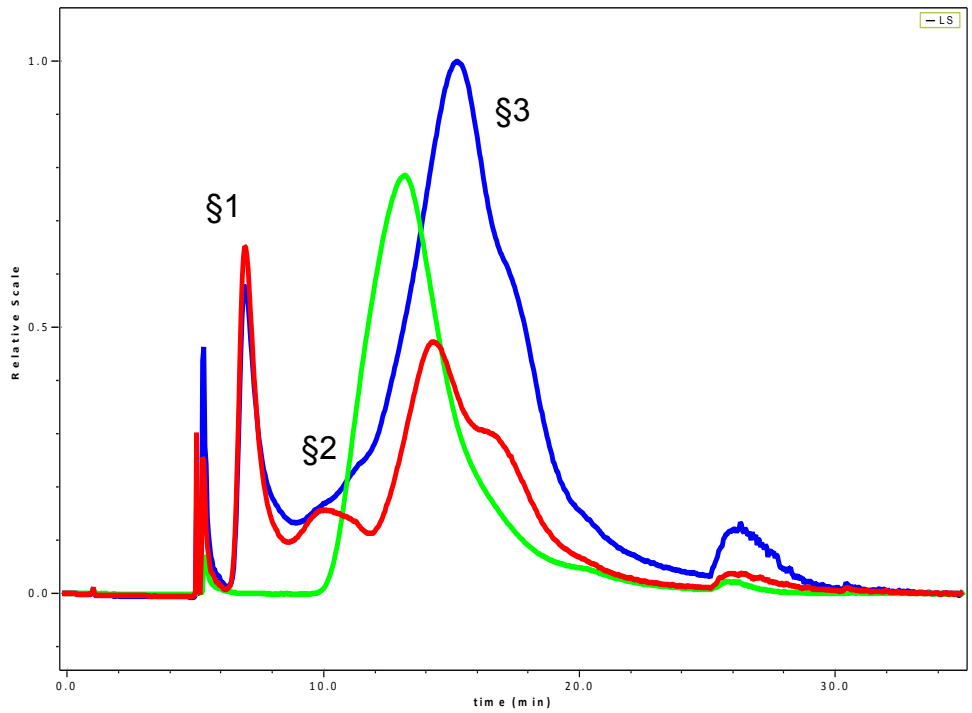

Figure 14: AF4-UV/Vis-MALS of serum, CP-4055 liposome, and serum+CP-4055 (Sample I)

Figure 15 shows the fractographic profile of the serum sample, CP-4055 liposome, and serum sample added with CP-4055 liposome (Sample II, Table 4).

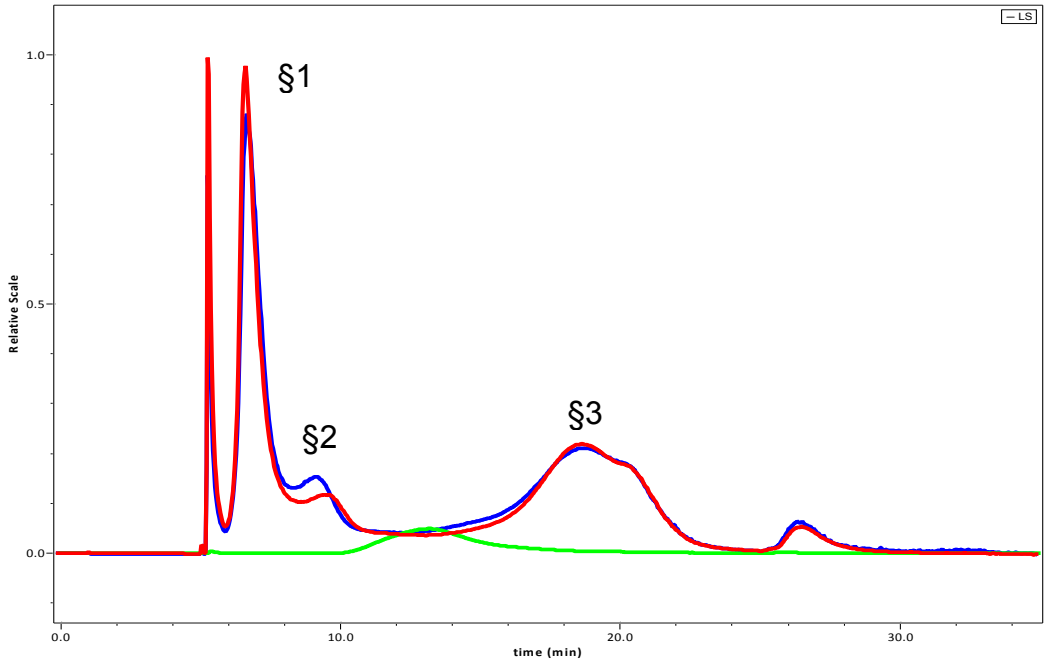

Figure 15: AF4-UV/Vis-MALS of serum, CP-4055 liposome, and serum+CP-4055 (Sample II)

Recoveries were roughly calculated: a concentration detector such as RI or PDA detector would be required, while the use of MALS detector is usually avoided because signal is proportional not only to sample concentration but also to other parameters like sample size and molecular weight and to the square of particle surface polarizability (dn/dc). On the other hand it was not possible to obtain any reliable signal from the RI detector because it is sensitive to the change in pressure inside the channel due to the cross-flow gradients of both method 1 and method 2, and at the same time UV-Vis detection was poor because of the lack of a convenient detection wavelength for serum and liposomes, since both absorption and extinction (scattering) phenomenon take place. For this reasons the use of MALS detector has been considered a reasonable approximation, and the evaluation of recoveries was done by means of the LS peak areas, following this equations:

$$A_{TOT} = A_{serum\ peak} + A_{liposome\ peak}$$

$$\text{Recovery \%} = A_{\text{sample I or II, peak}}/A_{TOT}$$

where A_{TOT} is the total peak area, meaning the sum of $A_{serum\ peak}$, the serum peak area, and of $A_{liposome\ peak}$, the area of liposome peak. Values of 98% and 95% of recoveries were found for sample I and sample II.

From the comparison of the fractionation profiles for serum (red traces in Figure 14 and Figure 15) and liposomes (green traces in Figure 14 and Figure 15), we can observe that in the retention time range for CP-4055 (10-15 min) no species are eluted in serum sample. This is evident in Figure 15 for sample II; while in Figure 14 for sample I there is a partial overlap with the peak of lipoproteins (§3). Moreover, this peak shows lower retention time with respect to sample I, however, also in sample II (Figure 15) the peak maximum for liposome corresponds to a minimum in the serum sample profile. In the fractionation profiles of the mixtures sample I and sample II (blue trace, in Figure 14 and Figure 15), a slight increase in the LS signal is present in retention interval typical for liposome. This increase is more evident in sample II where the serum amount in the mixture is lower. These results may indicate that liposomes were partially eluted within their typical retention interval and partially overlapped to the peak ascribed to serum lipoproteins, this hypothesis is confirmed by the almost total recovery obtained for both sample I and II. From the overlap of the typical profiles for serum and CP-4055 liposome, it is then reasonable to assume that the separation of liposomes from serum proteins is feasible. Indeed, it is not possible with the current method to deeper understand the behaviour of vesicles in presence of blood serum components. Instead, an increase of method selectivity may improve separation between immunoglobulins and lipoprotein peaks. Taking into account that no serum components are eluted in the typical retention

time interval of liposomes in sample II, an interaction between liposomes and other blood serum species could be easily monitored by enrichment of the CP-4055 band.

An attempt to pursue this objective has been done by fractionating sample on an analytical scale with the flow program of method 2 and using a longer channel, and a spacer width of 350 µm. In Figure 16 the fractographic profiles of liposome, serum and liposomes + serum samples are reported (sample prepared and injected according to Table 4).

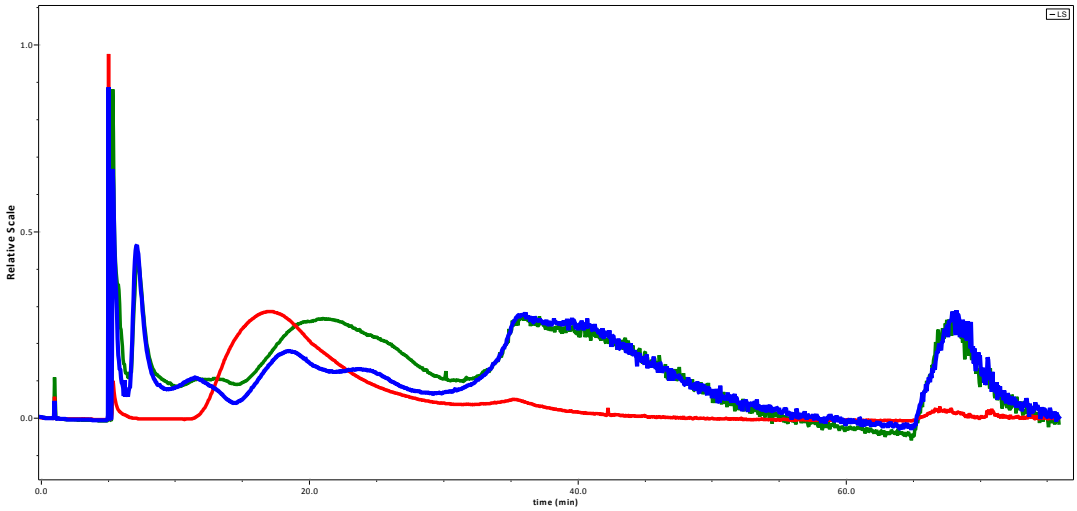

Figure 16: AF4-MALS of **liposome**, **serum**, **serum + liposome (sample II).**

The method contains an isocratic step at the beginning (Figure 11), which has the scope to improve the separation in the region between immunoglobulins and lipoproteins, where liposomes elutes. However it is evident that liposomes continue to exit with lipoproteins, when blends samples are injected (green trace). As a general conclusion it seems that the method 2 do not produce improvements on the separation, and a co-elution of liposome with serum lipoproteins persists. It is known that high amount of injection is a factor which limits separation power in AF4 [36, 62, 63]. Therefore an overloading study was performed to discriminate whether possible changes in the band shape of lipoproteins are due to actual interaction occurring between lipidic vesicles and serum lipoproteins rather than to aspecific phenomenon due to the method itself.

A specific approach was followed for this aim (samples were prepared according to Table 5). First of all (Figure 17a) the liposome to serum ratio of 1:20 was chosen and injection with decreasing amount were done (4 µL, 2 µL, and 0,5 µL). In the resulting fractograms, the retention times of lipoprotein bands where monitored and compared to that liposomes injected with the same method (indicated by the green arrow in the figure). This operation provides the injection volume giving no overloading; the resulting fractogram is then compared to the serum profile injected with the same volume to evaluate differences between serum profile and serum + liposome profiles which might be due to interactions. The results are reported in Figure 17b (fractographic profiles of a serum and liposomes + serum samples, at the ratio of 1:20, with 0.5 µL as injected volume). In Figure 17c the fractographic profiles of samples with liposome to serum ratios of 1:20; 1:10; 1:5 and liposomes alone using 4 µL as injected volume are reported.

By decreasing the total injected amount (Figure 17a) a decrease in retention time for the lipoproteins band was observed, retention time shifts from 20 minutes when 4 µL are injected to 17 minutes when 2 µL were injected and finally to 16 minutes for the 0,5 µL of injected volume; on the same time for the 0,5 µL injection a peak maximum close to the retention time typical for liposome appears. This result indicates the presence of overloading effects. When the injected amount is 0.5 µL the resolution is good and it allows the distinction of different subpopulation. Moreover, by the comparison of profiles for serum and liposomes + serum samples at 0.5 µL as injected volume (Figure 17b) it can be noticed that the initial parts of the fractionation (until retention time of liposomes) are superimposable. In the retention interval of interest, the lipoproteins band (liposomes-LDL-VLDL), there is a shift at higher retention times in the serum + liposomes sample. This effect can be related to co-elutuion and/or complexation of lipoproteins and liposomes. Moreover, the field release is higher with samples with liposomes, this can be explained by an iperaggregation phenomena of liposomes. The trend of RMS radius is good, from 10

nm (high abundant proteins) to 100 nm (field release) in which aggregates particles and chylomicrons species are eluted. In Figure 17c, by the injections of liposomes + serum samples with an increased amount of liposomes (black trace), a weak band at retention time typical for liposome appears. This effect is less evident with respect to injections at different volumes; however, it can confirm potential aspecific interactions between liposome and lipoproteins due to overloading effects. Therefore, it can be concluded that

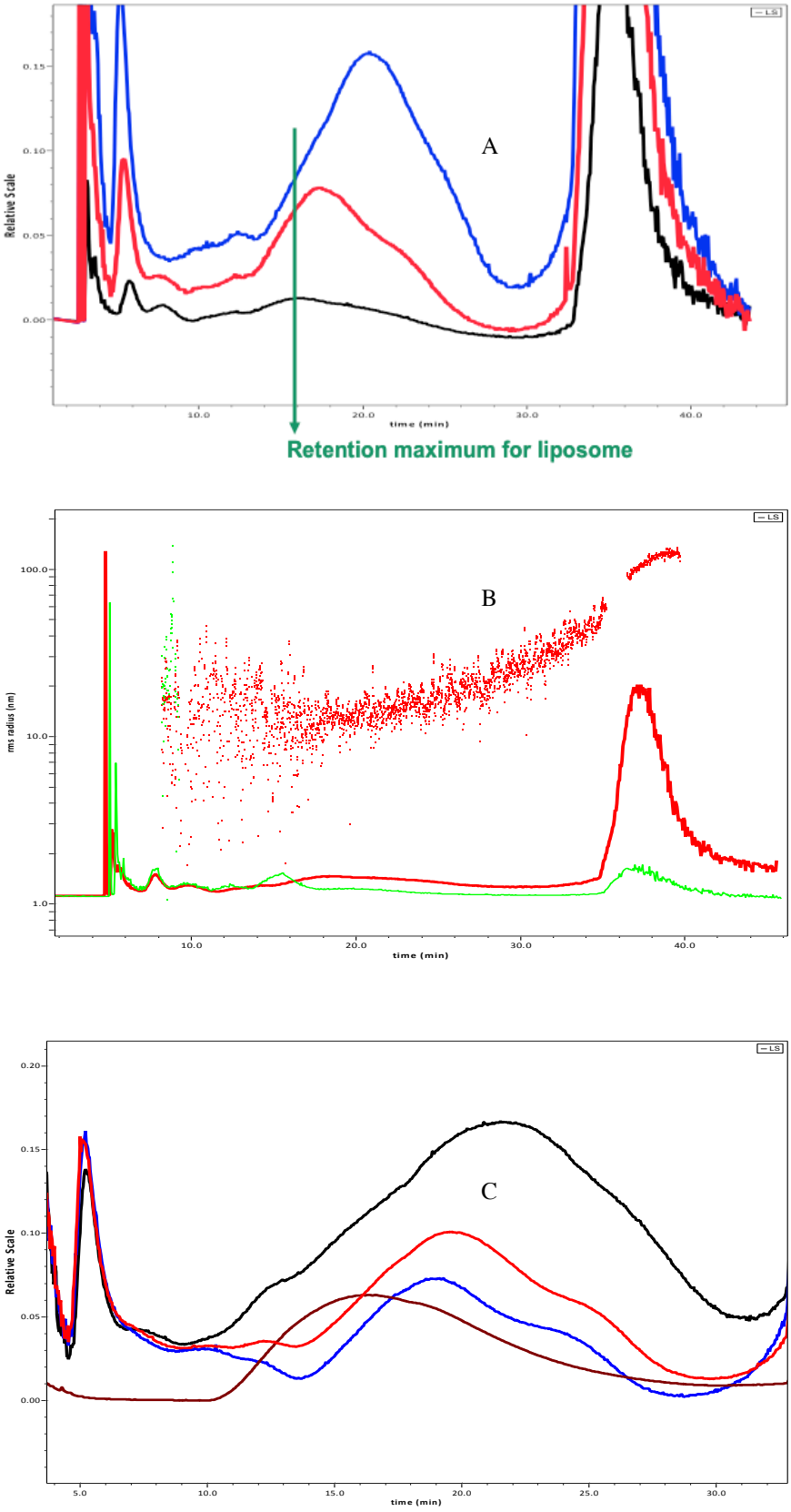

Figure 17: (a) AF4-MALS of a liposomes+serum 1:20 sample, injection volume: **4 µL**; **2 µL**; **0.5** µL; (b) 0.5 µL of **serum + liposome** and **serum** samples; (c) AF4-MALS of samples with liposome to serum ratios: **1:20**; **1:10**; **1:5** and **liposomes**

co-elution of liposomes and lipoproteins exists, together with some overloading issues. As a consequence the use of a higher spacer, a micro-preparative method with a spacer thickness of 490 µm, was considered as further step in the method development.

The injected volume was increased from 4 µL to 15 µL. In Figure 18 the profiles of liposome and liposomes + serum samples at different injection volumes are reported.

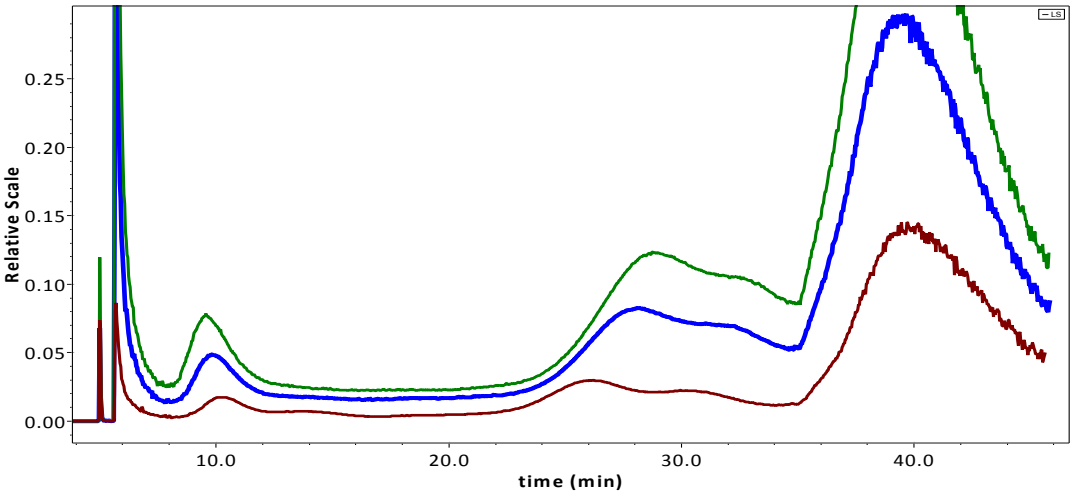

Figure 18: AF4-MALS of 4 ul liposomes+serum; 10 ul liposomes+serum; 15 ul liposomes+serum

The three profiles are characterized by the same patterns: a sharp band at the beginning of the elution step (minute 10) followed by a weak band ascribed to immunoglobulins (14 minutes) and a narrow, bimodal and intense band starting at 22 minutes, followed the field release band at the end of the method. For completeness the three injection of Figure 18 were compared to the corresponding injection of blood serum (Figure 19). In this case it is evident that the lipoprotein band eluting after minute 22 changes shape after interaction with liposomes, and, on the same time, the peak of liposomes alone which is expected to lays between immunoglobulins and lipoproteins does not appear in the fractogram. Furthermore in Figure 18 the intensity of signals are proportional to the injected amount and the retention times are comparable.

For this reasons it is reasonable to assume that the overloading issues are fixed and that at the same time the use of method 2 with a 490 µm spacer (the micro-preparative scale

channel) gives interesting insight on the mechanism of interaction of liposomes with blood serum components.

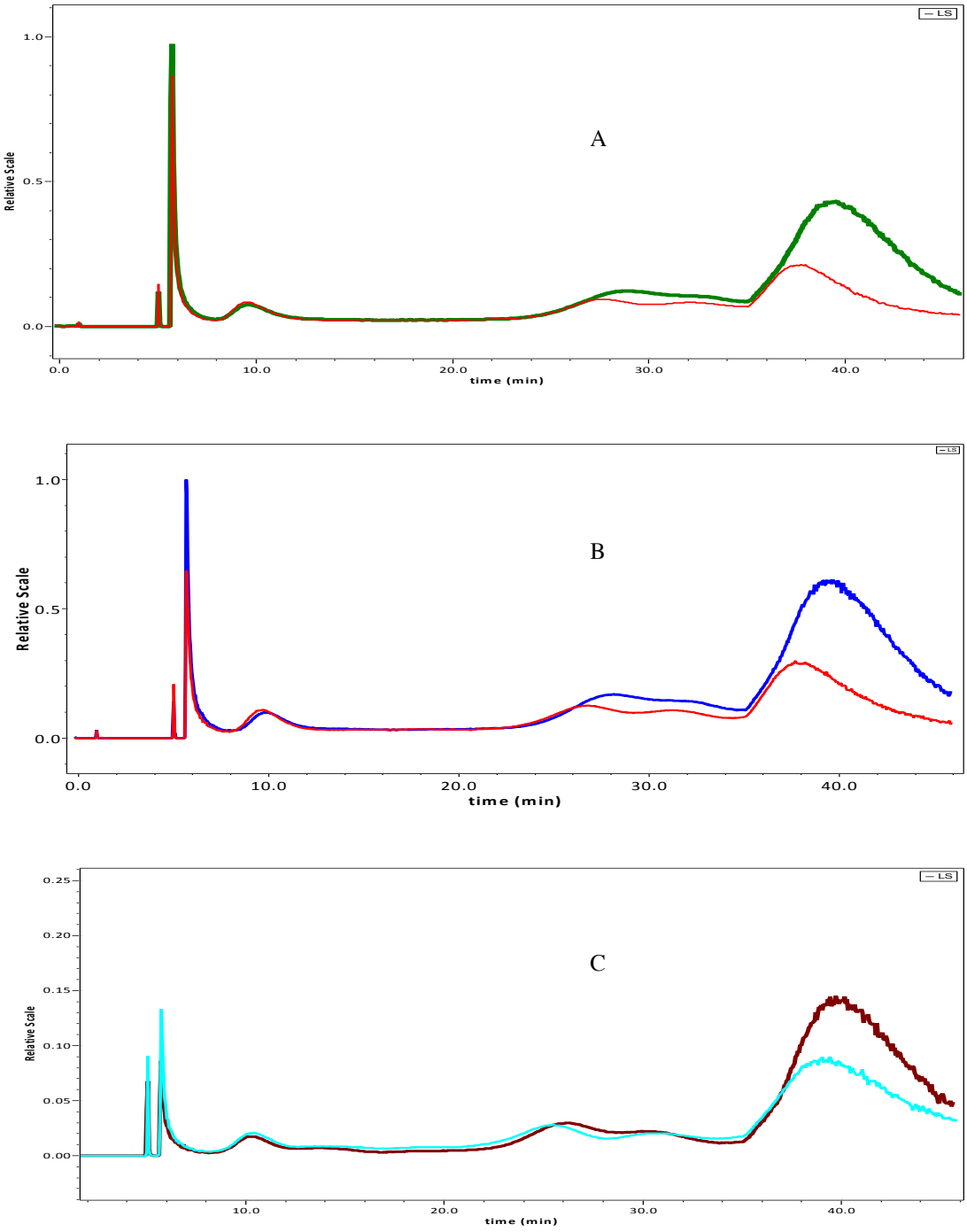

Figure 19: (a) AF4-MALS of 15 ul of serum and liposomes+serum; (b) AF4-MALS of 10 ul of **serum** and **liposomes+serum; (c)** AF4-MALS of 4 ul of **serum** and **liposomes+serum**

However it would be considered weak to speculate about liposome to lipoproteins interaction only on the basis of the interpretation of fractographic patterns, especially when

dealing with complex samples: it reasonable to assume that blood serum samples are prone to change with respect to time: phenomenon like aggregation of lipoproteins and/or sedimentation of chylomicrons which could act as filter are likely to be involved; obviously such phenomenon could affected the results. On the other had, as already explained, elacytarabine infusions are administered in the time frame of 24 hours: on the scope to give further insights on the behaviour of liposomes, the aging of serum and liposomes + serum sample was studied with respect to time. It has been mandatory, given the circumstances, to monitor in the same time frame also the serum sample to discriminate aging effects by complexation phenomena. Due to the good separation efficiency in the lipoproteins region of interest and the increased injected amount suitable also for further sample collection and analysis, the volume of 15 µL was chosen as injection volume to continue with the study of liposomes interactions.

5.4.2 - Liposome-lipoproteins interactions: incubation time, serum/liposome ratio

Figure 20 a, b and c show the profiles of liposomes + serum samples at the different ratios of 1:20, 1:50 and 1:100, at different incubation times (t=0, 12 h and 24 h; Table 8) while Figure 21 a, b and c show the profiles of liposomes + serum samples at the different ratios of 1:20, 1:50 and 1:100, at the same incubation time.

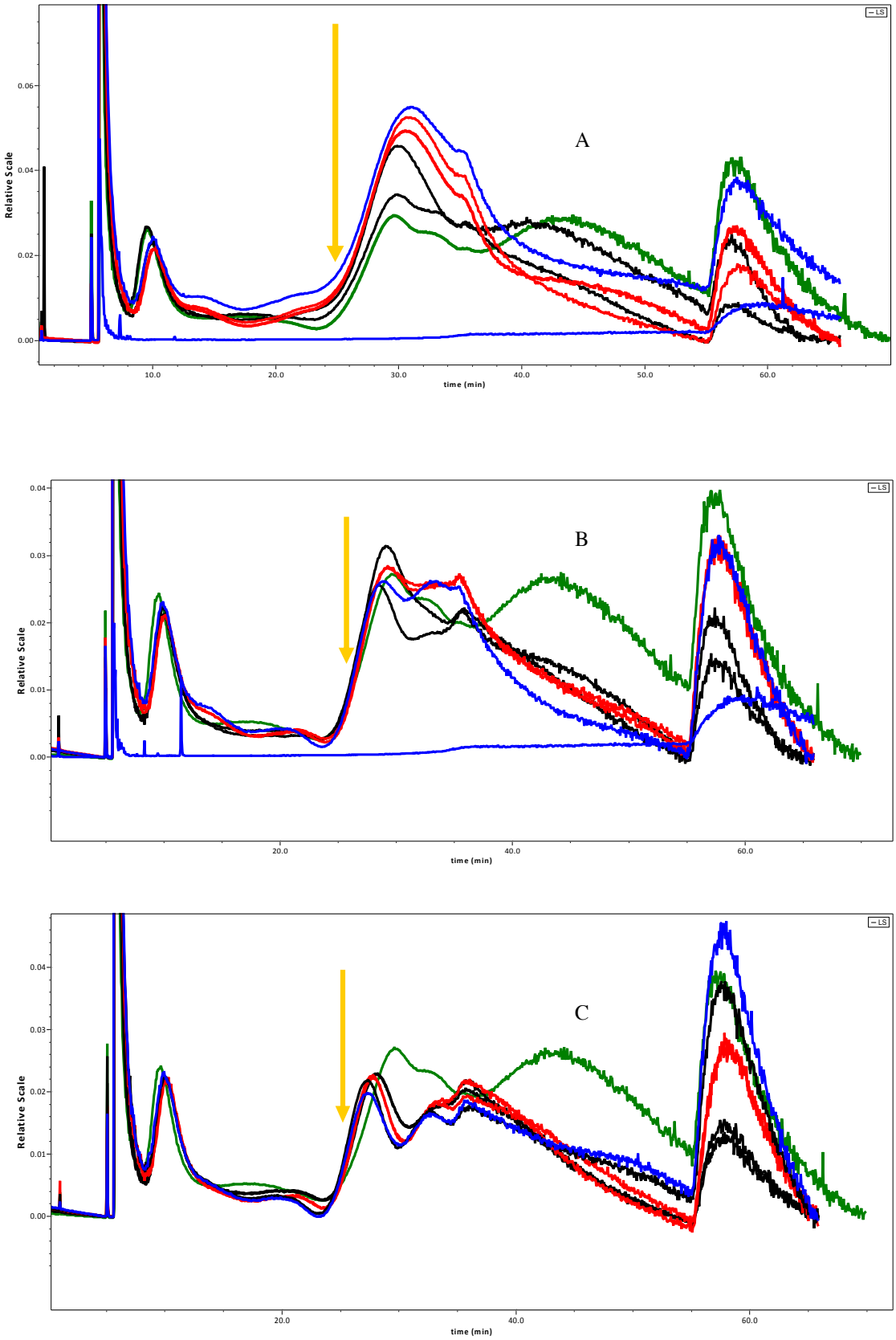

Figure 20: (a) AF4-MALS of serum; liposomes+serum 1:20 at t=0 (2 runs), t=12 h (2 runs); t=24 h (2 runs). Typical retention time for liposome; (b) AF4-MALS of serum; liposomes+serum 1:50 at t=0 (2 runs), t=12 h (2 runs); t=24 h (2 runs). Typical retention time for liposome; (c) AF4-MALS of serum; liposomes+serum 1:100 at t=0 (2 runs), t=12 h (2 runs); t=24 h (2 runs). Typical retention time for liposome

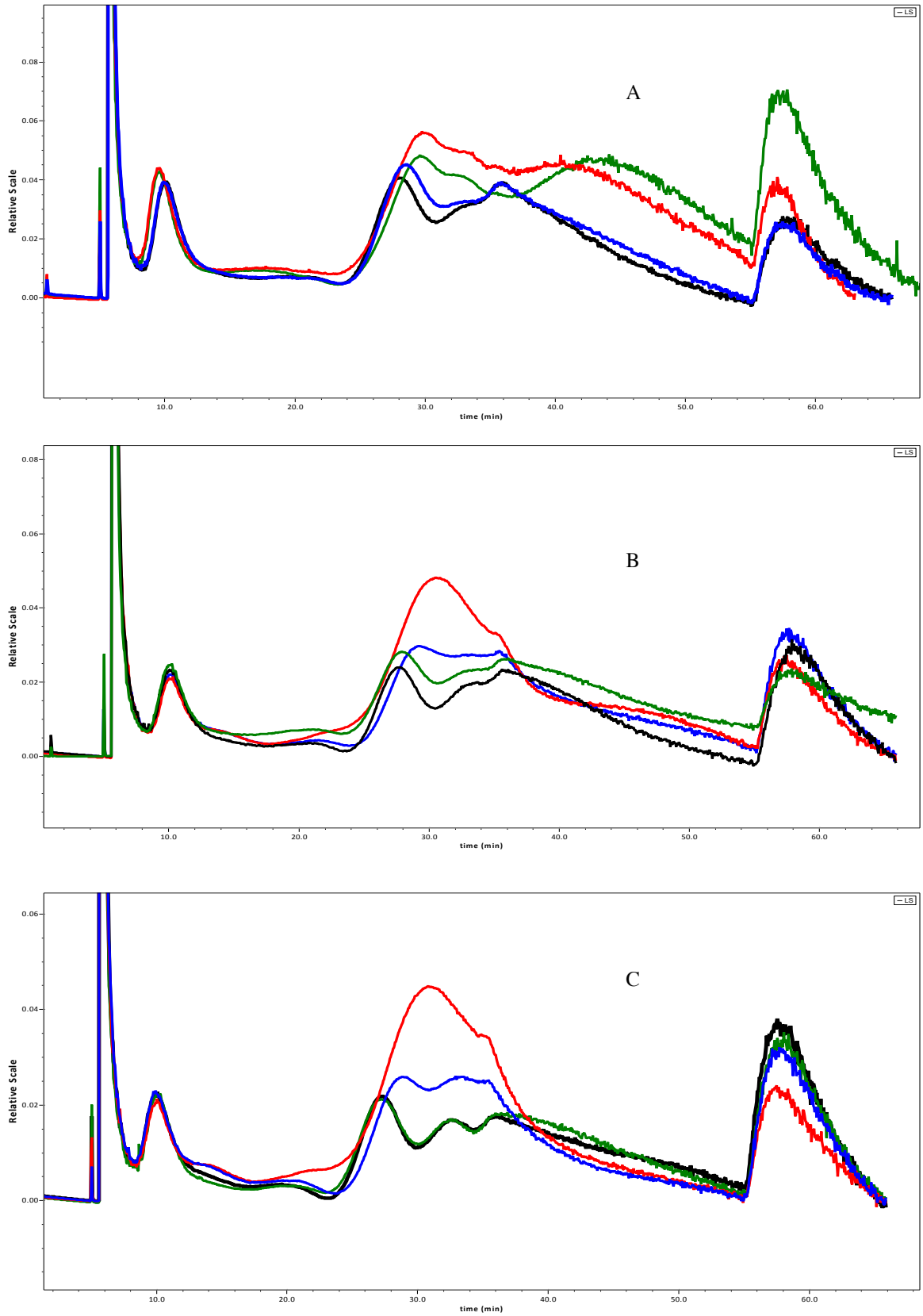

Figure 21: (a) AF4-MALS of **serum** and liposomes+serum (**1;20**; **1:50**; **1:100**) samples at t=0; (b) AF4-MALS of **serum** and liposomes+serum (**1;20**; **1:50**; **1:100**) samples at t=12 h; (c) AF4-MALS of **serum** and liposomes+serum (**1;20**; **1:50**; **1:100**) samples at t=24

From the comparison among different incubation times for liposomes + serum in Figure 20a we can notice that at t=0 the profile of liposomes + serum is slight different from those of serum sample; a slight increase in the signal at retention time typical for liposome starts to appear. Peak shapes at t=12 and t=24 hours are the same, and slightly different with respect to t=0, with increased intensity for the lipoproteins band due to the increased incubation/interaction with liposomes. In Figure 20 b the peak shape does not vary significantly at t=0, 12 and 24 h and a it is observed slight increase in the signal at retention time typical for liposome appears. In Figure 20 c (1:100 sample ratio) peak shape does not change at t= 0, 12 and 24 and slight increase in the signal at retention time typical for liposome appears.

From the comparison among different liposomes + serum ratio 1:20, 1:50 and 1:100 (Figure 21 a, b and c) at the same incubation time we can notice that at t=0 (a), a slight increase in the retention band intensity at retention time typical for liposomes appears for the 1:100 and 1:50 samples and it becomes more pronounced for 1:20 sample. The effect of incubation time is evident at t=12h and t=24h (b and c): the increase in liposome band intensity becomes significantly more evident for 1:20 sample.

Moreover, in general, the band eluting after 40 min that is associated to chylomicrons present an high variability in intensity and a general lower intensity on lipsoomes + serum samples with respect to serum sample alone. However, the serum sample was the first sample fractionated, it’s possible that the chylomicrons tend to sediment over time and their recovery becomes lower. Moreover, it should be note that the AF4 method is not optimized for such a big species.

As a general conclusion, by comparing the different incubation times for liposomes to serum ratio 1:20; 1:50 and 1:100 it is suggested that, depending on the liposomes/serum ratio, the differences among t=0 and t=12h and t=24h are more evident**.** From the evaluation of the profiles of different liposome to serum ratios the value of 1:100 is the

lower limit for the detection of liposome in serum. For this sample, the liposomes are still detectable in the fractogram. In the next section the potential interactions occurring between liposomes and lipoproteins are further studied by means of a conformational analysis of the species eluting on the lipoproteins band.

5.4.3 - Conformational analysis

Conformational studies with SEC or FIFFF and MALS have been done for a variety of samples, from proteins to biopolymers to nanoparticles [64-71]. They consists on the comparison of rh versus RMS values of samples, and they required the iphenation of a separation technique such as FIFFF to a detector able to give information on the size of the sample gained through the use of at least one non correlated method. Consequently the general approach is to plot the rg values coming from MALS detection versus the hydrodynamic radius values coming from the calibration of the FFF method (in which retention time is proportional to the diffusion coefficient and hence to the sample hydrodynamic size) or from the use of a DLS instrument.

The approach here taken is to fractionate samples and with the on-line coupling of MALS detector compute the RMS values on real time. After fractionation the samples were then collected and DLS analysis was performed off-line.

Figure 22 a, b and c reports the profile of serum, liposomes + serum and liposomes samples and the collected fractions are indicated.

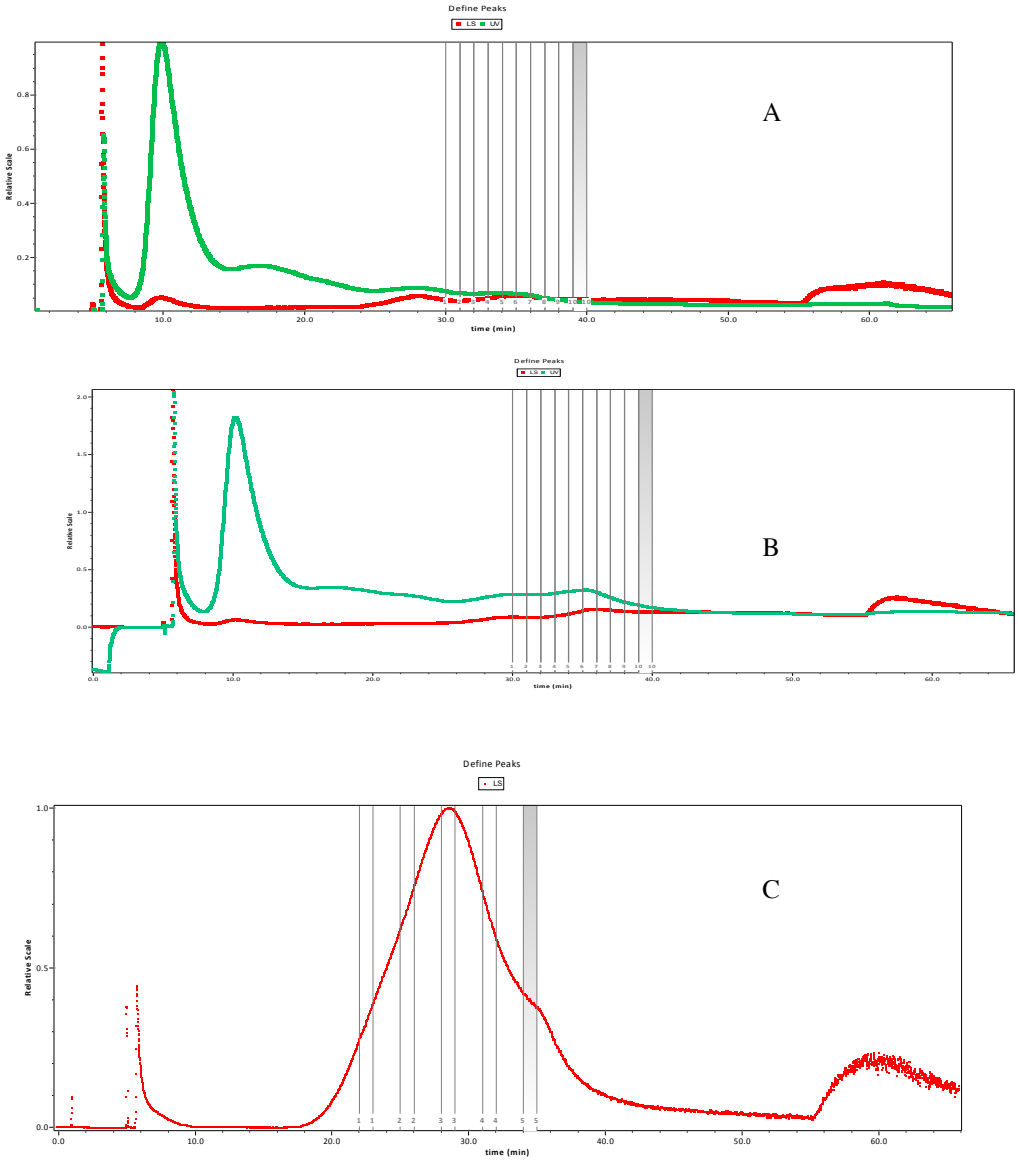

Figure 22: LS and **UV@280** nm signals for serum (a), liposomes+serum (b) and liposomes (c); collected fractions for conformational analysis

In Figure 26 the conformation analysis results on serum, liposomes and liposomes+serum samples are reported as RMS *vs* r_h.

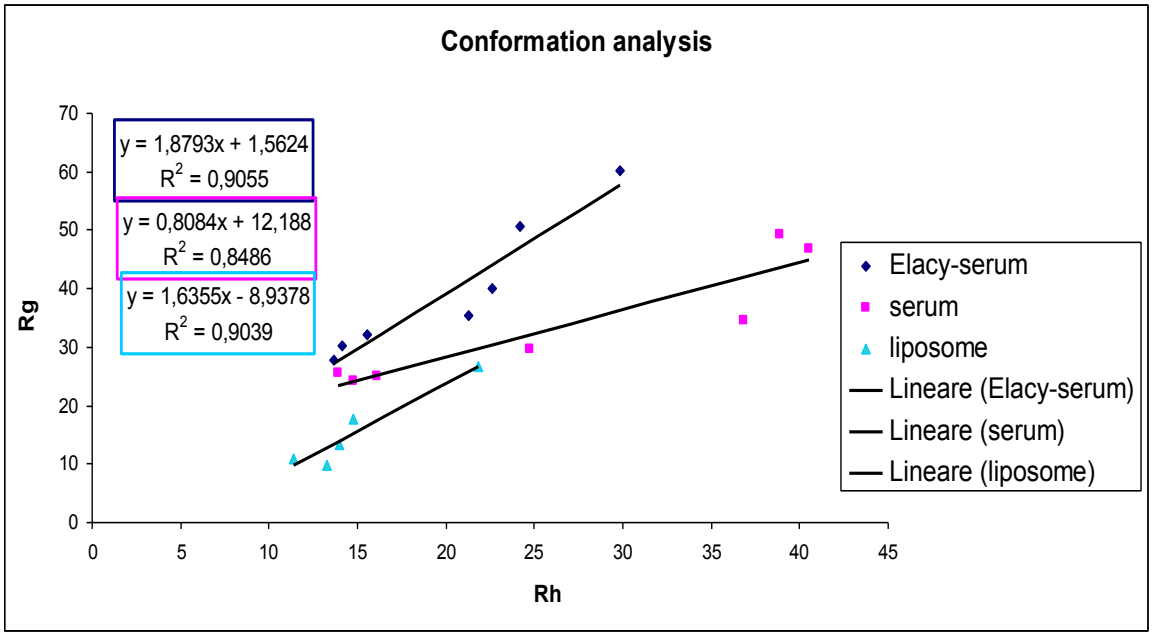

Figure 23: rg vs rh of **liposome**, **serum** and **liposomes+serum** samples.

In Figure 23 the conformational analysis is reported as a plot of rms versus rh. The results for serum and liposome + serum sample are also reported as RMS *vs* retention time and r_h *vs* retention time (Figure 24), in order to study the conformation with respect to fractionation profile.

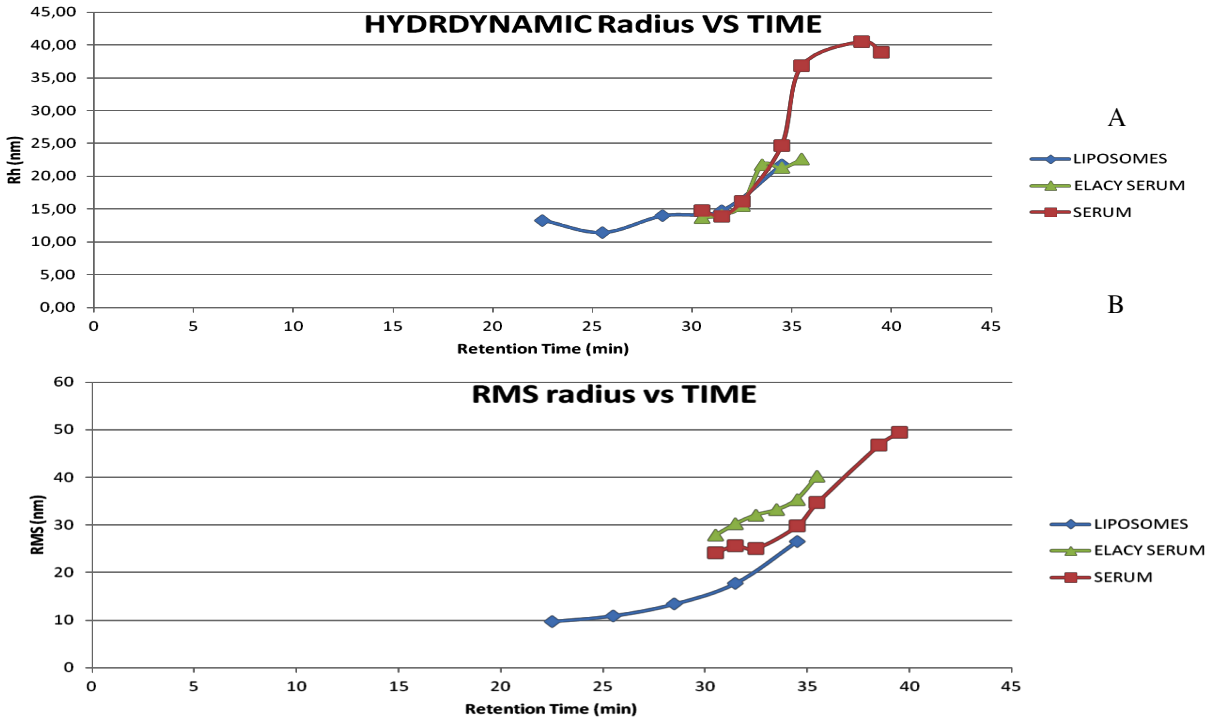

Figure 24: r_g vs retention time (a) and r_h vs retention time (b) for **serum**, **liposomes**, and **liposomes+serum** samples

We obtained 3 different values of rg/rh for serum, liposomes and liposomes+serum samples; indicating different conformations. From the results one can summarize that the lipoproteins show an indicative value for rg/rh ~ 0.8 indicative of compact spherical particles, while liposomes show a value for rg/rh ~ 1.8.

The value measured for liposomes + serum samples was ~ 1.6, suggesting an aggregation phenomenon between lipoproteins and liposome or a potential disruption of liposomes and reassembly. In order to investigate this issue, the conformation analysis was studied with respect to retention times.

The r_g at the same retention time is higher for liposomes + serum sample with respect to serum and liposomes samples (Figure 24b), while the r_h values shifts at higher retention times for liposomes + serum samples (Figure 24a). These results indicate aggregations phenomena.

5.4.4 - HPLC-UV drug analysis of collected fractions

The last aim of this work is to determine the serum proteins responsible for uptake of elacytarabine drug molecules. Figure 25 is an example of fractionation profile of a liposomes + serum 1:20 sample, and time interval of the collected fractions is reported on the box (F1 to F7). The same fractions were collected from liposomes + serum 1:20 and 1:100 samples at t=0 and t=24h, and they were are chosen to monitor all the different species that were attributed in the fractogram, that is HAS (F1), IgG (F2), LDL (F3), lipoproteins band 1 (F4), lipoproteins band 2 (F5), chylomicrons (F6) and field release (F7), as reported in Table 11. The method used is the micro-preparative one (flow conditions of Figure 11, detector flow is 1 mL/min and fractions were collected for 2 minutes and the operation repeated for 2 times, for a total sample volume of 4 mL each fraction.

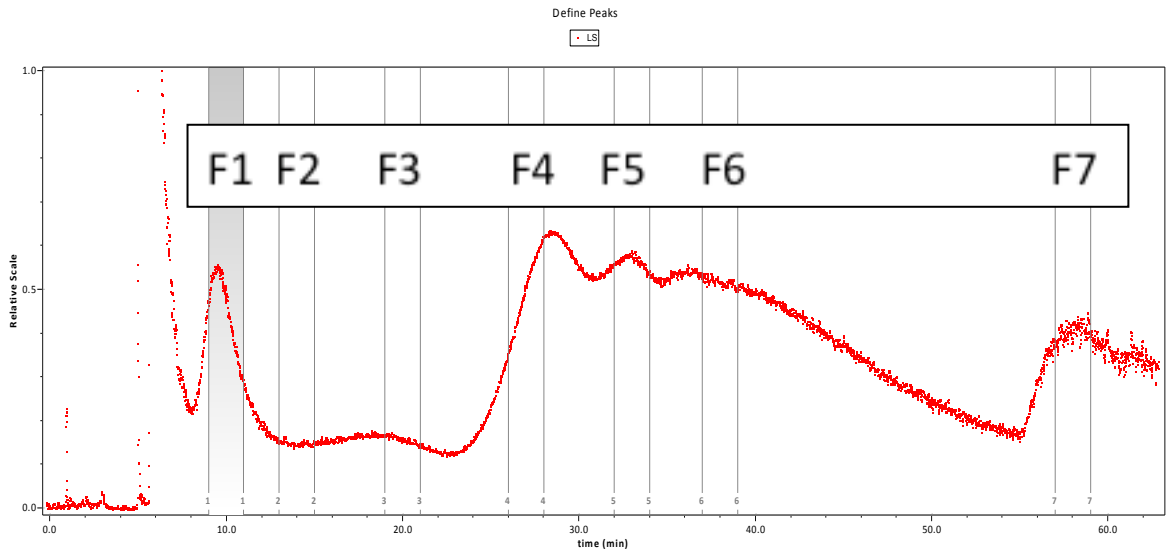

Figure 25: AF4-MALS of liposomes+serum. 1-7 collected fractions (in this example, run 187, liposome to serum ratio is 1:20)

In Figure 25 a scheme of collected fractions and pooled runs is reported.

2 min (2 mL fraction) F1: 9-11 min (HSA) F2: 13-15 min (IgG) F3: 19-21 min (LDL) F4: 26-28 min (*lipoproteins* band) F5: 32-34 min (*lipoproteins* band) F6: 37-39 min (*chylomicrons?*) F7: 57-59 min (field release)	Fractionated samples: 2 pooled runs for sample 1/20 at t=0 and t=24h 2 pooled runs for sample 1/100 at t=0 and t=24h

Table 11: collected fractions; fractionated samples

Figure 26 shows the results of HPLC-UV analysis. Elacytarabine peaks were calculated and converted in concentrations (gL/mL) as a function of fraction number. The results indicate that the higher amount of drug was found in fraction 2, the IgG fraction. It might be that on these fractions the HDL are eluted; so they are responsible for interactions with liposomes. LDL gives no interaction with the drug molecules, while the elacytarabine were also found in fractions 4 and 5, the lipoproteins fractions, with high amount.

The developed method is able to give fractions suitable for the HPLC-UV drug analysis, with only two pooled injections. Also the limit of detection, was calculated and found to be satisfactory for further, systematic studies (LoD < 0.007 µg/mL).

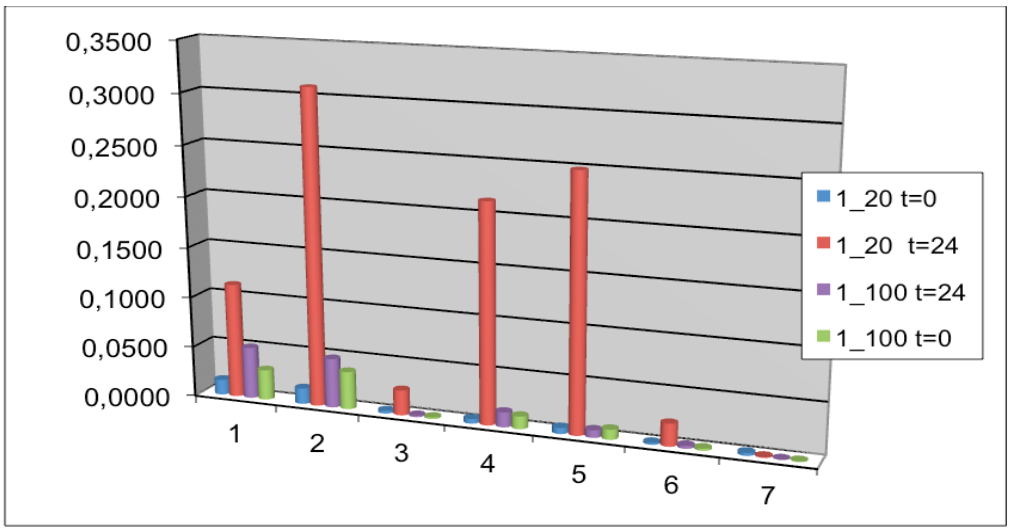

Figure 26: results of HPLC-UV analysis of collected fractions. mg/ml of elacytarabine vs fraction numbers for -1:20 liposomes+serum sample at **t=0** and **t=24 h**; and for -1:100 liposomes+serum samples at **t=0** and **t=24 h**.

5.5 - Conclusions

From the results one can summarize that:

(1) an analytical scale method for the size-based separation of serum component and for the size characterization of liposomes was developed. The goal was the improvement of the separation in the retention range between IgG and lipoproteins in a way to 'create' separative space for the elution of liposomes in between. The objective was not pursued: results indicate that liposomes still continue to exit with lipoproteins but it was not possible to discriminate whether co-elution is due to sample interactions or to aspecific phenomenon due to the method.

(2) The nature of co-elution of liposomes and lipoproteins was further investigated. An overloading study was performed in order to understand if it is an aggregation or an aspecific issue due to the method. The results indicate that there is an overloading effect due to the injected amount; and aggregation phenomena occurred.

(3) A micro-prep AF4-MALS method was then developed employing a channel height of 490 μm in order to avoid overloading and to allow increasing the injected amount. Higher sample loads were possible and the separation of lipoprotein - IgG - albumin was satisfying; and some differences between serum and liposomes + serum samples can be observed in the lipoproteins range.

(3) The liposomes/lipoproteins interactions were studied. Different incubation times for serum/liposome ratio 1:20; 1:50 and 1:100 were compared. Depending on the serum/liposome ratio, the differences among t=0 and t=12h and t=24h are more evident. Moreover, the comparison of fractionation profiles of different liposome to serum ratios confirms the presence of interactions with increased effect over time.

(4) Conformation analysis studiy on the "lipoproteins elution band", confirmed aggregation of liposomes and lipoproteins.

(5) An HLPC-UV analysis of elacytarabine distribution was performed on collected fractions with good analytical performances. The results indicate that the higher amount of drug was found in the IgG fraction. The hypothesis is that on this fraction the HDL are eluted; so they interact with liposomes. Elacytarabine was also found in fractions collected from the “lipoproteins” fractions, with high amount.

Section 3: FlFFF of functional nanoparticles in the context of drug delivery applications and nanorisk assessment

Chapter 6 – Characterization of Metal Organic Frameworks, a new material for azidothymidine delivery

6.1 - Introduction

One of the most used strategies in HIV therapy is the inhibition of retrotranscription and synthesis of proviral DNA. The class of drugs that exerts such a function is the Nucleoside Reverse Transcriptase Inihibitors (NRTI). NRTI are drug molecules whose chemical structure is the modified version of a natural nucleoside. These compounds suppress replication of retroviruses by interfering with the reverse transcriptase enzyme. The nucleoside analogues cause premature termination of the proviral (viral precursor) DNA chain. This class of drugs includes, among the other, azidothymidine (AZT).

AZT exerts its activity, like all NRTIs, *via* the metabolization to the triphosphate derivative [72, 73]. Phosphorylation takes place in the host's cells prior to nucleoside analogue incorporation into the viral DNA. However the process, which is actuated by the intracellular kinases, has very low efficiency [74]. Therefore the strategy to overcome this problem is to administer directly the triphosphate derivative of AZT (AZT-TP). Its molecular structure is reported in Figure 27.

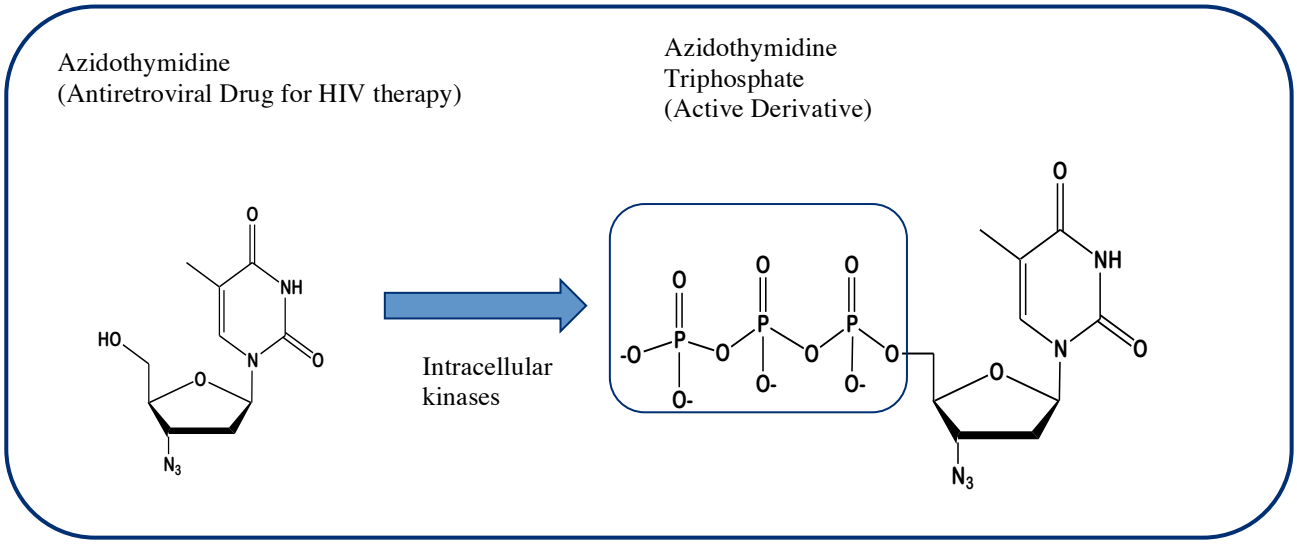

Figure 27: Azidothymidine triphosphate

However AZT-TP has some important problems which hinder its efficacy, like (a) short plasma half-life (1 h), (b) dose-dependent toxicities, (c) demands of frequent administration of high doses to maintain therapeutic drug levels (d) fluctuations of plasma drug concentration in intravenous administration with an initial high concentration that increases the risk of haematological toxicities and subsequent low drug levels those are below the therapeutic threshold (e) extensive first pass metabolism in oral administration. To overcome this bottleneck alternative strategies of administration are required.

Metal organic frameworks (MOFs) have gained increasing attention in the recent years due to their application in a variety of fields, such as gas storage, gas/vapor separation, catalysis, luminescence, as nanostructured materials. [75]. Moreover, in drug delivery they are used as carrier able to modulate the drug release of hosted entity like drug molecules, gene or proteins, to solubilize poorly soluble drugs and protect drugs from physiological degradation, [76]. They have been proposed also as valuable non-toxic nano-carriers for many anticancer and antiviral drugs like busulfan, cidofovir, doxorubicin and AZT-TP [77]. As nanostructured carriers, MOFs have to meet requirement such as bioavailability, non-toxicity and stability. Furthermore it has recently been reported that for medical applications a certain amount of chemical instability in the material becomes a desirable property, since the purpose of the carrier is to deliver and release the drug and once this function is completed it can degrade in situ [78].

The MOF used in this work is the MIL-100 (Material of Institute Lavoisier), whose structure is reported in Figure 28. Several ways of synthesis have been studied for this material, from hydro-solvothermal synthesis under dynamic or static, ambient or autogenous pressure conditions, assisted or not by microwave irradiation. The most interesting results come from the microwave assisted hydrothermal synthesis which is up to now the fastest one and gives high yields of small (<100 nm) and low polydispersed nanoparticles [79].

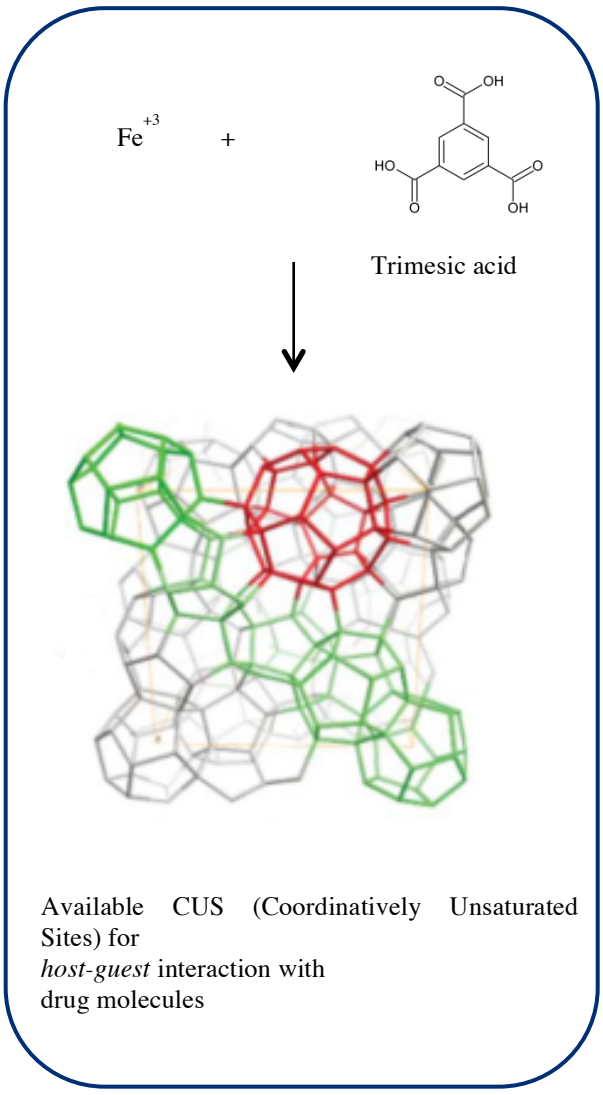

Figure 28: MIL-100 structure

MIL-100 is composed by Fe^{III} ions coordinated to a non-toxic, biocompatible carboxylic acid (trimesic acid). The resulting structure has coordinatively unsaturated sites (CUS) able to interact with host molecules.

The literature reports that AF4-MALS have been successfully used for the size-analysis, study of stability and drug release of NPs of different composition, since it allows for accurate size distribution analysis, investigation of NPs aggregation in native conditions, separation of the unbound constituents of the functional NPs and determination of the optical features of the NPs (separated from other dispersion components including free chromophores, or free drugs) [41]. Some example of its use on drug delivery nanoparticles

are the characterization of lipidic/liposomes particles [39, 80, 81], organic polymer particles like micelles (amphiphilic molecules), polymerosomes, dendrimers, nanocapsules and polymeric NPs [82, 83], [84-87] and biopolymer particles [88-92].

Given the importance of size distribution, morphology, size stability and functionality of drug vectors, in this work we propose AF4 coupled with MALS detection for the characterization of MOFs sample as carrier of NRTI drugs for the first time, with the following goals:

(1) to study the particle size distribution of MOFs;

(2) to study the particle size stability of MOFs over 24 hours;

(3) to qualitative evaluate the interaction of MIL-100 with 3 azidothymidine derivatives. For this aim four samples were chosen: the nude particles and the particles after interaction with drug in 3 different degrees of phosphorilation: azydothymidine (AZT, not phosporylated drug), azydothymidine monophosphate (AZT-MP) and azydothymidyne triphosphare (AZT-TP).

6.2 – Materials and methods

6.2.1 - Samples

MIL-100 (Fe) nanoMOFs were received from UMR CNRS 8612, Institute Galien Paris-Sud, as EtOH wet material, and stored in the dark at room temperature. Synthesis is achieved by means if an hydrothermal microwave assisted reaction described elsewhere [93]. An aliquot of wet material was suspended in a few mL of ethanol, then centrifuged (10 min, 10000 rpm) and subsequently washed two times with milli-Q water to completely remove the ethanol. Four samples were prepared, one was unconjugated MOF and the other three were drug conjugated MOFs (azidothymidine, azydothymidine monophosphate and azytothymidine triphosphate; MOF-AZT, MOF-AZT-MP, and MOF-AZT-TP, respectively). Aliquots of the centrifugate were taken and re-dispersed in water or aqueous solution of drug to achieve a final concentration of 0.02 mg/ml of the starting solid MOFs material and 0.02 mg/ml of MOFs and 0.1 mM of drug for the drug conjugated particles. 3’-azido-3’-deoxythymidine (AZT, Azido 3'- deoxythymidine, Moravek), 3’-azidothymidine monophosphate (AZT-MP, 3'-Azido-3'-deoxyD-thymidine 5'-monophosphate sodium salt, Carbosinth), 3’-azidothymidine triphosphate (AZT-TP, 3'-Azido-2',3'-dideoxythymidine-5'-Triphosphate lithium salt, TriLink) were used as received. Drugs were loaded within MOFs simply by impregnation (nanoparticles were incubated with aqueous solution of drug at room temperature for some minutes).

6.3 - Instrumental setup

6.3.1 – Separation and detection systems

AF4-MALS analysis was performed by using a 1100 Series HPLC system (Agilent Technologies, Palo Alto, CA), connected to a control module to control AF4 flow rates and operations (Eclipse 3, Wyatt Technology Europe, Dernbach, Germany). On-line detection

of the eluted species was performed with a MALS DAWN HELEOS detector (Wyatt Technology Corporation, Santa Barbara, CA). Carrier solutions were degassed using an on-line vacuum degasser Agilent, 1100 series (Agilent Technologies).

The separation device is a flat channel with a trapezoidal shape and capillary height. The channel was 152 mm long (Wyatt Technology Europe), equipped with a polyethersulfone membrane (Nadir), with a molecular weight cutoff of 10 kDa. The channel spacer was 350 µm tick, with trapezoidal shape (upstream width b_0 = 16 mm; downstream width b_L = 4 mm).

Figure 29 reports the flow program for the separation.

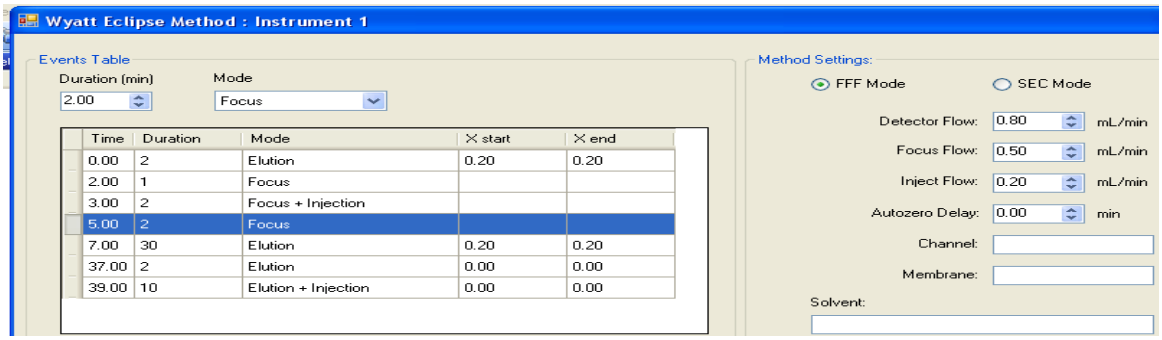

Figure 29: flow condition for the separation of MOF nanoparticles

It was set up as follows: two minutes of elution (cross-flow 0.2 ml/min) were applied to equilibrate the baselines on the detectors, then one minute focus-flow (0.5 mL/min) was applied to equilibrate the flows in the channel. Then 2 minutes injection (at a flow rate of 0.2 mL/min) in focus mode allow the sample to reach the channel, and two further minutes of focus were used to allow for a complete relaxation. After the focus step the elution starts with an isocratic cross flow step of 0.2 mL/min for 30 minutes. I final step of 10 minutes with no cross-flow was added to wash the channel and ensure complete elution of all particles.

6.3.2 – Zeta potential measurements

The nanonoparticles zeta potentials were measured with a Malvern® Nano-ZS instrument, Zetasizer Nano series, UK.

6.4 – Results and discussion

6.4.1 – MOFs particle size distribution

Figure 30 reports the Light scattering signal of the four samples at t=0. MOF particles were reconstituted, drug was added and the sample has been injected immediately after preparation.

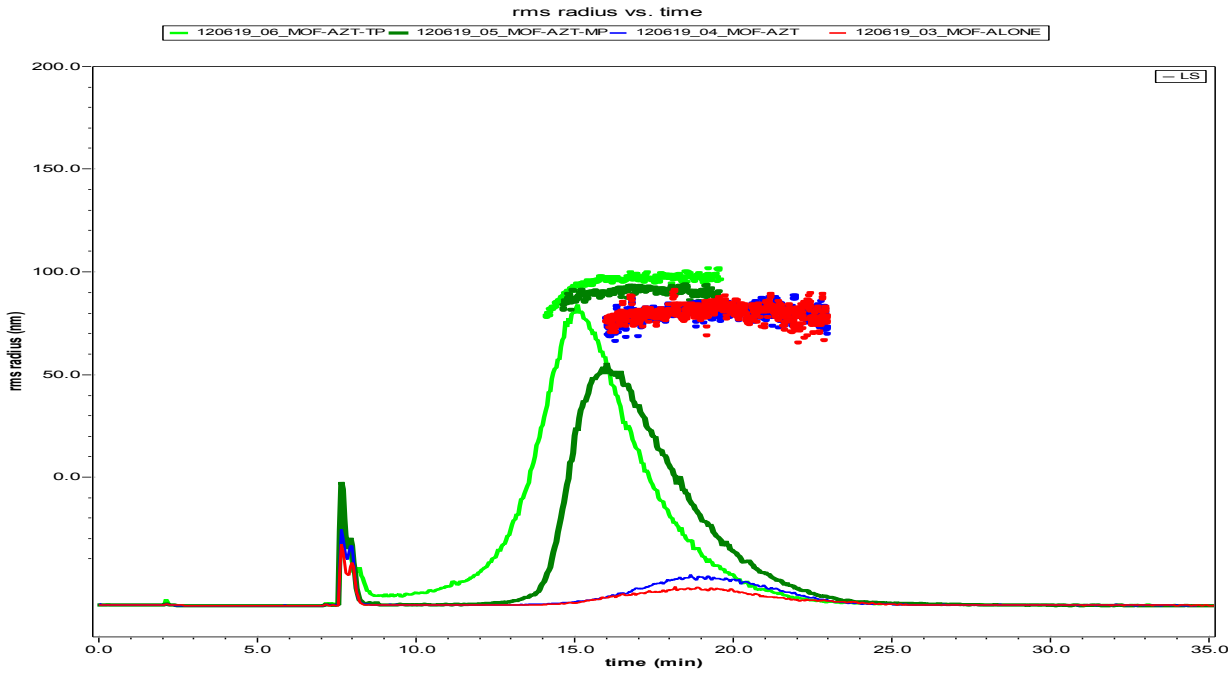

Figure 30*: fractograms of MOF samples immediatey after preparation. MOF-AZTTP; MOF-AZT-MP; MOF-AZT; Unconjugated MOF.*

All the fractograms are constituted of a first peak at minute 8, corresponding to the beginning of the elution step. It is due to both very small particles and to large aggregates that are not retained with the flow program of Figure 29. Then the main elution band appears, with variable intensity for the four samples. Unconjugated MOF has the weakest signals compared to the other samples, and the ratio between the void peak and the elution band is approximately 1, indicating that a certain amount of the starting material did

not take part in the nano porous MOF structure. Both the Gaussian shape of the peak and the monomodal distribution indicate a quite monodisperse sample, the RMS traces confirm this observation and the particle size is calculated to be around 80 nm. The same observations hold true for the MOF-ATZ-MP sample, furthermore it has about the same particle size distribution (85 nm). MOF-AZT-MP has a much more intense signal, with the left part of the peak quite Gaussian while the right branch is prolonged toward high retention time making the peak asymmetric. Particle size distribution is higher than those of unconjugated MOF and MOF-AZT, being about 90 nm. MOF-AZT-TP, has the most intense peak, it is also symmetrical, with a particle size higher than all the other samples, about 96 nm. RMS radii values are summarized in Table 12.

6.4.2 – MOF conjugation with drugs

From the variations of particle size and particle surface charge some considerations about the conjugation of MOF with the various azidothymidine derivatives are possible. Conjugation is here evaluated, by the means of MALS detection through the calculation of RMS radii and by zeta potential measurements of particles. Particle size distribution gives information on possible changes of the mass distribution of the particle itself once the interaction with other molecules, in this case drug molecules, occur. Zeta potentials gives information on particle charge, which depends upon the species bind to particle surface.

The RMS radius distributions of the four MOF samples at t=0 and at t=24 hours are listed in Table 12. Since all the samples are monodispersed, it make sense to report the distributions as a single value.

Sample	rms (nm)	
	1 hour (t=0)	24 hours (t=24)
MOF	80.79 ± 2.16	85.59 ± 2.22
MOF-AZT	80.78 ± 2.19	80.37 ± 3.11
MOF-AZT-MP	90.19 ± 2.03	89.75 ± 2.22
MOF-AZT-TP	96.78 ± 2.38	96.37 ± 2.21

Table 12: rms radius values expressed in nm of samples immediately after preparation and after 24 hours.

Zeta potential measurements are reported in Figure 31.

In Figure 30 and Table 12, it can be noticed that unconjugated MOF and MOF-AZT have exactly the same size (about 80 nm). therefore very poor interaction between azidothymidine and MOF can be hypothesized. When AZT-MP and AZT-TP are added to the particles, the distribution promptly increases to 90 nm and 96 nm. For this reason, it is possible to assume that the conjugation occurs. That fact that particles were reconstituted

and the AZT-MP solution immediately added indicates also a fast kinetic of conjugation: complexation of nanoparticles takes place in the minutes scale.

A hypothesis about the mechanism of complexation might be that the phosphate groups of AZT-MP and AZT-TP are involved on the conjugation and play a key role on the binding.

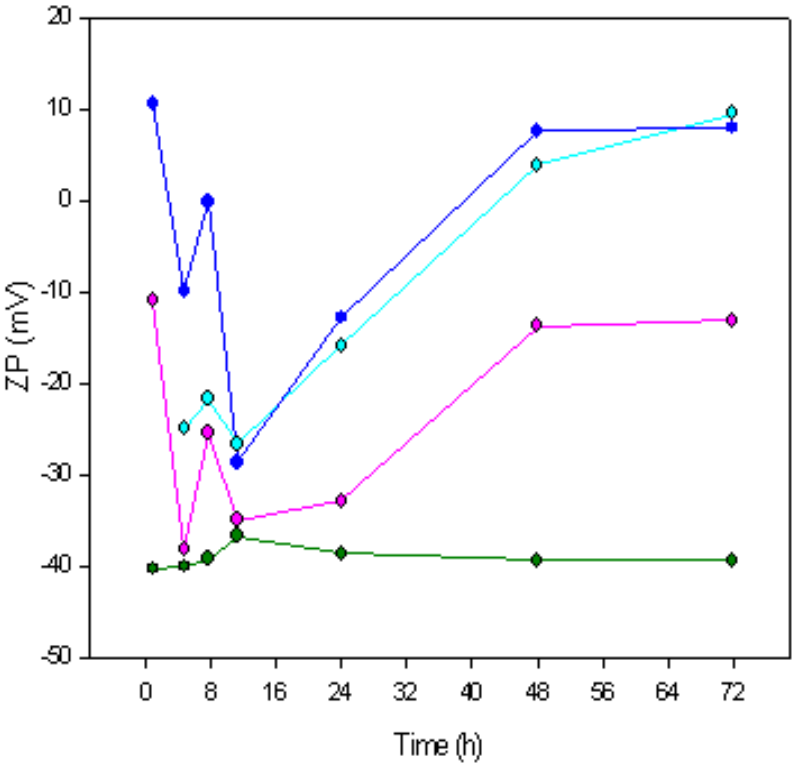

Figure 31: zeta potential of MOF, MOF-AZT, MOF-AZT-MP, and MOF-AZT-TP.

In Figure 31 all the particles have fluctuating surface charge, but on the average MOF-AZT-MP and MOF-AZT-TP have a negative charge which absolute value is higher when compared to MOF-AZT and most of all to MOF. These trends confirm that AZT-TP and AZT-MP actually bind MOF particles, while AZT gives poor interaction. Also the role of phosphate groups is confirmed to be crucial for the binding.

Zeta potential has also a key role on the elution behavior of particles because it influences relaxation inside the channel and retention time. Despite the theory would suggest smaller particles to elute first, in Figure 30 it can be noticed that the retention time is inverted

because larger particles elutes first. Since the channel membrane is negatively charged, conjugated particles are repelled away the membrane and they travel at higher position compared to unconjugated ones, where the flow stream is higher. The result is that bigger particles, in this case, elutes before the smaller ones (MOF-AZT-TP and MOF-AZT-MP have lower retention time than unconjugated MOF and MOF-AZT).

6.4.3 – Stability studies over 24 hours

In Figure 32 are reported the LS fractograms of unconjugated MOF samples immediately after preparation (red fractograms and rms distributions) and after 24 hours (black fractograms and rms distributions).

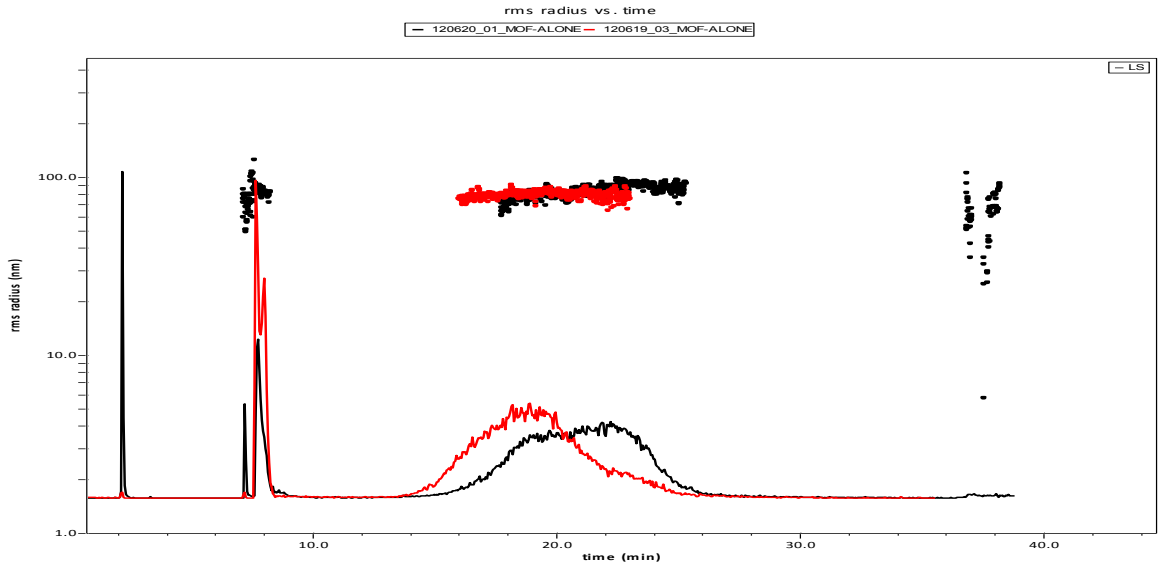

Figure 32: unconjugated MOF samples, at t=0 and after 24 hours, t=24

At t=0, the fractogram is constituted by Gaussian, monomodal distribution band, with a maximum at 18 minutes followed by a small shoulder at 22 minutes. After 24 hours (black traces), the trend is inverted, since unconjugated MOF samples gives a fractogram characterized by a band having two distinct maximum, the lower one at 18 minutes and the second, highest one, at 22 minutes. Despite the root mean square distributions are superimposable, this change in band shape indicates the start of an aggregation phenomenon.

The same analysis was performed on MOF-AZT samples, and results are reported in Figure 33. Immediately after preparation the fractogram is constituted by a Gaussian, intense and symmetric band. The maximum in the retention time band at t=0 is at 15 minutes, at this retention time after 24 hours of incubation the fractogram has only a weak

band (slightly shifted toward higher retention times, at about 16 minutes) and a second main band at 29 minutes.

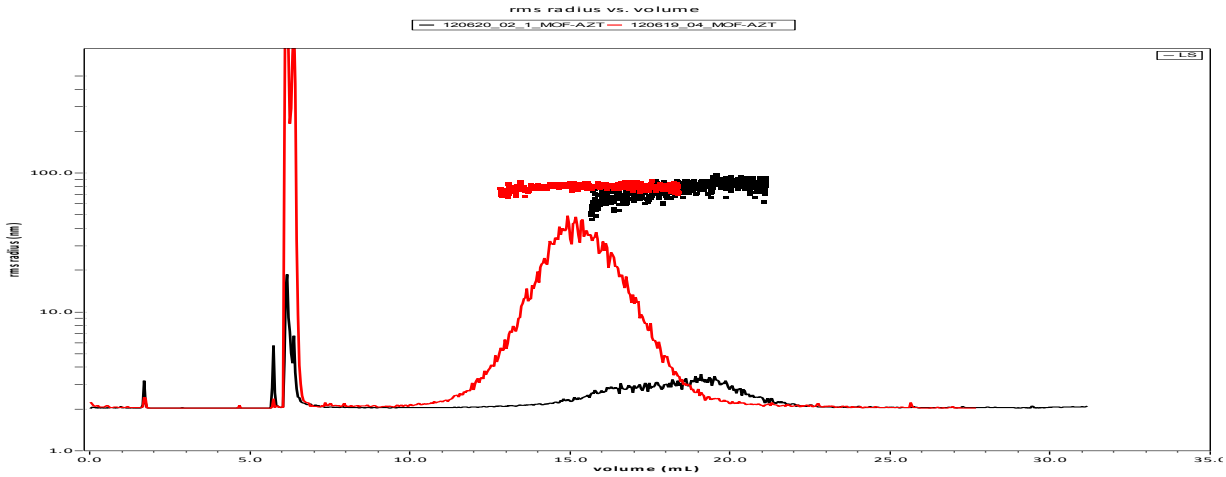

Figure 33: MOF-AZT sample, injection at t=0 and at t=24 hours.

Also in this case a the RMS traces do not indicates significative changes on the particle size distribution, however the fractogram shape suggests some aggregation on the sample.

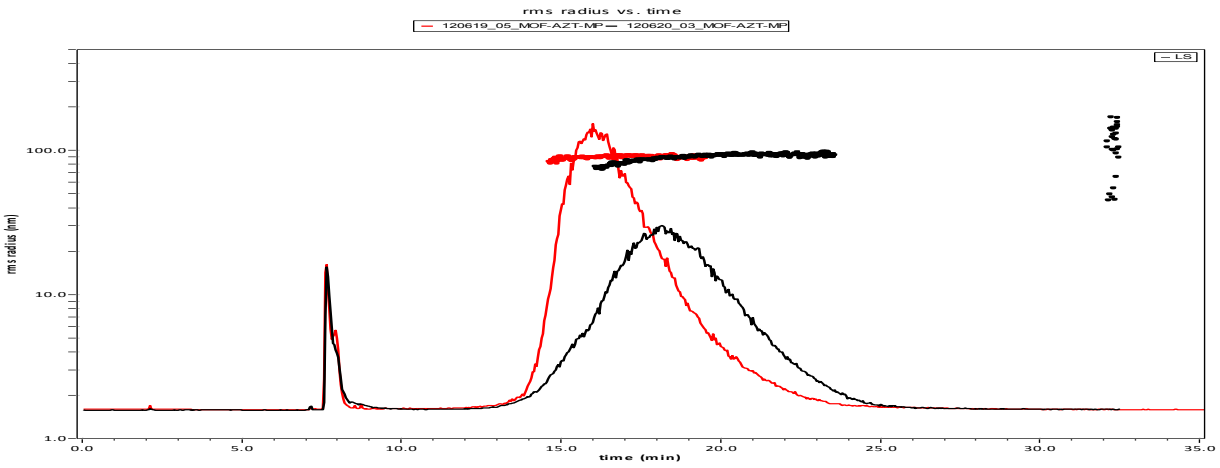

Figure 34: MOF AZT-MP sample, injection immediately after preparation and MOF-AZT-MP at t=24 hours.

Figure 34 shows the fractograms of the MOF-AZT-MP system. The two bands relative to t=0 and t=24 hours both indicate monomodal distributions. The dispersion seems to be stable in the 24 hours time frame, since there is only a little variation in the LS signal intensity, and the PSD given by the RMS radius does not vary with time.

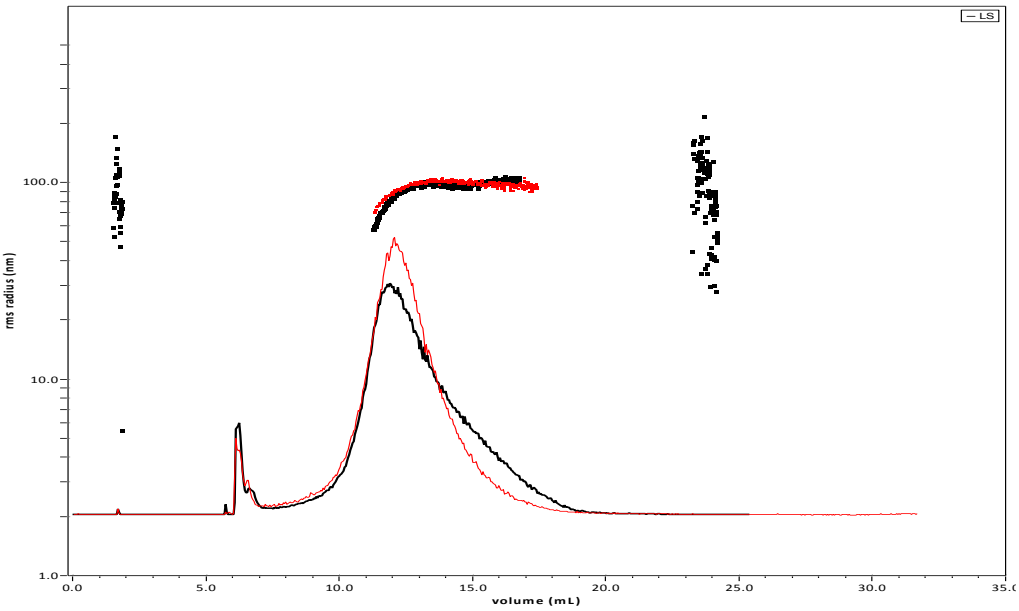

Figure 35: MOF AZT-TP at t=0, MOF AZT-TP at t=24 hours

Figure 35 shows the fractograms of the MOF-AZT-TP system. Elution bands are both quite symmetric, and signal intensities are comparable. Also the retention times are equal (12 minutes), indicating the stability of samples.

Zeta potential, is known to influence nanoparticle stability. For this reason one can assume that the aggregation phenomena suggested by the fractograms of unconjugated MOF and MOF-AZT (Figure 32 and Figure 33) are due to the absence of phosphate groups that leads to a particle charge that is more fluctuating and with values closer to 0 (Figure 31) compared to that of MOF-AZT-MP and MOF-AZT-TP.

6.5 - Conclusions

From a general point of view, the MOF particles here studied show no significative changes in RMS radius in the time frame of 24 hours. Phosphate groups contribute to the stability of particles giving a strong negative charge to the particle surface, so that the stability partially depends from conjugation. As a result, MOF-AZT-TP and MOF-AZT-MP are the most stable system, and their fractograms do not change with time. Unconjugated MOF and MOF-AZT seem to be stable as well according to the RMS radii, but fractogram shapes clearly indicate aggregation phenomena.

Conjugation with drugs was studied both with zeta potential measurements and through RMS distribution analysis. AZT gives poor conjugation, while AZT-MP and AZT-TP are uptaken from MOF particles.

AF4-MALS is here shown once again to be a useful methodology to analyze particles used in drug delivery application. The size separation together with the unique gentle separation mechanism is crucial to avoid loss of aggregates and to detect them, allowing for the identification of aggregates even when they are present in sufficient small amount to do not vary significantly the particle size distribution.

Morphological characterization is straightforward from the evaluation of RMS distributions, the same is for particle size stability. A starightforward evaluation of the drug conjugation was possible as well.

Chapter 7 – Hollow Fiber FlFFF coupled to ICP-MS for the rapid detection of metal nanoparticles

7.1 – Introduction

It is today a subject of increasing relevance for the scientific and industrial community the definition of protocols for the quality control and risk assessment of nanoparticles and nanodevice - engineered materials in general.

In the previous chapters are discussed various aspects of the characterization of particles for application in medicine, a field that for historical reasons has rigid and defined protocols of controls aimed to ensure the quality of the materials in use. However, the number of nanoparticle-containing product is immense, and many of them were put on the market before the international community started to focus on the theme of nanorisk. In this chapter the characterization of nanoparticles is devoted to assess the risk involved onto the use of a widely spread material-containing nanoparticles: tattoo inks. This material has been chosen for two main reasons, the first of which is that it is widely used, while the second one is because tattoo inks are injected on the skin by deposition under the first superficial layer of epidermis, where they lay for the rest of the individual's life without any, or at least not known, mechanism of metabolism. Being the time of residence of inks under the skin virtually infinite, the hypothesis of either instant or gradual release on the body fluids of dangerous or potentially hazardous substances has not to be excluded.

The characterization of a set of tattoo inks is here proposed with the purpose to perform an elemental characterization and then to investigate whether metal NPs are present or not in the samples. For the first aim an AF4 and an HF5 methods are developed to size separate and characterize the inks, by means of MS compatible carrier solutions. AF4 and HF5 performances are then briefly discussed. HF5 was then hyphenated with ICP-MS for the element identification and to determine the elemental composition of anoparticles contained in the inks.

7.2 – Materials and methods

7.2.1 - Samples

All original samples (red, white, brown, orange and black inks) were used as received from manufacturer without any chemical pre-treatment. Inks were diluted 1:2000 in 0.1% Triton X-100. The diluted samples were sonicated for 15 min prior to injection. The sample dilution in surfactant and the sonication had the purpose of disrupting large particles aggregates, which could interfere with the separation process and/or be out of the FFF operational range or even lead to aggregates formation (NPs coating the surface of existing aggregates).

Triton X-100 surfactant was purchased from Fluka.

7.2.2 - Methods

For the HF5 separation, the injection volume was 2µL. Milli-Q water was used as mobile phase, both for simplicity (compatibility with water-soluble tattoo inks) and because pure water is more suitable than buffers which contain salts for the coupling with ICP-MS. The HF5 employed separation methods and flow conditions ere described in Figure 36.

Start Time (min)	End Time (min)	Duration (min)	Mode	Vx Start (mL/min)	Vx End (mL/min)
0.00	1.00	1.00	Focus		
1.00	4.00	3.00	Focus + Inject		
4.00	14.00	10.00	Elution	0.30	0.10
14.00	24.00	10.00	Elution	0.10	0.10
24.00	26.00	2.00	Elution + Inject	0.00	0.00

Figure 36: flow conditions for HF5 separation.

Focus Flow was 0.85 mL/min and detector flow was 0.5 mL/min. The method starts with one minute of focus, followd by 3 minutes of sample injection and focusing. Afterwards ten minutes of elution with a cross flow gradient linearly decreasing from 0.30 to 0.10 mL/min and 10 minutes of isocratic cross flow of 0.10 mL/min allow for sample separation. At the

end of the method 2 minutes of elution and injection with no cross flow were put to wash the system. The channel was 17 cm long cylindrical PES membrane with a 0.8 mm internal diameter and a 10 kDa cut-off. Both UV signals (at 280 nm) and LS signals were recorded.

In Figure 37, the flow conditions for the AF4 method are reported.

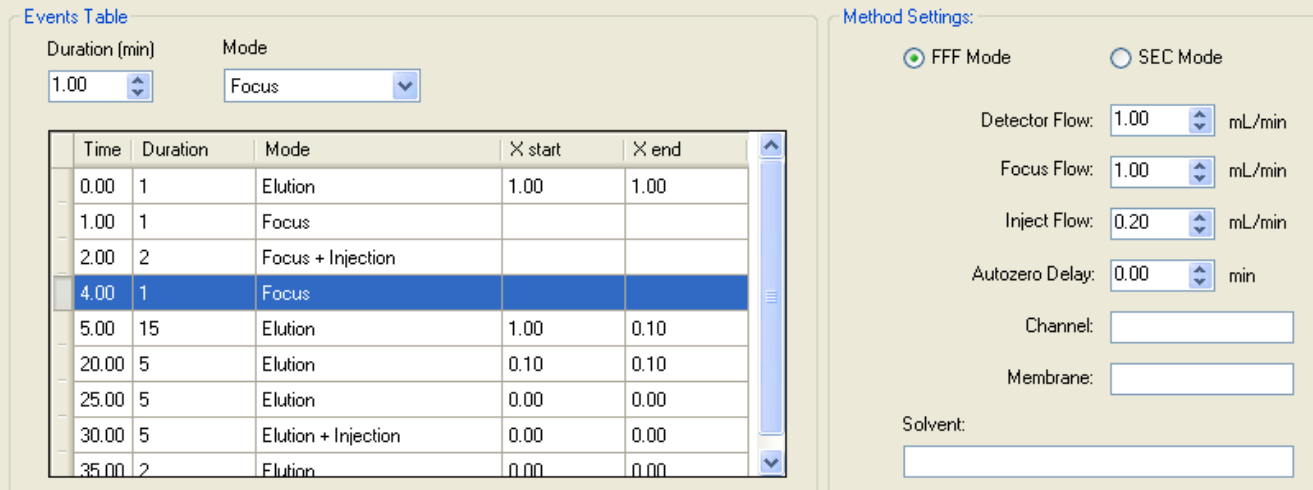

Figure 37: Flow conditions for AF4 separation

Also in this case injection volume was 2 µL. The channel was 265 mm long equipped with a regenerated cellulose ultrafiltration membrane (cut-off 10 kDa) and a spacer 250 µm tick with trapezoidal shape. Detector flow and focus flow were 1 mL/min each, inject flow was 0.2 mL/min. Elution and focus steps at the beginning of the method were put to equilibrate the flows in the separation system. Afterward sample was injected and focused for 3 minutes. For the separation of NPs a cross flow gradient from 1.00 mL/min to 0.1 mL/min followed by 5 min of 0.1 mL/min cross-flow was used.

7.3 - Instrumental setup

Separation systems were an Eclipse 3+ for AF4 separation (Wyatt Technology Europe) and an Eclipse DUALTEC (Wyatt Technology Europe) for HF5 separation, equipped with a

1100 and a 1200 Agilent HPLC systems, respectively. Detection was operated by a MALS detector (model Dawn Heleos, Wyatt Technology Europe).

ICP instrument was an iCAP Qc ICP-MS (Thermo Scientific), on-line coupled with a Dualtech (Wyatt Technology) separation system. After separation sample was indrotucted on the ICP by means of a PFA-ST nebulizer, equipped with a Quartz glass spraychamber (Quartz 2.0 mm ID injector, Ni sample cone, Ni skimmer cone). The quadrupole cell was a Qcell, operating in KED mode. He flux was 4.8 mL/min.

7.4 – Results and discussion

The HF5 method was applied to the fractionation of black ink sample in order to obtain characteristic size-based fractionation profiles, results are reported in Figure 38.

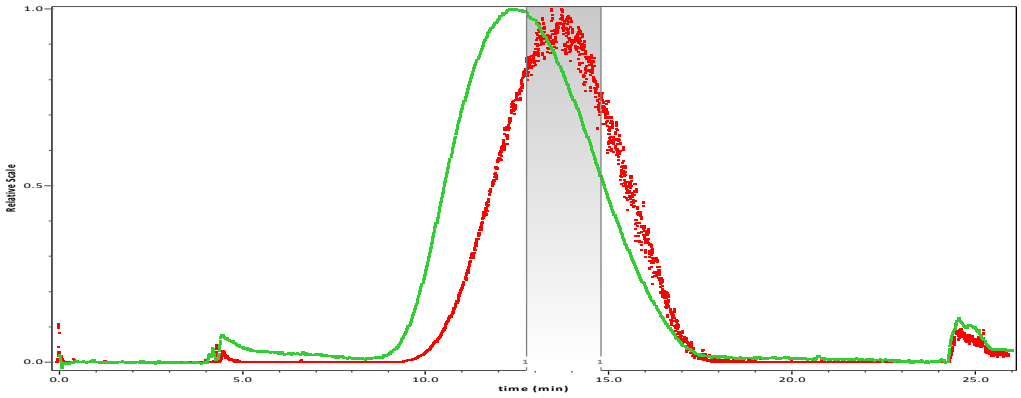

Figure 38: UV signal at 280 nm (green line) and light scattering signal at 90° (red points).

The elution UV profile shows a slightly tailed and broad (over 8 min) gaussian peak indicating a monomodal distribution of nanoparticles continuously distributed, the LS signal maximum is shifted to higher retention time with respect to UV signal, because LS is more sensible to bigger particles. In Figure 39 the AF4-MALS profile and RMS values for Black ink sample are reported. The fractionation results in a gaussian and symmetric peak eluting in a wide interval range and with a peak maximum at 10 min.

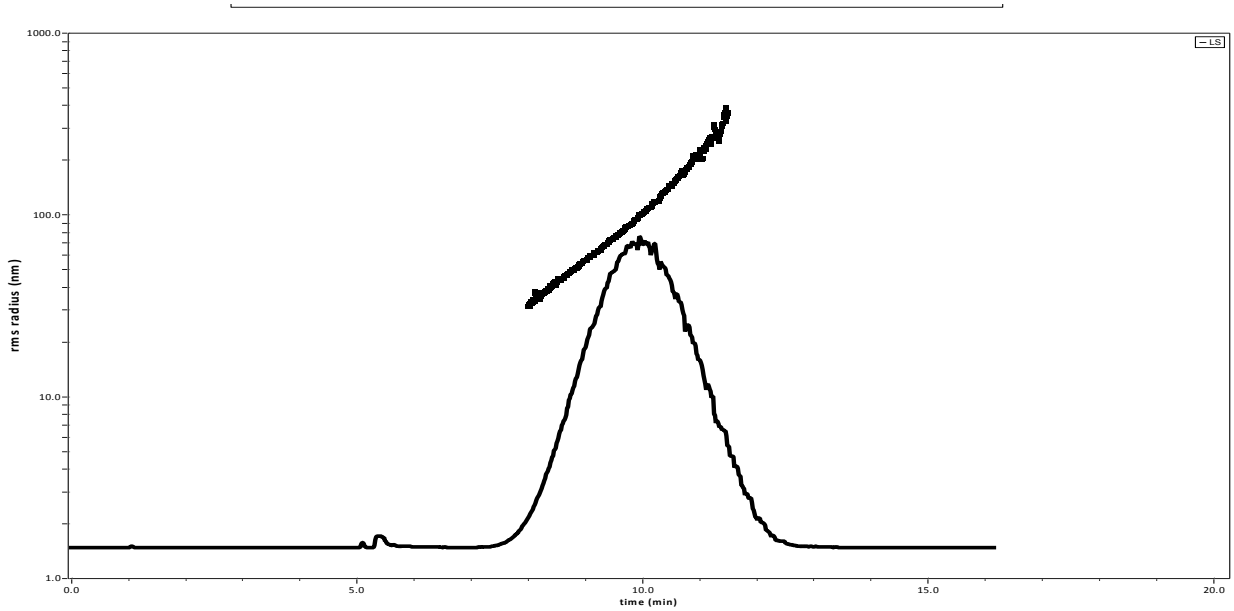

Figure 39: Fractogram and RMS distribution of Black sample.

Such a gaussian band indicates a monomodal distribution of a single population of nanoparticles continuously distributed in the range 30 nm – 300 nm (as indicated by values of RMS distribution). Sample is therefore highly polydispersed.

HF5 peak is 7 minutes, while AF4 peak is 5 minutes. Being the detector flow 0.5 mL/min and 1 mL/min respectivley, it means that HF5 allows to fractionate the particles in a lower volume with a lower dilution factor. HF5 can operate at low flow rates, which makes it the ideal candidate for coupling off/online with mass spectrometry. Therefore the HF5 separation techniques was then coupled to ICP-MS for a fast screening of further smples. The aim was at first to detect metals and then ascertain which of them constitutes nanoparticles. For this aim at first Flow Injection Analysis (FIA) were performed. FIA is based on the injection of a liquid sample into a continuous carrier stream ao that the sample is transported toward a detector that continuously records the the signal due to the passage of the sample meaterial through the flow cell [94].

In the case of HF5 a flow injection analysis indicates that no sample components cross the permeable, accumulation wall of the HF5 channel and all the species are detected. This approach was used for the total elemental quantification. Result are reported in Figure 40.

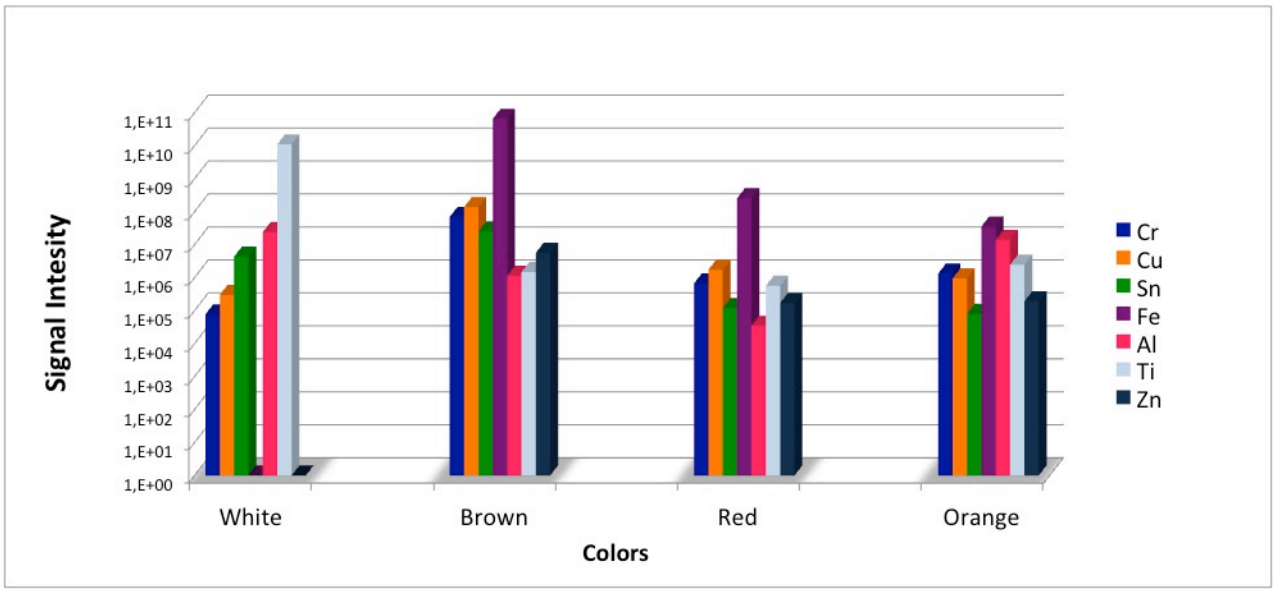

Figure 40: Relative amount of Cr, Cu, Sn, Fe, Al, Ti, Zn in White, Brown, Red and Orang tattoo inks obtained by means of FIA

The graph of Figure 40 reports the relative amount of elements on every ink. White Ink contains mainly Ti, brown ink contains high amount of Cu, while Red ink contains high amount of Fe.

Brown, red and white inks were injected a second time with the method of Figure 36 in order to determine which elements are assembled on nanoparticles. Results are reported in Figure 41a (Cu detection in Brown inks), Figure 41b (Fe detection in Brown inks), Figure 41c (Fe detection in Red inks), Figure 41d (Ti detection in white inks).

In Figure 41(a) and (b) retained peaks with maximum at approximately 330 seconds and after 1000 seconds indicates that nanoparticles are eluting and that the ICP-MS response indicates that they are mainly composed of Cu and Fe. Figure 41(c) indicates that red ink contains Fe nanoparticles while white ink contains big and highly retained Ti particles according to Figure 41(d).

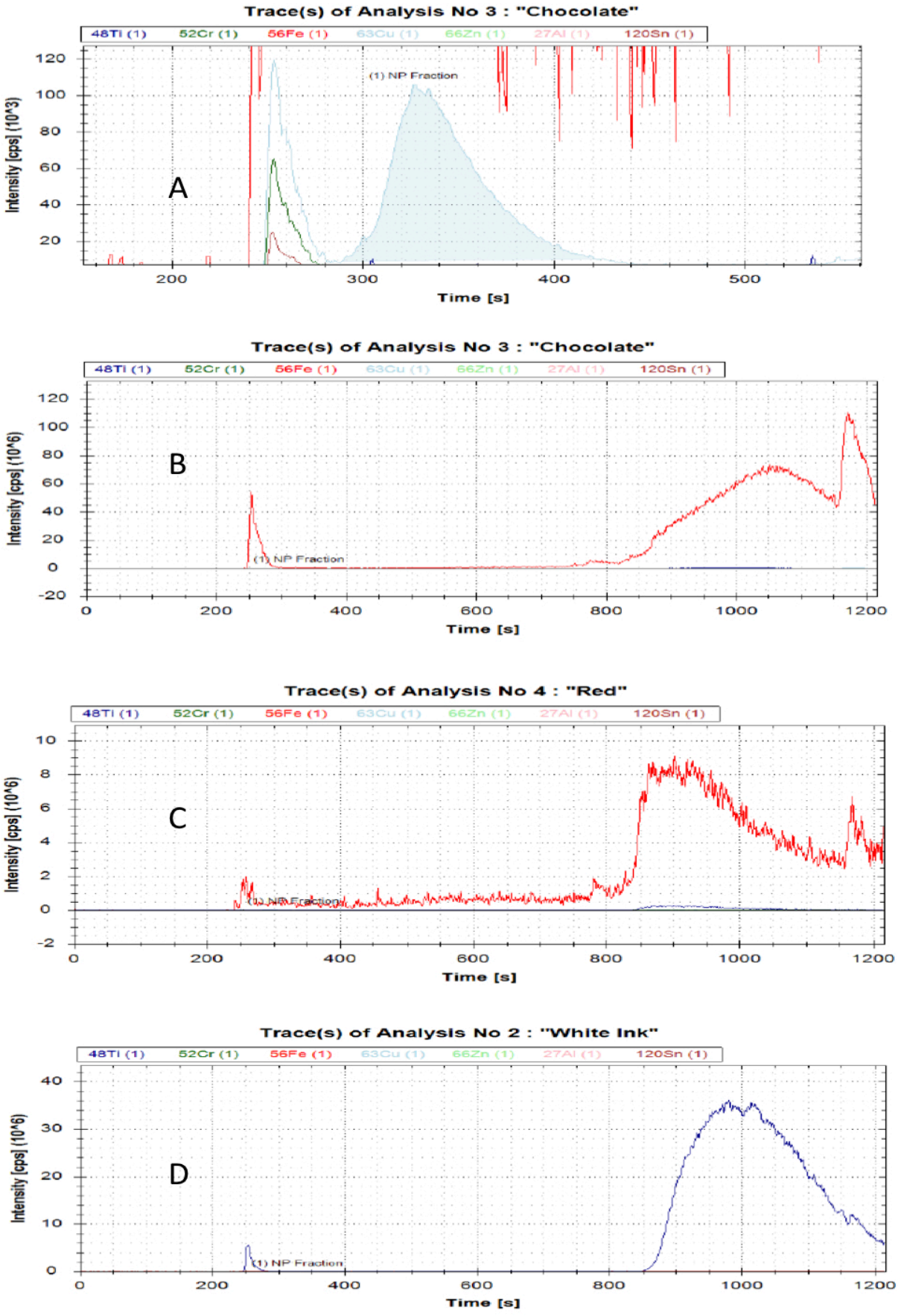
Trace(s) of Analysis No 3 : "Chocolate"
48Ti (1)
52Cr (1)
56Fe (1)
63Cu (1)
66Zn (1)
27Al (1)
120Sn (1)
(1) NP Fraction
A
Intensity [cps] (10^3)
Time [s]
Trace(s) of Analysis No 3 : "Chocolate"
B
Intensity [cps] (10^6)
Time [s]
Trace(s) of Analysis No 4 : "Red"
C
Intensity [cps] (10^6)
Time [s]
Trace(s) of Analysis No 2 : "White Ink"
D
Intensity [cps] (10^6)
Time [s]

Figure 41: (a) Cu detection in Brown ink, (b) Fe detection in Brown ink, (c) Fe detection in red ink, (d) Ti detection in white ink.

7.5 - Conclusions

In this study it is highlighted that in HF5 the longitudinal flow rate (also known as detector flow rate) was 0.5 mL/min. This is the maximum flow rate value – under the specifications of the manufacturer. Based on the sample characteristics and on the separation performance objectives (resolution, efficiency ecc.), a detector flow rate lower than 0.5 mL/min is usually employed. Furthermore the HF5 cartridge is commercially available in a disposable format - the separation device can be easily replaced between subsequent injections, thus eliminating the sample carry-over effect. Considering the fact that the same sample amount was injected (2 µL) and the fact the peak volume is lower for HF5, it is proved that HF5 provides better sensitivity when compared to AF4. HF5 operates at lower flow rates (which also makes it ideal for the trace analysis and for the on-line coupling with ICP-MS, making possible the online analysis of samples to correlate samples properties to different size subpopulations). The HF5 separation device has a channel volume of 85 µL while the flat channel has channel volume of 465 µL (in the configuration used in this study). The volume of flat channel is five-fold the HF5 channel volume, this means that the latter provides much lower sample dilution and therefore the UV and LS signals are more intense.

According to these premises the HF5 was suitably coupled to ICP-MS for the fast analysis of sample of ink for tattoo. Rather than an in dept characterization of sample which is indeed possible, it is here shown that HF5-ICP-MS can be used also as a tool for fast metal nanoparticle screening. It is of particular relevance the possibility to work both in FIA mode, a procedure that allows for a rapid metal identification and subsequentely fractionate the sample in order to identify which species actually form nanoparticles.

References

1. Chaudhry, Q., et al., *Applications and implications of nanotechnologies for the food sector.* Food Additives & Contaminants: Part A, 2008. **25**(3): p. 241-258.

2. Wiesner, M.R., et al., *Decreasing Uncertainties in Assessing Environmental Exposure, Risk, and Ecological Implications of Nanomaterials†‡.* Environmental Science & Technology, 2009. **43**(17): p. 6458-6462.

3. Barth, N., C. Schilde, and A. Kwade, *Influence of Particle Size Distribution on Micromechanical Properties of thin Nanoparticulate Coatings.* Physics Procedia, 2013. **40**: p. 9-18.

4. Gaumet, M., et al., *Nanoparticles for drug delivery: The need for precision in reporting particle size parameters.* European Journal of Pharmaceutics and Biopharmaceutics, 2008. **69**(1): p. 1-9.

5. Giddings, J.C., *FIELD-FLOW FRACTIONATION - ANALYSIS OF MACROMOLECULAR, COLLOIDAL, AND PARTICULATE MATERIALS.* Science, 1993. **260**(5113): p. 1456-1465.

6. P, R., et al., - *Field-flow fractionation and biotechnology.* - Trends Biotechnol. 2005 Sep;23(9):475-83., (- 0167-7799 (Print)): p. - 475-83.

7. Rambaldi, D.C., P. Reschiglian, and A. Zattoni, *Flow field-flow fractionation: recent trends in protein analysis.* Analytical and Bioanalytical Chemistry, 2011. **399**(4): p. 1439-1447.

8. S. Williams, R.K., *Field-Flow Fractionation in Biopolymer Analysis*. X ed, ed. Springer.

9. Thielking, H., D. Roessner, and W.-M. Kulicke, *Online Coupling of Flow Field-Flow Fractionation and Multiangle Laser Light Scattering for the Characterization of Polystyrene Particles.* Analytical Chemistry, 1995. **67**(18): p. 3229-3233.

10. Wyatt, P.J., *Light scattering and the absolute characterization of macromolecules.* Analytica Chimica Acta, 1993. **272**(1): p. 1-40.

11. Bangham, A.D. and R.W. Horne, *Negative staining of phospholipids and their structural modification by surface-active agents as observed in the electron microscope.* Journal of Molecular Biology, 1964. **8**(5): p. 660-IN10.

12. Papahadjopoulos, D. and J.C. Watkins, *Phospholipid model membranes. II. Permeability properties of hydrated liquid crystals.* Biochimica et biophysica acta, 1967. **135**(4): p. 639-52.

13. Olson, F., et al., *Preparation of liposomes of defined size distribution by extrusion through polycarbonate membranes.* Biochimica et biophysica acta, 1979. **557**(1): p. 9-23.

14. Hope, M.J., et al., *Production of large unilamellar vesicles by a rapid extrusion procedure - Characterization of size distribution, trapped volume and ability to mantain a membrane-potential.* Biochimica Et Biophysica Acta, 1985. **812**(1): p. 55-65.

15. Mayhew, E., et al., *High-Pressure continuous-flow system for drug entrapment in liposomes.* Methods in Enzymology, 1987. **149**: p. 64-77.

16. Milsmann, M.H., R.A. Schwendener, and H.G. Weder, *The preparation of large single bilayer liposomes by a fast and controlled dialysis.* Biochimica et biophysica acta, 1978. **512**(1): p. 147-55.

17. Szoka, F., Jr. and D. Papahadjopoulos, *Procedure for preparation of liposomes with large internal aqueous space and high capture by reverse-phase evaporation.*

Proceedings of the National Academy of Sciences of the United States of America, 1978. **75**(9): p. 4194-8.

18. Gregoriadis, G., *Liposomes: European research.* Science (New York, N.Y.), 1978. **201**(4352): p. 211-3.

19. Gregoriadis, G., *Liposomes in therapeutic and preventive medicine: the development of the drug-carrier concept.* Annals of the New York Academy of Sciences, 1978. **308**: p. 343-70.

20. Hamori, C.J., et al., *TARGETING ZINC PROTOPORPHYRIN LIPOSOMES TO THE SPLEEN USING RETICULOENDOTHELIAL BLOCKADE WITH BLANK LIPOSOMES.* Pediatric Research, 1993. **34**(1): p. 1-5.

21. Liu, D.X., A. Mori, and L. Huang, *ROLE OF LIPOSOME SIZE AND RES BLOCKADE IN CONTROLLING BIODISTRIBUTION AND TUMOR UPTAKE OF GM1-CONTAINING LIPOSOMES.* Biochimica Et Biophysica Acta, 1992. **1104**(1): p. 95-101.

22. Colas, J.C., et al., *Microscopical investigations of nisin-loaded nanoliposomes prepared by Mozafari method and their bacterial targeting.* Micron, 2007. **38**(8): p. 841-7.

23. Ruozi, B., et al., *AFM, ESEM, TEM, and CLSM in liposomal characterization: a comparative study.* International journal of nanomedicine, 2011. **6**: p. 557-63.

24. Kuntsche, J., J.C. Horst, and H. Bunjes, *Cryogenic transmission electron microscopy (cryo-TEM) for studying the morphology of colloidal drug delivery systems.* International journal of pharmaceutics, 2011. **417**(1-2): p. 120-37.

25. Ruozi, B., et al., *Atomic force microscopy and photon correlation spectroscopy: two techniques for rapid characterization of liposomes.* European journal of

pharmaceutical sciences : official journal of the European Federation for Pharmaceutical Sciences, 2005. **25**(1): p. 81-9.

26. Balashev, K., et al., *Kinetics of degradation of dipalmitoylphosphatidylcholine (DPPC) bilayers as a result of vipoxin phospholipase A2 activity: an atomic force microscopy (AFM) approach.* Biochimica et biophysica acta, 2011. **1808**(1): p. 191-8.

27. Eshuis, A., et al., *EXPERIMENTAL-DETERMINATION OF PARTICLE-SIZE DISTRIBUTIONS IN COLLOIDAL SYSTEMS BY DYNAMIC LIGHT-SCATTERING - APPLICATION TO POLYSTYRENE LATEX SPHERES AND TO NONIONIC MICROEMULSIONS.* Langmuir, 1985. **1**: p. 289-293.

28. Stock, R.S. and W.H. Ray, *MEASUREMENT OF THE PARTICLE-SIZE DISTRIBUTION OF LATEX-PARTICLES BY DYNAMIC LIGHT-SCATTERING.* Abstracts of Papers of the American Chemical Society, 1985. **190**: p. 12-PME.

29. Wagner, J., *PARTICLE-SIZING BY DYNAMIC LIGHT-SCATTERING.* Chemie Ingenieur Technik, 1986. **58**: p. 578-583.

30. Goldburg, W.I., *Dynamic light scattering.* American Journal of Physics, 1999. **67**(12): p. 1152-1160.

31. Bryant G., J.C.T., *Improved Particle Size Distribution Measurements Using Multiangle Dynamic Light Scattering.* Langmuir, 1995(11): p. 2480 - 2485.

32. Brandl M., I.L., *Determination of the size distribution of liposomes by SEC fractionation, and PCS analysis and enzymatic assay of lipid content.*
. AAPS PharmSciTech, 2002. **3**(2).

33. Grabielle-Madelmont, C., S. Lesieur, and M. Ollivon, *Characterization of loaded liposomes by size exclusion chromatography.* Journal of Biochemical and Biophysical Methods, 2003. **56**(1-3): p. 189-217.

34. Ingebrigtsen, L. and M. Brandl, *Determination of the size distribution of liposomes by SEC fractionation, and PCS analysis and enzymatic assay of lipid content.* AAPS PharmSciTech, 2002. **3**(2): p. E7-E7.

35. Hupfeld, S., et al., *Liposome size analysis by dynamic/static light scattering upon size exclusion-/field flow-fractionation.* Journal of Nanoscience and Nanotechnology, 2006. **6**(9-10): p. 3025-3031.

36. Hupfeld, S., *Size Characterisation of Liposomes Using Asymmetrical Flow Field-Flow Fractionation - Factors Influencing Fractionation and Size Determination*, in *Department of Pharmacy*. 2009, University of Tromsø, Norway: Tromsø. p. 80.

37. Hupfeld, S., D. Ausbacher, and M. Brandl, *Asymmetric flow field-flow fractionation of liposomes: optimization of fractionation variables.* Journal of Separation Science, 2009. **32**(9): p. 1465-1470.

38. Hupfeld, S., D. Ausbacher, and M. Brandl, *Asymmetric flow field-flow fractionation of liposomes: 2. Concentration detection and adsorptive loss phenomena.* Journal of Separation Science, 2009. **32**(20): p. 3555-3561.

39. Hupfeld, S., et al., *Liposome fractionation and size analysis by asymmetrical flow field-flow fractionation/multi-angle light scattering: influence of ionic strength and osmotic pressure of the carrier liquid.* Chemistry and Physics of Lipids, 2010. **163**(2): p. 141-147.

40. Evjen, T.J., et al., *Physicochemical characterization of liposomes after ultrasound exposure - Mechanisms of drug release.* Journal of Pharmaceutical and Biomedical Analysis, 2013. **78-79**: p. 118-122.

41. Zattoni, A., et al., *Flow field-flow fractionation for the analysis of nanoparticles used in drug delivery.* Journal of Pharmaceutical and Biomedical Analysis, 2014. **87**(0): p. 53-61.

42. Sahoo, S.K., F. Dilnawaz, and S. Krishnakumar, *Nanotechnology in ocular drug delivery.* Drug discovery today, 2008. **13**(3-4): p. 144-51.

43. George H. Rothblat, M.d.l.L.-M., Veronique Atger, Ginny Kellner-Weibel, and M.C.P. David L. Williams, *Cell cholesterol efflux: integration of old and new observations provides new insights.* Journal of lipid research, 1999. **40**: p. 781 - 796.

44. Kenji Inoue, S.K., Tadahiko Tsuru, Makoto Araie, Yousuke Seyama, *Cholestanol Induces Apoptosis of Corneal Endothelial and Lens Epithelial Cells.* Investigative Ophthalmology & Visual Science, 2000. **41**(5).

45. Vey, N., *Elacytarabine – A New Agent in the Treatment of Relapsed/Refractory Acute Myeloid Leukaemia.* European Oncology & Haematology, 2012. **8**(2): p. 111–15.

46. Galmarini, C.M., et al., *Potential mechanisms of resistance to cytarabine in AML patients.* Leukemia research, 2002. **26**(7): p. 621-629.

47. Gati, W.P., et al., *Sensitivity of acute leukemia cells to cytarabine is a correlate of cellular es nucleoside transporter site content measured by flow cytometry with SAENTA-fluorescein.* Blood, 1997. **90**(1): p. 346-353.

48. Hubeek, I., et al., *The human equilibrative nucleoside transporter 1 mediates in vitro cytarabine sensitivity in childhood acute myeloid leukaemia.* British Journal of Cancer, 2005. **93**(12): p. 1388 – 1394.

49. Adema, A.D., et al., *Metabolism and accumulation of the lipophilic deoxynucleoside analogs elacytarabine and CP-4126.* Investigational new drugs, 2012. **30**(5): p. 1908 - 1916.

50. Knapper, S., et al., *Elacytarabine in relapsed/refractory acute myeloid leukaemia: An evaluation of clinical efficacy, pharmacokinetics, cardiac safety and effects on lipid profile.* Leukemia research, 2013.

51. Ahrabi, S., F. Myhren, and O.H. Eriksen, *Parenteral formulations of elacytarabine derivatives*. 2013, Google Patents.

52. Ferezou, J. and A.C. Bach, *Structure and metabolic fate of triacylglycerol- and phospholipid-rich particles of commercial parenteral fat emulsions.* Nutrition, 1999. **15**(1): p. 44-50.

53. Bonté, F. and R.L. Juliano, *Interactions of liposomes with serum proteins.* Chemistry and Physics of Lipids, 1986. **40**(2–4): p. 359-372.

54. Pownall, H.J., et al., *Kinetics of lipid-protein interactions: interaction of apolipoprotein A-I from human plasma high density lipoproteins with phosphatidylcholines.* Biochemistry, 1978. **17**(7): p. 1183-1188.

55. Mady, M.M. and M.M. Ghannam, *Stability of anionic liposomes in serum and plasma.* African Journal of Pharmacy and Pharmacology, 2011. **5**(16): p. 1898-1905.

56. Liu, D., et al., *Interactions of serum proteins with small unilamellar liposomes composed of dioleoylphosphatidylethanolamine and oleic acid: high-density lipoprotein, apolipoprotein A1, and amphipathic peptides stabilize liposomes.* (0006-2960 (Print)).

57. Cwiklinska, A., et al., *Interaction Between VLDL and Phosphatidylcholine Liposomes Generates New gamma-LpE-like Particles.* Lipids, 2014. **49**(2): p. 143-153.

58. Semple, S.C., A. Chonn, and P.R. Cullis, *Interactions of liposomes and lipid-based carrier systems with blood proteins: Relation to clearance behaviour in vivo.* Advanced Drug Delivery Reviews, 1998. **32**(1–2): p. 3-17.

59. Tadin-Strapps, M., et al., *siRNA-induced liver ApoB knockdown lowers serum LDL-cholesterol in a mouse model with human-like serum lipids.* Journal of Lipid Research, 2011. **52**(6): p. 1084-1097.

60. Qureshi, R.N., et al., *Determination of cholesterol and triglycerides in serum lipoproteins using flow field-flow fractionation coupled to gas chromatography-mass spectrometry.* Analytica Chimica Acta, 2011. **706**(2): p. 361-6.

61. Zattoni, A., et al., *Hollow-fiber flow field-flow fractionation of whole blood serum.* Journal of chromatography. A, 2008. **1183**(1-2): p. 135-42.

62. Arfvidsson, C. and K.G. Wahlund, *Mass overloading in the flow field-flow fractionation channel studied by the behaviour of the ultra-large wheat protein glutenin.* (0021-9673 (Print)).

63. Caldwell, K.D., et al., *Sample overloading effects in polymer characterization by field-flow fractionation.* Journal of Applied Polymer Science, 1988. **36**(3): p. 703-719.

64. Yanagisawa, M., et al., *SEC-MALS study on aggregates of chitosan molecules in aqueous solvents: Influence of residual N-acetyl groups.* Carbohydrate Polymers, 2006. **66**(2): p. 192-198.

65. M Yanagisawa, A.I., *SEC-MALS-QELS Study on the Molecular Conformation of Cellulose in LiCl - Amide Solutions.* Biomacromolecules, 2005. **6**: p. 1258-1265.

66. Runyon, J.R., M. Ulmius, and L. Nilsson, *A perspective on the characterization of colloids and macromolecules using asymmetrical flow field-flow fractionation.*

Colloids and Surfaces A: Physicochemical and Engineering Aspects, 2014. **442**(0): p. 25-33.

67. Alftrén, J., et al., *Comparison of molecular and emulsifying properties of gum arabic and mesquite gum using asymmetrical flow field-flow fractionation.* Food Hydrocolloids, 2012. **26**(1): p. 54-62.

68. Bourgoin, A., E. Zablackis, and J.B. Poli, *Characterization of α-carrageenan solution behavior by field-flow fractionation and multiangle light scattering.* Food Hydrocolloids, 2008. **22**(8): p. 1607-1611.

69. Chiaramonte, E., et al., *Amylose and amylopectin in starch by asymmetric flow field-flow fractionation with multi-angle light scattering and refractive index detection (AF4–MALS–RI).* Journal of Cereal Science, 2012. **56**(2): p. 457-463.

70. Håkansson, A., M. Ulmius, and L. Nilsson, *Asymmetrical flow field-flow fractionation enables the characterization of molecular and supramolecular properties of cereal β-glucan dispersions.* Carbohydrate Polymers, 2012. **87**(1): p. 518-523.

71. Wagner, M., et al., *Characterization of cationic polymers by asymmetric flow field-flow fractionation and multi-angle light scattering—A comparison with traditional techniques.* Journal of Chromatography A, 2014. **1325**(0): p. 195-203.

72. Dutschman, G.E., et al., *Metabolism of 2 ',3 '-dideoxy-2 ',3 '-didehydro-beta-L(-)-5-flurocytidine and its activity in combination with clinically approved anti-human immunodeficiency virus beta-D(+) nucleoside analogs in vitro.* Antimicrobial Agents and Chemotherapy, 1998. **42**(7): p. 1799-1804.

73. Furman, P.A., et al., *Phosphorylation of 3'-azido-3'-deoxythymidine and selective interaction of the 5'-triphosphate with human immunodeficiency virus reverse transcriptase.* Proceedings of the National Academy of Sciences, 1986. **83**(21): p. 8333-8337.

74. M. Kukhanova, A.K., W. Prusoff, Y-C. Cheng, *Design of Anti-HIV Compounds from Nucleoside to Nucleoside 5-Triphosphate Analogs. Problems and Perspectives.* Current Pharmaceutical Design, 2000. **6**(5): p. 585 - 598.

75. Kuppler, R.J., et al., *Potential applications of metal-organic frameworks.* Coordination Chemistry Reviews, 2009. **253**(23-24): p. 3042-3066.

76. Della Rocca, J., D. Liu, and W. Lin, *Nanoscale Metal-Organic Frameworks for Biomedical Imaging and Drug Delivery.* Accounts of Chemical Research, 2011. **44**(10): p. 957-968.

77. Horcajada, P., et al., *Porous metal-organic-framework nanoscale carriers as a potential platform for drug delivery and imaging.* Nature Materials, 2010. **9**(2): p. 172 - 178.

78. Horcajada, P., et al., *Metal-Organic Frameworks in Biomedicine.* Chemical Reviews, 2012. **112**(2): p. 1232-1268.

79. Chalati, T., et al., *Optimisation of the synthesis of MOF nanoparticles made of flexible porous iron fumarate MIL-88A.* Journal of Materials Chemistry, 2011. **21**(7): p. 2220-2227.

80. Kalu*ƒ*ëerovi*ƒ*á, G.N., et al., *Liposomes as vehicles for water insoluble platinum-based potential drug: 2-(4-(Tetrahydro-2H-pyran-2-yloxy)-undecyl)-propane-1,3-diamminedichloroplatinum(II).* European Journal of Medicinal Chemistry, 2012. **54**(0): p. 567-572.

81. Kang, D.Y., et al., *Size characterization of drug-loaded polymeric core/shell nanoparticles using asymmetrical flow field-flow fractionation.* (1618-2650 (Electronic)).

82. Schädlich, A., et al., *Tumor Accumulation of NIR Fluorescent PEG‚ÄìPLA Nanoparticles: Impact of Particle Size and Human Xenograft Tumor Model.* ACS Nano, 2011. **5**(11): p. 8710-8720.

83. Schadlich, A., et al., *How stealthy are PEG-PLA nanoparticles? An NIR in vivo study combined with detailed size measurements.* (1573-904X (Electronic)).

84. Gaulding, J., A. South, and L.A. Lyon, *Hydrolytically degradable shells on thermoresponsive microgels.* Colloid and Polymer Science, 2013. **291**(1): p. 99-107.

85. Shimoda, A., et al., *Dual crosslinked hydrogel nanoparticles by nanogel bottom-up method for sustained-release delivery.* Colloids and Surfaces B: Biointerfaces, 2012. **99**(0): p. 38-44.

86. Ma, P.L., M.D. Buschmann, and F.M. Winnik, *One-Step Analysis of DNA/Chitosan Complexes by Field-Flow Fractionation Reveals Particle Size and Free Chitosan Content.* Biomacromolecules, 2010. **11**(3): p. 549-554.

87. Augsten, C. and K. M√§der, *Characterizing molar mass distributions and molecule structures of different chitosans using asymmetrical flow field-flow fractionation combined with multi-angle light scattering.* International journal of pharmaceutics, 2008. **351**(1‚Äì2): p. 23-30.

88. Fraunhofer, W., G. Winter, and C. Coester, *Asymmetrical Flow Field-Flow Fractionation and Multiangle Light Scattering for Analysis of Gelatin Nanoparticle Drug Carrier Systems.* Analytical Chemistry, 2004. **76**(7): p. 1909-1920.

89. Zillies, J.C., et al., *Method for Quantifying the PEGylation of Gelatin Nanoparticle Drug Carrier Systems Using Asymmetrical Flow Field-Flow Fractionation and Refractive Index Detection.* Analytical Chemistry, 2007. **79**(12): p. 4574-4580.

90. Garcea, R.L. and L. Gissmann, *Virus-like particles as vaccines and vessels for the delivery of small molecules.* Current Opinion in Biotechnology, 2004. **15**(6): p. 513-517.

91. Chuan, Y.P., et al., *Quantitative analysis of virus-like particle size and distribution by field-flow fractionation.* Biotechnology and Bioengineering, 2008. **99**(6): p. 1425-1433.

92. Pease, L.F., 3rd, et al., *Quantitative characterization of virus-like particles by asymmetrical flow field flow fractionation, electrospray differential mobility analysis, and transmission electron microscopy.* (1097-0290 (Electronic)).

93. Agostoni, V., et al., *'Green' fluorine-free mesoporous iron(III) trimesate nanoparticles for drug delivery.* Green Materials, 2013. **1**(4): p. 209-217.

94. Ružicka J, *Flow Injection Analysis*. 3rd ed. 1988. 528.